FEB 15 1994

Sta. 21 (20)

ENGINEERING DATA TRANSMITTAL

	Page 1 of _1_
	1. EDT 603784

2. To: (Receiving Organization) Multifunction Waste Tank Facility	3. From: (Originating Organization) Central Engineering	4. Related EDT No.: N/A
5. Proj./Prog./Dept./Div.: Project 236A	6. Cog. Engr.: A. M. Tallman	7. Purchase Order No.: N/A
8. Originator Remarks: Seismic hazard analysis for the Hanford Site. Key words: earthquake, ground motion, natural phenomena, seismic hazard.		9. Equip./Component No.: N/A
		10. System/Bldg./Facility: N/A
11. Receiver Remarks:	JAN 1996 RECEIVED EDMC	12. Major Assm. Dwg. No.: N/A
		13. Permit/Permit Application No.: N/A
		14. Required Response Date: February 28, 1994
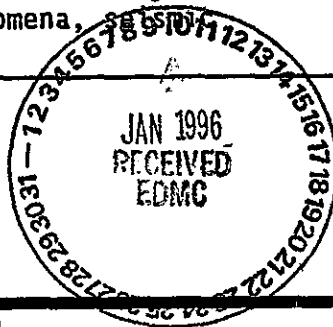
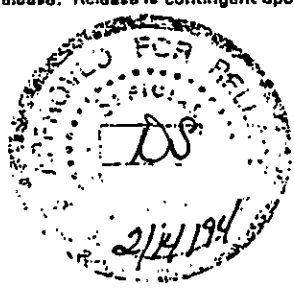### 15. DATA TRANSMITTED

(A) Item No.	(B) Document/Drawing No.	(C) Sheet No.	(D). Rev. No.	(E) Title or Description of Data Transmitted	(F) Impact Level	(G) Reason for Trans- mittal	(H) Origi- nator Dispo- sition	(I) Receiv- er Dispo- sition
1	WHC-SD-W236A-TI-002		0	Probabilistic Seismic Hazard Analysis, DOE Hanford Site, Washington	Q	1,2	1	

16. KEY

Impact Level (F)	Reason for Transmittal (G)	Disposition (H) & (I)
1, 2, 3, or 4 (see MRP 5.43)	1. Approval 4. Review 2. Release 5. Post-Review 3. Information 6. Dist. (Receipt Acknow. Required)	1. Approved 4. Reviewed no/comment 2. Approved w/comment 5. Reviewed w/comment 3. Disapproved w/comment 6. Receipt acknowledged

17. SIGNATURE/DISTRIBUTION
(See Impact Level for required signatures)

(G) Rea- son	(H) Disp.	(J) Name (K) Signature (L) Date (M) MSIN	(J) Name (K) Signature (L) Date (M) MSIN	(G) Rea- son	(H) Disp.
1,2	1	Cog.Eng. A. M. Tallman H5-60	M. D. Stine E6-50	2	
1,2	1	Cog. Mgr. T. J. Conrads H5-55	K. R. Fecht H6-06	2	
1,2	1	QA A.K. Sharma for 2/1/94 H5-60	S. K. Farnworth H5-55	2	
		Safety	J. M. Light B4-08	2	
		Env.	D. J. Green H5-53	2	
2		L. K. Severud H5-60	R. L. Fritz B4-08	2	
2		S. P. Reidel H6-06	A. C. Rohay (PNL) K6-84	2	

18. A. M. Tallman Signature of EDT Date Originator	19. J. M. Light 2/4/94 Authorized Representative Date for Receiving Organization	20. T. J. Conrads 2/11/94 Cognizant/Project Engineer's Manager Date	21. DOE APPROVAL (if required) Ltr. No. [] Approved [] Approved w/comments [] Disapproved w/comments

Date Received: 12/22/93	INFORMATION RELEASE REQUEST	Reference: WHC-CM-3-4

Complete for all Types of Release

Purpose				ID Number (include revision, volume, etc.)
[]	Speech or Presentation	[]	Reference	WHC-SD-W235A-TI-002, REV.0
	[] Full Paper (Check only one suffix)	[X]	Technical Report	
	[] Summary	[]	Thesis or Dissertation	List attachments.
	[] Abstract	[]	Manual	N/A
	[] Visual Aid	[]	Brochure/Flier	
[]	Speakers Bureau	[]	Software/Database	Date Release Required
[]	Poster Session	[]	Controlled Document	
[]	Videotape	[]	Other	12/28/93

Title Probabilistic Seismic Hazard Analysis, DOE Hanford Site, Washington	Unclassified Category UC-	Impact Level Q

New or novel (patentable) subject matter? [X] No [] Yes If "Yes", has disclosure been submitted by WHC or other company? [] No [] Yes Disclosure No(s).	Information received from others in confidence, such as proprietary data, trade secrets, and/or inventions? [X] No [] Yes (Identify)
Copyrights? [X] No [] Yes If "Yes", has written permission been granted? [] No [] Yes (Attach Permission)	Trademarks? [X] No [] Yes (Identify)

Complete for Speech or Presentation

Title of Conference or Meeting N/A	Group or Society Sponsoring N/A		
Date(s) of Conference or Meeting N/A	City/State N/A	Will proceedings be published? [] Yes [X] No Will material be handed out? [] Yes [X] No	
Title of Journal N/A			

CHECKLIST FOR SIGNATORIES

Review Required per WHC-CM-3-4	Yes	No	Reviewer - Signature Indicates Approval Name (printed)	Signature	Date
Classification/Unclassified Controlled Nuclear Information	[]	[X]			
Patent - General Counsel	[X]	[]	S. W. Berglin	S.W.Berglin	12/36/3
Legal - General Counsel	[X]	[]	S. W. Berglin		
Applied Technology/Export Controlled Information or International Program	[]	[X]			
WHC Program/Project	[X]	[]	R. L. Fritz		12/28/93
Communications	[]	[X]			
RL Program/Project	[X]	[]	R. M. Hiegel		1/4/94
Publication Services	[X]	[]	D. J. Hastings	Hastings	1/7/94
Other Program/Project	[]	[X]			

Information conforms to all applicable requirements. The above information is certified to be correct.

	Yes	No	INFORMATION RELEASE ADMINISTRATION APPROVAL STAMP
References Available to Intended Audience	[]	[X]	Stamp is required before release. Release is contingent upon resolution of mandatory comments.
Transmit to DOE-HQ/Office of Scientific and Technical Information	[]	[X]	
Author/Requestor (Printed/Signature) Date A. M. Tallman 1/17/93			
Intended Audience [] Internal [] Sponsor [X] External			
Responsible Manager (Printed/Signature) Date T. J. Conrads 12/17/93		Date Cancelled	Date Disapproved

SUPPORTING DOCUMENT		1. Total Pages 154	

2. Title	3. Number	4. Rev No.
Probabilistic Seismic Hazard Analysis, DOE Hanford Site, Washington	WHC-SD-W236A-TI-002	0

5. Key Words	6. Author
Earthquake, ground motion, natural phenomena, seismic hazard. APPROVED FOR PUBLIC RELEASE 2/14/94 D. Salis	Name: A. M. Tallman for Geomatrix Consultants, Inc. *A. M. Tallman* Signature Organization/Charge Code 23000/DTTTC

7. Abstract

The seismic hazard analysis presents the characterization of the seismic sources and the tectonic model of the Hanford Site and surrounding region and the probabilistic seismic hazard analysis methodology and results for five areas of the Hanford Site. This analysis supersedes WHC-MR-0023.

10. RELEASE STAMP

OFFICIAL RELEASE
BY WHC
DATE FEB 15 1994
Sta. 21

9. Impact Level Q

GEOMATRIX

PROBABILISTIC SEISMIC
HAZARD ANALYSIS
DOE HANFORD SITE, WASHINGTON

Prepared for

Westinghouse Hanford Company
2920 George Washington Way
Richland, Washington

December 1993
Project No. 2169

Geomatrix Consultants

TABLE OF CONTENTS

TALBE OF CONTENTS (continued)

LIST OF TABLES

LIST OF FIGURES

TABLE OF CONTENTS (continued)

LIST OF FIGURES (continued)

TABLE OF CONTENTS (continued)

LIST OF FIGURES (continued)

TABLE OF CONTENTS (continued)

LIST OF FIGURES (continued)

TABLE OF CONTENTS (continued)

LIST OF FIGURES (continued)

TABLE OF CONTENTS (continued)

LIST OF FIGURES (continued)

TABLE OF CONTENTS (continued)

LIST OF FIGURES (continued)

PROBABILISTIC SEISMIC HAZARD ANALYSIS, DOE HANFORD SITE, .WASHINGTON

1.0 INTRODUCTION

This report presents the results of a probabilistic seismic hazard analysis conducted for five areas at the DOE Hanford Site, Washington. Figure 1-1 shows the locations of the sites for which seismic hazard computations were performed. The sites are labeled as A, B, C, D, and E and correspond to the following areas of the Hanford Site.

> A 200 West Area
> B 200 East Area
> C 300 Area
> D 400 Area
> E 100 K area

The seismic hazard analysis presented in this report is the result of an evolutionary process in the development of a probabilistic seismic hazard model for the region. The starting point was the study of Power and others (1981) performed for the Washington Public Power Supply System's nuclear reactor sites WNP-1/4 and WNP-2, also located on the Hanford Site. That study was subsequently applied to the DOE Hanford Site areas with modification of the earthquake recurrence rate assessments (Woodward-Clyde Consultants, 1989). The model presented here was developed with input from Geomatrix Consultants, Westinghouse Hanford Company, Pacific Northwest Laboratories, and Washington Public Power Supply System (The Supply System). The individuals involved in the assessments were:

Geomatrix Consultants	Michael Angell
	Kevin Coppersmith
	Laurel Di Silvestro
	Robert Youngs
Pacific Northwest Laboratories	Alan Rohay
Washington Public Power Supply System	William Kiel
Westinghouse Hanford Company	Stephen Reidel
	Ann Tallman

The models, parameters, and their relative weights presented in this report represent a consensus of the team developed through multiple meetings and discussions. The model represents the team's assessment of the current state of scientific knowledge about the seismic potential and earthquake ground motion characteristics of the Hanford region. Work is continuing to evaluate the appropriateness of the assumptions regarding the characteristics of earthquake ground motions at the individual sites.

GEOMATRIX
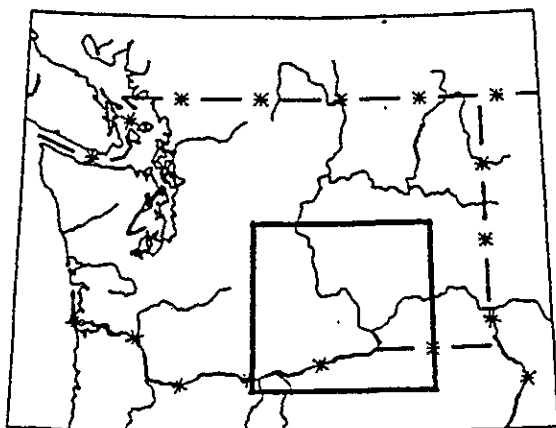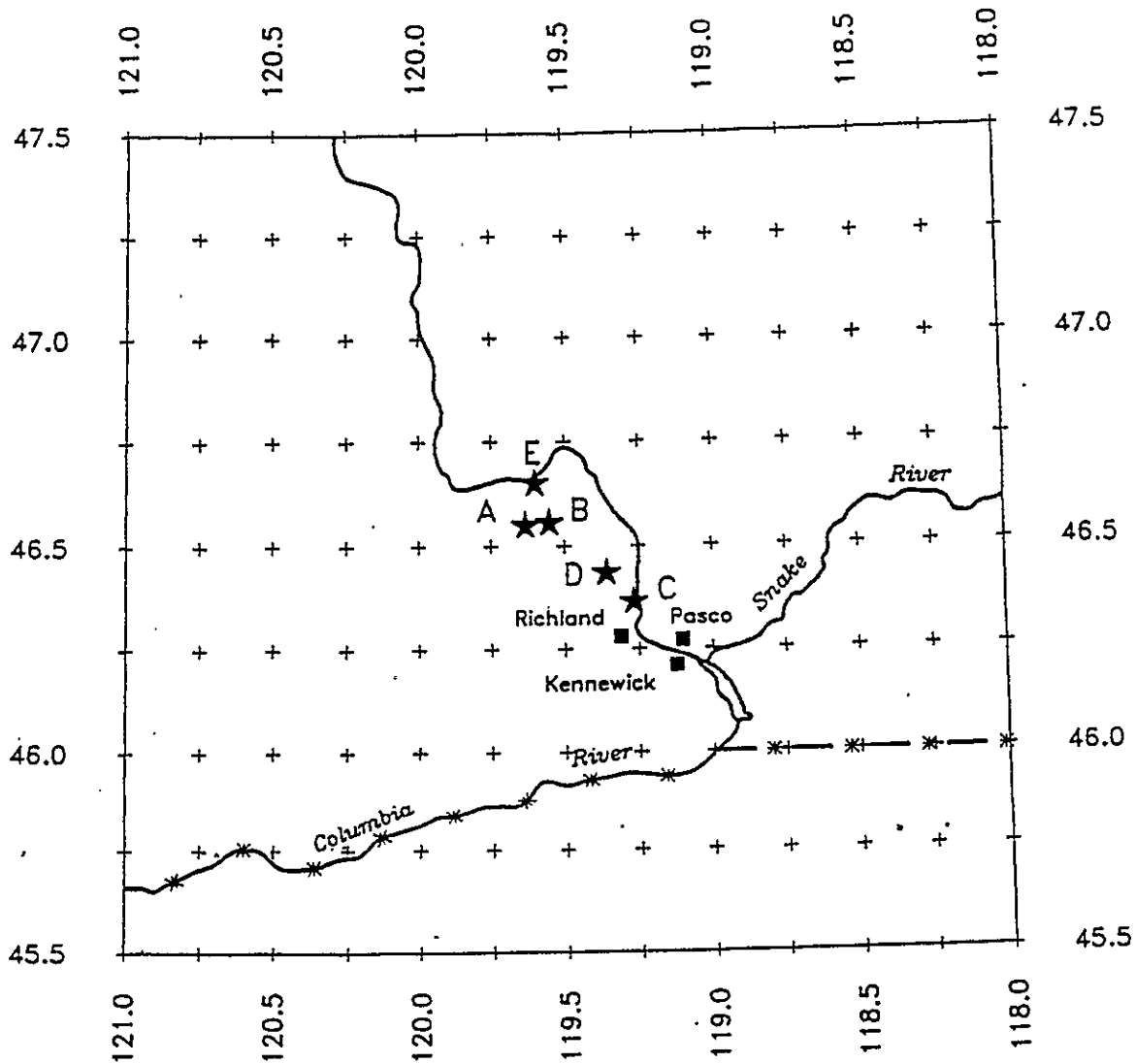
Scale 1 : 2,000,000

★   Hanford DOE sites

Figure 1-1   Location of DOE sites analyzed in this study.

2.0 SEISMIC HAZARD ANALYSIS METHODOLOGY

For this study, probabilistic seismic hazard analysis (PSHA) is defined as an evaluation of the probability or likelihood that various levels of ground motion will be exceeded during a specified time period. The analysis procedure was originally proposed by Cornell (1968). Since that time there has been significant progress in our understanding of the earthquake process and in the techniques for evaluation of the relevant seismological, geological, and geophysical data. The analysis methodology used in this study is similar to that used in the 1981 study and incorporates the significant advances that have been made in PSHA (e.g., Coppersmith and Youngs, 1990; Coppersmith, 1991). Section 2.1 outlines the mathematical formulation used. Following that, the important considerations involved in selecting the analysis models and input parameters are discussed.

2.1 HAZARD FORMULATION

In probabilistic terms, seismic hazard is defined as the likelihood that various levels of ground motion will be exceeded at a site during a specified time period. It is commonly assumed that the occurrence of individual main shocks can be represented as a Poisson process. Following the approach developed by Cornell (1968), the probability that at a given site a ground motion parameter, Z, will exceed a specified level, z, during a specified time period, t, is given by the expression:

$$P(Z > z | t) = 1.0 - e^{-v(z) \cdot t} \le v(z) \cdot t \tag{2-1}$$

where $v(z)$ is the average frequency during time period t at which the level of ground motion parameter Z exceeds z at the site resulting from earthquakes on all sources in the region. The inequality at the right of Equation (2-1) is valid regardless of the appropriate probability model for earthquake occurrence, and $v(z) \cdot t$ provides an accurate and slightly conservative estimate of the hazard for probabilities of 0.1 or less, provided $v(z) \cdot t$ is the appropriate value for the time period of interest.

The frequency of exceedance, $\nu(z)$, is a function of the randomness in the time, size, and location of future earthquakes and randomness in the level of ground motions they may produce at the site. It is computed by the expression:

$$\nu(z) = \sum_N \alpha_n(m^o) \int_{m^\bullet}^{m^\bullet} f(m) \left[\int_0^\infty f(r|m) \cdot P(Z>z|m,r) dr \right] dm \qquad (2\text{-}2)$$

where $\alpha_n(m^o)$ is the frequency of earthquakes on source n above a minimum magnitude of engineering significance, m^o; $f(m)$ is the probability density function for event size between m^o and a maximum event size for the source, m^u; $f(r \mid m)$ is the probability density function for distance to the earthquake rupture; and $P(Z>z \mid m,r)$ is the probability that, given a magnitude m earthquake at a distance r from the site, the ground motion exceeds level z.

The distance density function, $f(r \mid m)$, is developed by specifying the geometry of the seismic sources and allowing earthquake ruptures to occur randomly over the source volume. In this study individual faults are modeled as segmented planar features, with the earthquake rupture modeled as a rectangular area randomly located on the fault plane. Area sources are modeled by closely spaced fault traces, each being an individual fault plane. The rate term $\alpha_n(m^o)$ and the density function $f(m)$ are specified by developing a recurrence relationship for the source. The density function $f(m)$ is limited on the upper end by developing an estimate of the maximum magnitude for the source. The approaches used to develop these functions and parameters are described in the next section.

The probability functions contained in Equations (2-1) and (2-2) represent the uncertainties inherent in the natural phenomena of earthquake generation and seismic wave propagation. For the Hanford region (usually the case in any region) there are considerable uncertainties about the appropriate models and model parameters required to apply Equation (2-2) arising from limited data and/or alternative interpretations of the available data. This study explicitly

incorporates these additional uncertainties into the analysis to provide a quantitative assessment of the uncertainty in the seismic hazard estimate.

The uncertainty in modeling the natural phenomena is incorporated into the hazard analysis through the use the logic tree methodology employed in the previous studies (Power and others, 1981; Woodward-Clyde Consultants, 1989). The logic tree formulation for seismic hazard analysis (Kulkarni and others, 1984; Youngs and others, 1985, 1987, 1988; Coppersmith and Youngs, 1986) involves specifying discrete alternatives for states of nature or analysis model parameter values and judgments on the relative likelihood that each discrete alternative is correct. The relative likelihoods of the different parameter values are typically based on subjective judgment, but may be specified by an objective statistical analysis if the available data warrant an assessment. The components of the logic trees developed for this study are described in the next section. The selection of the parameters and models for each source and the bases for parameter selection and relative weighting are discussed in Chapters 3 and 4.

2.2 DEVELOPMENT OF SEISMIC HAZARD MODEL

The seismic hazard at a site is a function of the location and geometry of potential sources of future earthquakes, the frequency of occurrence of various size earthquakes on these sources, and the characteristics of seismic wave propagation in the region. In the methodology used here, these elements are analyzed within a probabilistic framework that addresses both the randomness of the earthquake process and the uncertainty in modeling the process. The seismic hazard model consists of two basic components: a model of the sources of potential future earthquakes and a model of the effects at the site, due to potential of future earthquakes. Each potential earthquake source is characterized by parameters that describe its location, geometry, maximum magnitude, and earthquake recurrence. The methods used in this study to characterize the seismic sources are state-of-the-art and provide for the specific inclusion of detailed aspects of fault behavior (e.g., Coppersmith, 1991). To allow for independent review of the assessments made in this study, we document in Sections 3 and 4 the basis for

GEOMATRIX

each seismic source characteristic in terms of the data and interpretations leading to the values in the seismic hazard model.

Figure 2-1 displays the overall logic tree representing the seismic hazard model developed for this study. The logic tree is laid out to provide a logical progression from general aspects/hypotheses regarding the characteristics of seismicity and seismic wave propagation in the region to specific input parameters for individual faults and fault segments. The rationale for developing the various levels of the logic tree is discussed below.

The first node of the logic tree represents the uncertainty in selecting the appropriate strong ground motion attenuation relationship. Attenuation was placed first in the tree because it is felt that a single relationship (whichever relationship may be "best" at representing ground motion attenuation) is applicable to all earthquake sources in the region. The selection of attenuation relationships is discussed in Section 4.

At this point the logic tree is expanded into three subtrees, one for each of the seismic source types included in the analysis to model the additive hazard from multiple sources: folds of the Yakima Fold Belt, shallow basalt sources, and basement sources. To the right of this node of the logic tree each source is considered to be acting independently, and the distribution in the total computed hazard is obtained by convolving the independent distributions obtained for each seismic source.

The following nodes, related to characterizing the individual sources, include: source activity, source tectonic model, source geometry, maximum magnitude, earthquake recurrence, and magnitude distribution models. The specific node levels used and the resulting branches and associated relative likelihoods are dependent on the type of source assessed. Section 3 describes the logic trees for the seismic sources.

Several nodes of the logic tree relate to earthquake recurrence. For areal sources the recurrence relationships were based on recorded seismicity and the truncated exponential

magnitude distribution (Cornell and Van Marke, 1969) was used to define the recurrence relationships. The truncated exponential relationship is of the form

$$N(m) = N(m^0) \frac{10^{-b(m-m^0)} - 10^{-b(m^U-m^0)}}{1 - 10^{-b(m^U-m^0)}} \qquad (2\text{-}3)$$

where $N(m^0)$ is the annual frequency of occurrence of earthquakes of magnitude greater than a minimum magnitude, m^0; b is the Gutenberg and Richter (1954, 1956) b-value parameter; m^U is the maximum magnitude event than can occur on the source; and $N(m)$ is the annual frequency of occurrence of earthquakes of magnitude greater than m.

For fault sources, the earthquake recurrence rate is estimated based on an assessment of fault slip rate and a translation of the slip rate to seismic moment rate. To develop an earthquake recurrence relationship from slip rate, the seismic moment rate must be partitioned into earthquakes of various magnitudes according to a magnitude distribution or recurrence model. Two recurrence models are considered in this analysis: the characteristic earthquake model and the exponential model. These models describe the distribution of earthquake magnitudes. Youngs and Coppersmith (1985a, b) and Youngs and others (1992) have shown that the characteristic earthquake model is more appropriate for fault sources.

In applying Youngs and Coppersmith's (1985a, b) characteristic magnitude distribution, the maximum magnitude assessed for the fault, m^U, is taken to be the expected magnitude for the characteristic size event, with individual events uniformly distributed in the range of $m^U \pm \frac{1}{4}$ magnitude units, reflecting random variability in individual "maximum" ruptures. The form of the characteristic magnitude distribution used thus becomes

$$N(m) = N^c \frac{10^{-b(m-m^0)} - 10^{-b(m^U-\frac{1}{4}-m^0)}}{1.0 - 10^{-b(m^U-\frac{1}{4}-m^0)}} + N^c \qquad for \ m^0 \geq m > m^U-\frac{1}{4}$$

$$\qquad (2\text{-}4)$$

$$N(m) = N^c \frac{m^U+\frac{1}{4}-m}{1/2} \qquad for \ m^U-\frac{1}{4} \geq m > m^U+\frac{1}{4}$$

where the terms N^e and N^c represent the rate of exponential and characteristic events respectively. $N^c = N(m^U - \frac{1}{4})$, the cumulative frequency of characteristic events, and the total seismicity rate, $N(m^0) = N^e + N^c$. These terms can be specified directly from seismicity or by using the slip rate formulation of Youngs and Coppersmith (1985b)

$$N^e = \frac{\mu A_f S(1.0 - 10^{-b(m^U - \frac{1}{4} - m^0)})}{M_o(m^U + \frac{1}{4}) 10^{-b(m^U - \frac{1}{4} - m^0)} \left[\frac{b \cdot 10^{-c/2}}{c-b} + \frac{b \cdot 10^b(1.0 - 10^{-c/2})}{c} \right]}$$

$$N^c = \frac{\frac{1}{2}b\ln(10)N^e 10^{-b(m^U - \frac{1}{4} - m^0 - 1)}}{1.0 - 10^{-b(m^U - \frac{1}{4} - m^0)}}$$

(2-5)

where μ is the shear modulus of fault zone rock (assumed to be $3 \cdot 10^{11}$ dyne/cm^2), A_f is the fault surface area, S is the slip rate, and $M_o(m^U + \frac{1}{4})$ is the seismic moment for the upper limit event, $m^U + \frac{1}{4}$, given by the expression

$$M_o(m) = 10^{c \cdot m + d}$$

(2-6)

To provide a consistent interpretation for the exponential model, Youngs and others (1987) introduced a modification to the standard truncated exponential distribution in which the upper bound magnitude in the density function was treated as uniformly distributed over the range of $m^U \pm \frac{1}{4}$ magnitude units. The effect is to generalize the upper boundary of the magnitude distribution without altering the general shape of the recurrence relationship. The cumulative frequency for earthquakes of magnitude $m^U - \frac{1}{4}$ is again set equal to the annual frequency of maximum events assessed for the fault. In this modified form the distribution of events in the range $m^U \pm \frac{1}{4}$ remains nearly exponential. The formulation for the modified truncated exponential is

$$N(m)=N(m^0)\left[1.0-\frac{(1.0-10^{-b(m-m^0)})(\ln(f^U)-\ln(f'))}{b\cdot\ln(10)/2}\right] \qquad for \ m^0\geq m> m^{U}-\tfrac{1}{4}$$

$$N(m)=N(m^0)\left[1.0-\frac{(1.0-10^{-b(m-m^0)})(\ln(f^U)-\ln(f^i))}{b\cdot\ln(10)/2}-2(m-m^{U}+\tfrac{1}{4})\right] \qquad for \ m^{U}-\tfrac{1}{4}\geq m> m^{U}+\tfrac{1}{4}$$

$$(2\text{-}7)$$

with

$$f' = 10^{b(m^{U}-\tfrac{1}{4})} - 10^{bm^0}$$
$$f^u = 10^{b(m^{U}+\tfrac{1}{4})} - 10^{bm^0}$$
$$f^i = 10^{bm} - 10^{bm^0}$$

$$(2\text{-}8)$$

If the recurrence rate is specified by the rate of "characteristic" events, $N^c = N(m^U\text{-}\tfrac{1}{4})$, then the total rate of seismicity, $N(m^0)$ is given by

$$N(m^0) = \frac{N^c}{1.0 - \dfrac{(1.0-10^{-b(m^{u}-\tfrac{1}{4}-m^0)})(\ln(f^u)-\ln(f'))}{b\cdot\ln(10)/2}}$$

$$(2\text{-}9)$$

If the recurrence rate is given by slip rate then $N(m^0)$ is given by

$$N(m^0)=\frac{6\mu A_f S(c\dot{-}b)}{\dfrac{10^{c(m^{U}-\tfrac{1}{4})+d}}{10^{b(m^{U}-\tfrac{1}{4}-m^0)}-1.0}+\dfrac{4\cdot10^{cm^{U}+d}}{10^{b(m^{U}-m^0)}-1.0}+\dfrac{M_o(m^{U}+\tfrac{1}{4})}{10^{b(m^{U}+\tfrac{1}{4}-m^0)}-1.0}}$$

$$(2\text{-}10)$$

Figure 2-2 compares the shape of the exponential, modified exponential, and characteristic magnitude distributions. Shown on the left are the three distributions developed for an

assessed fault m^U of 7.25 with the frequency of events larger than magnitude 7 held constant in all three models. Shown on the right on Figure 2-2 are the magnitude distributions developed on the basis of equal rate of seismic moment release. As can be seen, the modified truncated exponential distribution is essentially equal to the truncated exponential distribution except near the upper bound. The characteristic magnitude distribution results in about a factor of 10 reduction in the frequency of small magnitude events compared to the exponential model when the absolute level of the distribution is fixed by either the frequency of the largest events or by the rate of moment release.

Attenuation Relationship	Sources	Activity	Tectonic Model	Segmentation	Source Geometry	Maximum Magnitude	Recurrence Rate	Magnitude Distribution
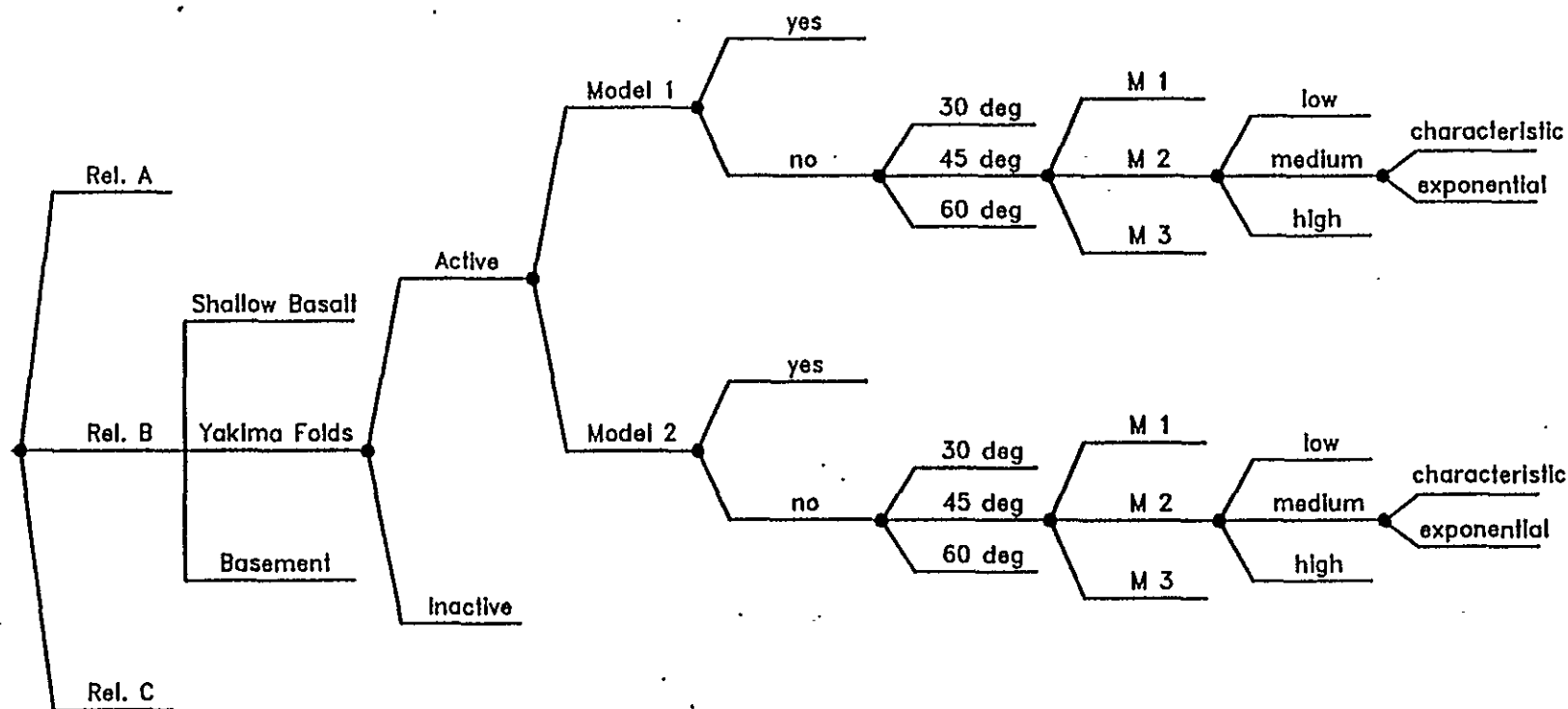
Figure 2-1   Basic seismic hazard model logic tree
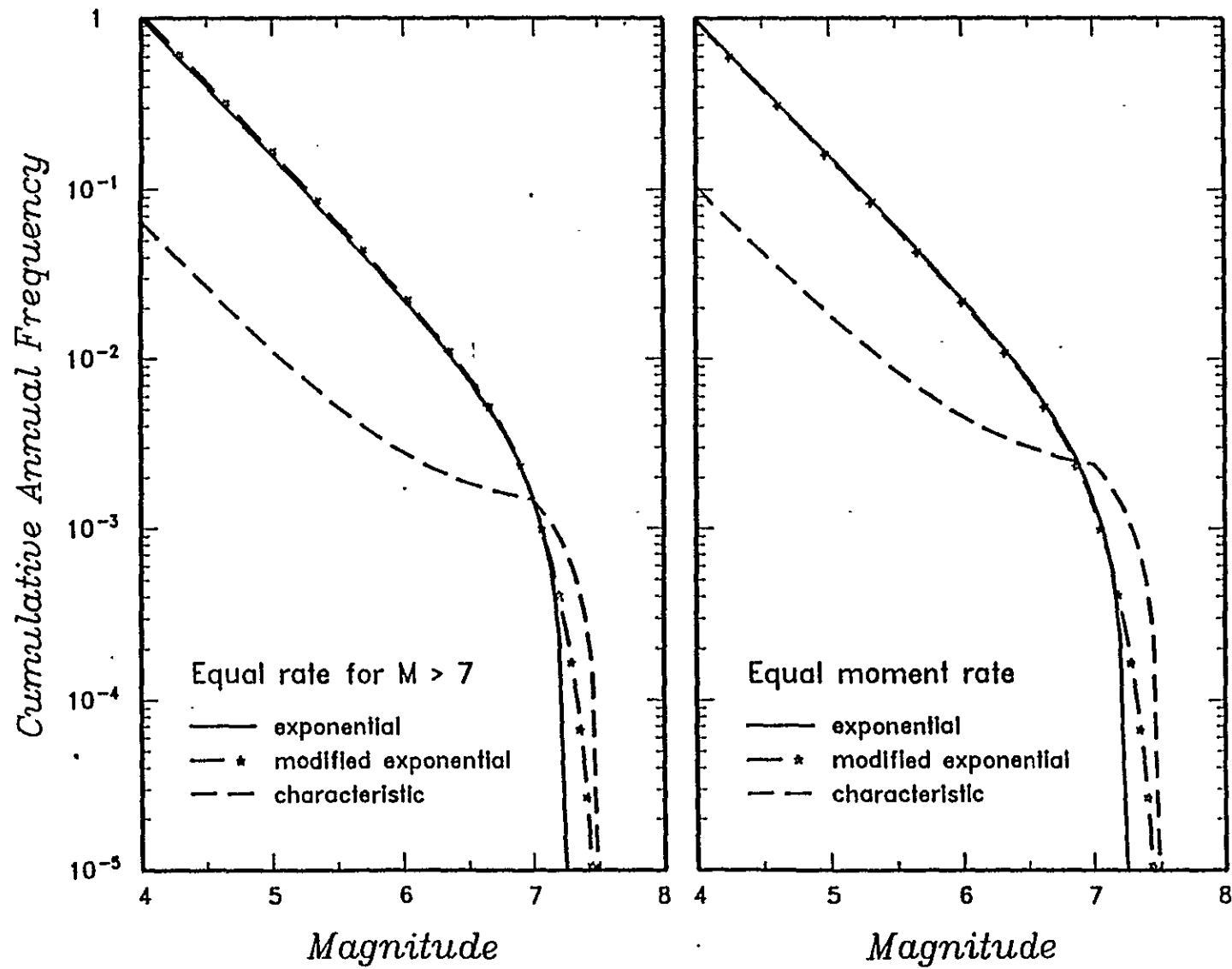
Figure 2-2   Magnitude distribution models used in analysis

3.0 SEISMIC SOURCE CHARACTERIZATION

In this section the characteristics of each potential earthquake source that might affect the seismic hazards at the DOE Hanford Site are presented. The source characteristics are presented and incorporated into the seismic hazard analysis through the use of logic trees. In Section 2.2 the basic elements of the logic trees were discussed. In this section the parameter values and associated weights that we include in the logic trees are documented. Sections 3.1 and 3.2 discuss the seismicity and seismic source model for the Yakima fold belt. Section 3.3 characterizes the Cascadia subduction zone lying along the coast of Washington and Oregon. The computed hazard and the influence of the important elements of the seismic source model are shown in Section 5.

3.1 REGIONAL SEISMICITY OF THE YAKIMA FOLD BELT

3.1.1 Earthquake Catalog

An earthquake catalog for the site region was compiled from the catalog presented in the FSAR for Washington Public Power Supply System's WNP-2 power plant for the time period of 1850 to 1969 and from the University of Washington seismic records for the period 1969 through March of 1991. Figure 3-1 shows the spatial distribution of earthquakes in the site region. A summary of the historical and instrumental seismicity of the region is presented in DOE (1988).

3.1.2 Earthquake Magnitude

The catalog contains a variety of magnitude measures. For larger and older events, magnitudes are reported as either local magnitude, M_L, or surface wave magnitude, M_S. In the magnitude range of the reported events, these two measures are essentially equivalent to moment magnitude, M, as proposed by Hanks and Kanamori (1979). Smaller magnitude events are reported in terms of coda-duration magnitude, M_C, which has been calibrated by the University of Washington to be equivalent to M_L. Comparisons of M_C and M_L estimates for individual events indicate that M_C may provide a slight over estimate of M_L although this

conclusion was based on a very limited data set (Malone, 1979). For this analysis, it was assumed that the two magnitude measures are equivalent.

The seismic hazard calculations were performed assuming that moment magnitude, M, (Hanks and Kanamori, 1979) is equivalent to M_L in the site region. There are not sufficient data available to confirm this assumption. However, it has been found that this assumption is a reasonable one for much of the western United States. For example, early investigations of the relationship between seismic moment, M_o and M_L for Basin and Range earthquakes by Doser and Smith (1982) suggested a significantly different relationship than that developed by Hanks and Kanamori for California earthquakes. However, more extensive analyses by Shemeta and Pechmann (1989) have shown that the Hanks and Kanamori (1979) moment-magnitude relationship, $M = \frac{2}{3}\log_{10}(M_o)-10.7$ is appropriate for Basin and range earthquakes. In addition, moment estimates for two moderate magnitude events in northwest Oregon indicated compatibility between M_L and M. Yelin and Patton (1991) report that the moment magnitude for the 1962 M_L 5.2 Portland earthquake is M 5.2. The magnitude estimates for the March 25, 1993 Scotts Mills earthquake are M_L 5.6 (Steve Malone, University of Washington, pers. comm.) and M 5.6 (John Nabelek, Oregon State University, pers. com.).

The magnitude estimates for the recent 1993 Klamath Falls events in southern Oregon also show consistency between estimates of M_L and seismic moment. The University of Washington reports M_C (calibrated to be equivalent to M_L) values of 5.9 and 6.0 for the two events. The National Earthquake Information Center reports magnitudes of M_L 5.9, M 5.9 for the first and M_L 5.9, M 5.9 for the second.

3.1.3 Identification of Dependent Events

The mathematical formulation used in this (and most) probablistic seismic hazard analysis is based on an assessment of the frequency of occurrence of independent earthquakes. It has been shown that the inclusion of dependent events (e.g., foreshocks and aftershocks) in the analysis results in about a 10 percent increase in the frequency of exceeding various ground motion levels (Merz and Cornell, 1973; Veneziano and Van Dyck, 1985). This increase is

small in comparison with the uncertainty estimates in the hazard due to uncertainty in estimating the rates of the independent events and would have a negligible effect on computed ground motion levels at specified return periods.

For this study, dependent events in the earthquake catalog were identified using the following procedure. The largest event in the catalog was identified and a spatial and temporal window was specified based on empirical criteria for the size of foreshock-aftershock sequences as a function of earthquake magnitude. All events falling within the window were flagged as dependent events. The next largest unflagged event was then selected and the process repeated down to the smallest magnitude event.

The three empirical criteria selected for identifying dependent events are shown on Figure 3-2. Youngs and others (1987) found that all three criteria performed well in identifying dependent events in the earthquake catalog for the Wasatch front in Utah. The three criteria were applied independently to this catalog, and earthquakes were identified as dependent events if flagged by at least two of the three criteria.

The use of the above method for identifying dependent events is based on the assumption that the time sequence of earthquakes in the Columbia Plateau follow typical mainshock-foreshock-aftershock behavior. However, the earthquakes within the basalt show pronounced clustering behavior. Johnson (1989a) performed a detailed analysis of clustering of earthquakes in eastern Washington and developed criteria for identifying earthquakes that form a cluster or swarm. Her criteria for the Columbia Plateau region indicate that events that occur within a time window of 14 days and a distance window of 4 km of each other should be considered part of a cluster of events. Using these criteria, the earthquake catalog was analyzed to identify cluster and noncluster earthquakes. The largest event in each cluster, together with the noncluster events, were then cataloged as independent events. Figure 3-3 compares the earthquake occurrence rates computed for independent earthquakes based on the aftershock sequence criteria shown on Figure 3-2, with the earthquake occurrence rates computed for independent events and the largest event of each cluster identified using the criteria developed

by Johnson (1989a). As indicated by the fitted recurrence relationships, the two approaches lead to similar estimates of the frequency of independent earthquakes and b-values. Also shown is the computed frequency of all earthquakes. The computed b-value for all events is similar to the value obtained by Rohay (1989) for the instrumental period (nominally 1970 to the present).

The computed recurrence relationships are used in the hazard analysis to estimate the frequency of magnitude 5 and larger earthquakes. Because small earthquakes in the Columbia Plateau tend to occur in swarms rather than classical mainshock-aftershock sequences, the recurrence relationships used were based on independent events and the largest event of clusters identified using Johnson's (1989a) criteria. As indicated on Figure 3-3, this approach results in a slightly greater estimate of the rate of events of magnitude 5 and larger than obtained using the empirical aftershock size criteria or considering all earthquakes.

3.1.4 Catalog Completeness

The time periods over which independent events of various magnitudes can be considered completely reported in the catalog must be established in order to properly estimate earthquake recurrence frequencies. Within the Yakima Fold Belt region, the estimated detection thresholds are approximately magnitude 2.0 for the period 1970 through 1974 and approximately 1.5 after 1975 (University of Washington, 1985).

The periods of complete reporting for the region were estimated by examining the variation in the rate of earthquake occurrence with time. Figure 3-4 presents plots of the observed frequency of occurrence of events in different magnitude intervals as a function of time before the present (defined as April 1, 1991), with the observed frequency equal to the number of events observed in the past T years divided by T. The magnitude intervals were centered on magnitudes estimated using unit intensities of II and greater in the Gutenberg and Richter (1956) intensity-magnitude relationship. Two plots are shown, one for all events and one for independent events (defined in Section 3.1.3). The rates shown for independent events are

without the effects of temporal clusters of earthquakes. The presence of clusters results in deviations from the assumed model of earthquake occurrence of independent Poisson arrivals.

The results shown indicate that the catalog can be considered complete for magnitudes in the range of 2.0 to 4.0 since 1970. Events smaller than magnitude 2 either do not appear to be completely reported over the whole Yakima Fold Belt region at the present time or these events exhibit a lower *b*-value than those larger than magnitude 2.0. The data for magnitudes greater than 4 are very limited. Rohay (1989) estimated catalog completeness for a larger region covering eastern Washington and concluded that earthquakes of intensity MMI V ($\sim M_L$ 4.3) have been completely reported since 1905 and earthquakes of intensity MMI VI ($\sim M_L$ 5) have been completely reported since 1890. These completeness estimates were used to compute earthquake recurrence rates for the study region.

3.1.5 Recurrence Calculations

Recurrence parameters of a truncated exponential frequency magnitude distribution (Equation 2-3) were fit to the data for each source zone or source zone combination using the maximum likelihood algorithm of Weichert (1980). Uncertainty in the values of $N(m^0)$ and b were specified by using Weichert's likelihood formulation to compute the relative likelihood of a set of discrete values for both $N(m^0)$ and b over a range of plus-or-minus two standard errors about the maximum likelihood values. The computed likelihoods of the discrete values were then normalized to form a joint distribution for the two recurrence parameters that properly accounts for the correlation between them.

Figure 3-5 shows the computed earthquake recurrence relationship for the Yakima Fold Belt region outlined on Figure 3-1 using the completeness periods defined in Section 3.1.4 and independent events, defined in Section 3.1.3. The maximum likelihood fits to the independent data yield *b*-values of 1.00 (± 0.04) for m^0 equal to 2.0 and 1.10 (± 0.07) for m^0 equal to 2.5. These recurrence relationships are compared to recurrence estimates for the Yakima Fold Belt region developed by Rohay (1989). The estimates are generally similar. The difference in *b*-value between the estimates for m^0 equal to 2.0 and 2.5 may reflect incomplete reporting

at the magnitude 2 level. The differences in the b-value are not statistically significant (<5 percent probability they are different) and fall within the distribution used to model the earthquake recurrence for this source.

Recurrence calculations for individual seismic source zones are discussed below.

3.2 SEISMIC HAZARD SOURCE MODEL FOR THE YAKIMA FOLD BELT

3.2.1 Tectonic Model

Earthquake activity in the Columbia Basin, central Washington, is attributed to three separate source regions of the seismogenic crust: (1) fault sources expressed at the surface as the Yakima Folds and related thrust/reverse faults; (2) a shallow basalt source that accounts for the observed seismicity within the Columbia River Basalt Group (CRBG) that is not spatially associated with the Yakima Folds; and (3) a crystalline basement source region that extends from the top of crystalline basement to the base of the seismogenic crust. These source regions are assumed to account for all observed seismicity and are developed within the framework of a regional crustal model based on available surface and subsurface geologic data, geophysical data, and seismicity data. Within the constraints provided by these data sets, various alternative interpretations are possible for the characterization of each of the three sources. The available data related to tectonic models for the region is discussed below, followed by a discussion of the characteristics of the three source types.

The model for the regional crustal structure of the Columbia Basin used in the source characterization is based primarily on interpretations of seismic refraction data. These data, developed from a series of experiments conducted in the mid-1980s (Rohay and Malone, 1983; Rohay and others, 1985; Glover, 1985; Catchings and Mooney, 1988) represent the majority of available information on the crustal structure and velocities in the Columbia Plateau. Figure 3-6 shows crustal-scale cross-sectional geometry along two north-south transects through the basin (119.5W and 120.0W) and an east-west tie-line. Figure 3-7 shows a larger scale cross section through the Columbia Plateau developed by Catchings and Mooney (1988). The crustal stratigraphy is interpreted in terms of the following layers:

- **Layer A:** Highly competent basalts of the Columbia River Basalt Group (CRBG) (compressional wave velocities of 5.2-5.7 km/sec)

- **Layer B:** Relatively incompetent sub-basalt basinal sediments (velocities of 5.0 km/sec)

- **Layer C:** Crystalline basement comprising the mid- to lower crust (velocities of 6.1-6.8 km/sec)

- **Layer D:** Ductile mantle (velocity of 7.5 km/sec)

The late Tertiary, Quaternary, and present-day tectonic stress field within the Columbia Basin is primarily compressive and oriented in a north-south direction, as indicated by the orientation of structures within the Yakima Fold Belt (Grolier and Bingham, 1971; Davis, 1977; Shannon and Wilson, 1977; Bentley, 1977; Swanson and others, 1979, 1980; DOE, 1988; Reidel and others, 1989); in-situ stress measurements (Kim and others, 1986), and several studies of the focal mechanisms of ongoing seismicity (Foxall and others, 1981; Rohay and Davis, 1983; DOE, 1988; Johnson, 1989b; Ludwin and others, 1992). Focal mechanisms for earthquakes located within the crystalline basement indicate that the orientation of maximum horizontal stress in the basement is generally the same as for the upper crust (DOE, 1988).

Based on the observed style and orientation of late Tertiary and Quaternary geologic structures and the earthquake focal mechanisms, the maximum compressive stress is assumed to be horizontal. Evidence includes the orientation of structures related to growth of the Yakima Folds, including east-west trending thrust faults and fold axes, NW-trending tear faults along the fold trends, and the limited evidence for northwest-trending strike-slip faulting in Wallula Gap. Although crustal extension is also evident at several locations around the Columbia Basin, these features are limited to secondary deformation associated with primary tectonic structures consistent with a horizontal maximum compressive stress. These features are: (1) localized extension in the hanging wall of several of the Yakima anticlines, such as Smyrna Bench at Saddle Mountain and Toppenish Ridge (Campbell and Bentley, 1981; Reidel, 1988; Geomatrix, 1990; West and Shaffer, in review), and (2) interpreted normal faulting in the Wallula Gap region (Washington Public Power Supply System, 1981; Mann and Meyer,

1993). The cause for extensional faulting in Wallula Gap is less well understood but can be attributed to either (A) extensional duplexing in a right-stepping discontinuity in the trace of a strike-slip fault (Mann and Meyer, 1993), or (B) a hanging wall extension with an orientation that is strongly influenced by the pre-existing tectonic fabric related to intrusion of the Ice Harbor dike swarm (S. Reidel, pers. comm, 1992).

There are several lines of evidence that suggest that the basinal sediments (layer B) beneath the basalts act as a detachment zone within the middle crust and accommodate regional compression by essentially aseismic distributed shear in a relatively "ductile" zone. This evidence includes (1) a distinct low level of seismicity within this zone, contrasted with relatively elevated levels of seismicity in the basalts and underlying crystalline basement (Fig. 3-7); (2) reversal of vergence and development of box-fold geometries along the strike of some of the Yakima Fold Belt folds, suggesting an underlying detachment; (3) structural and mechanical analysis that indicates the geometry of the Yakima Folds is consistent with critical wave length buckling of a strong elastic lid (basalts) over a relatively thick and incompetent substrate (basinal sediments) (Watters, 1989); and (4) downward-steepening of the faults (Reidel and others, 1989), suggesting ductile shortening and thickening within the basinal sediments (beneath the Columbia River basalts) to counteract the development of a void by displacement on steeply dipping reverse faults (see Coward, 1983).

The fold and thrust mechanisms of shortening exhibited by the Yakima Folds are, in most cases, restricted to the CRBG (layer A) and do not extend below the base of the basalts into the underlying Tertiary sediments or into the crystalline basement (i.e., the two regions of the crust are "uncoupled" in terms of seismic deformation). This interpretation is consistent with depth-to-detachment calculation of about 1.5 km for the Umtanum Ridge anticline (Price and Watkinson, 1989); observations in the field of an undeformed detachment horizon at the base of the CRBG in the Cleman Mountain anticline (Reidel and Campbell, 1989); and the preceding arguments for a strong mechanical contrast at the base of the CRBG. In addition, various estimates of the total strain represented by the Yakima Folds, including balancing and restoration methods, indicate the total shortening strain is relatively low (Bentley, 1980;

Laubscher, 1981; Reidel, 1984; Reidel and others, in press), suggesting the detachment system is local, not regional (see Reidel and others, 1989). Also, there is little evidence for regional late Tertiary to Quaternary deformation in the sediments underlying the CRBG (Campbell, 1988, 1989).

The seismicity that is occurring within the crystalline basement (layer C) is described by three alternative models for the basement source region, as discussed in Section 3.2.4: (1) reactivation of a failed rift in the present tectonic regime; (2) a broad region of subsiding basement separated from the surrounding relatively stable crust by potential fault sources; and (3) a random model that treats the entire basement as a zone of uniform seismicity.

Layer D is interpreted to exhibit velocities typical of upper mantle material subjacent to the Moho discontinuity. The absence of seismicity within this layer suggests that it lies below the brittle-ductile transition and strain is accommodated by aseismic crystal-plastic mechanisms. The geometry of layer D interpreted from geophysical data is a significant factor in distinguishing the failed rift model from the down-dropped block model (see Section 3.2.4).

3.2.2 Yakima Fold Sources

Figure 2-1 shows the basic structure of the seismic hazard model logic tree for the three source types that account for seismicity in the Columbia Basin: the Yakima Folds, Columbia River Basalt source, and basement sources. To define the geometry of seismic sources within the basalts, we first consider the possibility that faults associated with folds of the Yakima Fold Belt are potential seismic sources. Figures 3-8 and 3-9 shows the location of the major mapped folds in the vicinity of the site together with the spatial distribution of shallow and deep earthquakes, respectively. The lines on the figure denote the locations at which inferred south-dipping reverse faults underlying the folds would intersect the ground surface. These generally lie at the base of the steeply dipping north limb of the folds. As indicated on the figures, the seismicity is generally scattered and does not delineate any of the folds. The largest concentration of seismicity is that located just north of Saddle Mountains and is

confined primarily to focal depths shallower than 5 km. These events are not located where one would expect seismicity associated with reverse faults underlying the fold.

The general lack of spatial association of seismicity with inferred faults underlying the folds may be due to a low rate of seismic activity generated by the folds relative to the duration of the observed record, or the folds themselves may not in fact contain seismogenic faults. Because it is clear from the seismicity record that earthquakes occur within the Columbia River Basalt Group, we represent the basalts as a seismic source in all cases (see Section 3.2.3). We also consider the possibility that individual folds of the Yakima Fold Belt are seismogenic—meaning that they localize seismicity over and above that occurring within the basalts. This probability, which is termed the *probability of activity* in this study, varies with each fold. If a fold is active, then it may generate earthquakes along its length over and above those occurring randomly in the basalts. If a fold is not active, then earthquakes can still occur in proximity to the fold, but the presence of the fold has no effect on the spatial distribution of earthquakes.

Seismic source logic trees were developed for each of the folds because each fold is assumed to be potentially underlain by a fault, whether or not a fault is mapped at the surface. The characteristics of the fault (e.g., total slip and geometry) are specific to each fold and can be derived from the fold structure. Figure 3-10 shows the logic tree for the fold nearest the site, the Umtanum Ridge-Gable Mountain fold system. Similar logic trees were developed for the other folds within the vicinity of the Hanford Site. Tables 3-1 through 3-4 summarize the source parameters used to characterize the fault associated with each fold. For clarification, the Horse Heaven Hills is divided into two parts: the "Horse Heaven Hills NE" part that strikes to the northeast; and the "Horse Heaven Hills NW" part that strikes to the northwest.

Fold geometry/structural data for the Umtanum anticline (one of the largest, most well-exposed Yakima Folds) are considered representative of the style and amount of compressive deformation in the Yakima Fold Belt. Detailed analysis of this structure by Price and Watkinson (1989) indicates two large-scale mechanisms of shortening: initial shortening by

asymmetric buckling, followed by imbrication of the fold structure by late-stage "break-through faulting" on two discrete faults. Shortening represented by the earlier folding phase calculated by line-length balancing is about 0.75 km, or about 20 percent (according to Figure 17 in Price and Watkinson, 1989). Shortening by late-stage faulting is an additional 1.1 km (according to Figure 16 in Price and Watkinson, 1989). More importantly, depth-to-detachment calculations indicate the detachment accommodating horizontal shortening represented by the Umtanum anticline lies at 1.2 to 1.3 km. This is consistent with the results of previous studies that suggest the detachments lie within or directly beneath the Columbia River basalts (i.e., approximately 1.5 - 5 km) (Glover and others, 1985; Catchings and Mooney, 1988). These shallow depths to an underlying detachment imply that the faults associated with the folds likewise have a very limited downdip extent within the crust, thus constraining their seismogenic potential.

In the following sections we characterize those parameters that are used to define the seismic hazard potential of the Yakima Folds. These parameters are summarized in Tables 3-1 through 3-4: probability of activity, the degree of coupling between the CRBG and the crystalline basement, the segmentation and rupture length of faults underlying the folds, style of deformation, dip of the faults, seismogenic crustal thickness, maximum magnitudes, and slip rate.

3.2.2.1 **Probability of Activity.** The first assessment in the logic tree for the Yakima Fold sources is the likelihood that the structure is seismogenic, or active, within the present tectonic regime and will, therefore, localize seismicity above the levels occurring randomly within the region. The assessment of activity is made independently of whether or not the fault is assumed to be coupled (see Section 3.2.2.2). In the same manner as the assessment of activity is made for faults, the assessment of the activity of the Yakima Folds is based on such factors as: association with historical seismicity, evidence for late Quaternary fault displacements, geomorphic evidence for geologically recent deformation, association with neighboring structures showing evidence for Quaternary activity, pre-Quaternary history of deformation, and orientation relative to the present stress field. Evidence for Quaternary fault

displacements or geologically recent deformation are considered the strongest indicators of activity. A spatial association with seismicity such that there is a clear delineation along the fold is also an indicator of activity. However, the absence of a spatial seismicity pattern provides only a weak argument against activity, given the generally low rates of crustal deformation and the short time period of recording.

Table 3-1 lists the assigned probabilities of activity for each of the folds. The probability of activity is assessed to be relatively high for Toppenish Ridge (0.6), which exhibits geomorphic evidence for young deformation and stratigraphic evidence for late Quaternary displacement (Campbell and Bentley, 1981). On the other extreme, the Hog Ranch-Naneum Ridge anticline is assigned a low probability of activity of 0.1, reflecting a lack of any definitive evidence for Quaternary deformation and a highly uncertain relationship with the development of the Yakima Fold Belt and with the present stress field. Saddle Mountains is assigned a probability of activity of 0.5, reflecting possible geomorphic evidence for Quaternary faulting on Smyrna Bench (West and Shaffer, 1989), although such evidence is not present at other locations along the fold. There is a significant concentration of seismicity in the area of Saddle Mountains, but its spatial distribution does not delineate the presence of a fault beneath the Saddle Mountains fold (Geomatrix, 1990).

For the bulk of the Yakima Folds, the assessment of the probability of activity is relatively low (0.25), reflecting a lack of evidence for geologically-young displacement such as that observed at Toppenish Ridge and no clear spatial pattern in the seismicity. The principal reason for assigning a finite probability of activity to the folds is the evidence for post-10.5 million-year-old fold deformation and an inferred favorable orientation of the folds relative to the present stress regime.

In the hazard analysis, the CRBG and crystalline basement sources are assumed to exist in all cases. In the case where a fold source is assumed to be active (i.e., along the "yes" branch of the logic tree shown on Figure 3-10), the fold is further characterized by its coupling, geometry, etc., and it is added to the basalt and basement sources. In the case where a fold

is not active, the basalt and basement sources are all that are assumed to be active in the vicinity of the fold.

3.2.2.2 Coupling. The next assessment in the logic tree for the Yakima Fold sources is the degree to which there is a local mechanical linkage between the deformation within the CRBG in the upper 1.5 to 5.0 km of the crust and the deformation in the basement rocks beneath the sub-basalt sediments provided by a through-going fault. Specifically, a *coupled* source consists of a fault underlying a fold that extends from the surface or near-surface within the basalts down into basement through the entire width of the seismogenic crust. In contrast, the "uncoupled" scenario assumes that there is a mechanical discontinuity between the faults within the CRBG and faults within the basement. This model implies that a detachment zone or decollement exists between the basalt and basement rocks. In this model, the detachment zone may be either a floor thrust system (i.e., a subhorizontal zone into which listric thrust faults coalesce) located within or at the base of the basalts, or distributed aseismic deformation of the sub-basalt sediments. These sediments are characterized by low levels of seismicity and, presumably, lower strength than the overlying basalts or underlying crystalline rocks. In addition, the spatial distributions of shallow and deep seismicity show different patterns (DOE, 1988; Johnson, 1989b). Figure 3-11 shows the spatial pattern of well located (standard errors of location estimated to be less than or equal to 1.0) shallow (depth $\leq$ 5 km) and deep (depth $>$ 5 km) earthquakes. With the exception of the concentration of seismicity north of the Columbia river in the vicinity of Saddle Mountains (see Figure 3-8), the shallow and deep earthquakes display different spatial distributions.

The probability that individual folds are coupled has been assessed for groups of folds. This is because coupling is assessed primarily on the basis of structural features that are commonly shared among several folds. These include expression of Quaternary tectonic activity; structural style (fold trend, length and amplitude); degree of secondary deformation (e.g., normal faults on Saddle Mountains); paleoseismological evidence for slip per event (e.g., Toppenish Ridge); association with neighboring folds (e.g., Horse Heaven Hills NE with Toppenish Ridge); and location with respect to prominent basement structures (e.g., Horse

Heaven Hills NW with the southeast extension of the White River-Naches fault, Saddle Mountains with abrupt shallowing of crystalline basement). Table 3-1 lists the assigned probabilities of coupling for each fold.

The fold groups are the "Toppenish Group" - Toppenish Ridge, Columbia Hills (not included in the analysis), and Horse Heaven Hills NE; the "RAW Group" - the Rattlesnake-Wallula trend and Horse Heaven Hills NW; the "Central Group" - Umtanum Ridge-Gable Mountain, Manastash Ridge, Yakima Ridge, and Rattlesnake Hills; and three separate folds, Frenchman Hills, Saddle Mountain, and Hog Ranch-Naneum Ridge.

For Toppenish Ridge and related structures (i.e., Horse Heaven Hills NE, Columbia Hills) the probability of coupling is assessed to be 0.7, which is relatively high. The basis for this assessment is the abundant evidence for young displacements and stratigraphic evidence for individual, presumably coseismic, displacements along Toppenish Ridge (Campbell and Bentley, 1981). The amount of individual offsets, if coseismic, is suggestive of relatively large events. Large events would, in turn, imply significant downdip extent for the associated faults. The Toppenish Ridge area may be more active than the rest of the Columbia Basin and Yakima Fold Belt because it occupies a structural setting that appears to be more influenced by the present Cascade Arc. The Simco Volcanic field, an example of backarc volcanism, has been more prominent in a zone bounded on the north by Toppenish Ridge and on the south by the Columbia River. This field is expressed at the surface by a large number of volcanic cones and in the subsurface by an intrusion that has domed up the volcanic field. The domal uplift is centered on the Horse Heaven Hills. Toppenish Ridge also trends east-west and is on trend with an alignment in the Cascade Range that includes Mt. Adams and Mt. St. Helens.

For Saddle Mountains, the evidence of coupling is somewhat less conclusive, but normal faults have been mapped on Smyrna Bench that may represent upper plate deformation above a primary reverse fault, and the probability of coupling is assessed at 0.6. Earthquake swarm activity in the vicinity of Saddle Mountains does extend somewhat deeper than in other areas

(Figure 3-11), but these events do not delineate a reverse fault underlying the fold (Geomatrix, 1990).

For the Umtanum Ridge-Gable Mountain group, the probability is assessed to be 0.15 on the basis of a lack of clear evidence for large displacement events due to reverse faulting, changes in fold geometry along strike, and the other lines of evidence for shallow depth limit to faulting discussed above. For Frenchman Hills the potential for coupling is also assessed to be 0.15 because of the similarities of this fold to the other members of the central fold group.

The style of faulting assessed for the Yakima Fold sources is reverse faulting for all cases with the exception of RAW. For RAW and those structures closely associated with it, we consider the possibility of strike-slip faulting, although we favor reverse faulting for the observed deformation on the basis of the evidence presented in the WNP-2 FSAR (Washington Public Power Supply System, 1981; Power and others, 1981). Such evidence includes a consistent sense of structural relief across RAW, consistent direction of net tectonic transport across the trend, anticlinal axes that essentially follow a single trend rather than an en echelon pattern or rotated axes as expected for strike-slip, and a lack of kinematic indicators for young strike-slip displacement. Further evidence against strike-slip is the apparent absence of cumulative lateral offset of a north-south gravity anomaly across the projection of RAW (Washington Public Power Supply System, 1981; anomaly shown on Figure 3-21). Evidence for a strike-slip origin for RAW presented in the Power and others (1981) is limited to: horizontal and sub-horizontal striae developed on Quaternary fault surfaces within the Wallula fault zone to the southeast, and the orientation of RAW relative to the inferred north-south orientation of the maximum horizontal compressive stress direction. In addition, Mann and Meyer (1993) argue for a strike-slip origin for RAW on the basis of association with strike-slip faults to the southeast along the Olympia-Wallowa Lineament (OWL), analogy of the structural style of the Wallula fault zone to a strike-slip extensional duplex, possible evidence for dextral offset across RAW of stream channels near Wallula Gap, and a change in structural style along strike from predominantly normal slip at Wallula fault zone to reverse slip along RAW to the northwest.

On the basis of these arguments, the assessment of coupling for RAW includes both strike-slip and reverse coupled faults. The probability of a coupled reverse fault was assessed to be 0.3 and that of a coupled strike-slip fault was assessed to be 0.05. The probability the structure contains uncoupled reverse faults is thus 0.65.

3.2.2.3 Segmentation/Rupture Length. The next assessments in the logic tree (Figure 3-10) are the assessment of whether or not the fold and associated fault is segmented, and the assessment of maximum rupture lengths assigned to the fault. Segmentation is one of the approaches that assist in the estimation of maximum magnitudes in the following way. As shown in Figure 3-10, the assessment of segmentation is made assuming both that the fold is coupled and is not coupled. The maximum magnitude approaches will differ for these two cases. In the case where the fold is assessed to be both coupled and segmented (i.e., along the "yes" coupled and "yes" segmented branches), each segment is characterized separately by its geometry, maximum magnitude, and recurrence rates. As will be discussed in Section 3.2.2.6, the length of the segment and its downdip width will provide a fundamental constraint on maximum magnitude for the segment. In the case where the fold is coupled but not segmented, the entire fold is characterized as a whole and maximum magnitude estimates do not rely on segment lengths. In the case where the fold is assessed to not be coupled (i.e., to not extend into the crystalline basement) and to be segmented, each segment is again characterized by its own geometry, maximum magnitude, and recurrence rate. However, in this model the fault is assumed to have a limited downdip extent due to the limited basalt thickness. Therefore, the downdip width, rather than the segment length, provides the fundamental constraint on maximum magnitude estimates. Finally, in the case where the fold is assessed to not be coupled and to not be segmented, the entire fold is characterized as a whole and the maximum magnitude method is again reliant on the downdip width of the fault.

Detailed assessments of fold segmentation were presented for the Umtanum Ridge-Gable Mountain and the Rattlesnake-Wallula fold systems in Power and others (1981) and those assessments were adopted for this study. Since that time only one other fold, the Saddle Mountains anticline, has been analyzed for fold segmentation (Reidel, 1984) and his

GEOMATRIX

assessments of segment lengths were used in this study. Although Reidel and others (1989, and in press) provide arguments for segmentation of the Yakima Folds, the other folds have not been studied in detail for segmentation. These sites are farther from the Hanford site and are less important to the seismic hazard. Therefore, the other folds are treated as not segmented in this analysis.

As summarized in the WNP-2 FSAR, the Umtanum Ridge-Gable Mountain fold system is marked by changes in fold amplitude, fold geometry, and vergence along strike, suggesting that an underlying associated fault zone must also be segmented into separate sources. From this evidence, we conclude that it is somewhat more likely (0.6) that the fault is segmented along strike than unsegmented (0.4). If the fold is interpreted to be segmented and coupled, then each of the five segments is treated as an independent seismic source and the maximum magnitude is constrained by assuming that the entire length of the segment will rupture in a maximum event (the lengths of segments are given in Table 3-2). Similar arguments apply to the assessment of segmentation of the Saddle Mountains anticline, which is also given a likelihood of 0.6 of being segmented and 0.4 of being unsegmented. If the fault is assumed to be unsegmented and coupled, then the length of ruptures are estimated to be either the entire length of the fold or one-half the entire length. These rupture length estimates together with estimates of downdip width provide the constraints on maximum magnitudes for this case (Section 3.2.2.6).

In the case of the Rattlesnake-Wallula fold system (RAW), the variation along trend of the surface manifestation of deformation is quite pronounced, ranging from the Rattlesnake Mountain segment, to the "brachy-anticline" segment marked by doubly-plunging anticlines, to the Wallula Gap fault segment. This change in character along strike makes it more likely (0.7) that the fold system is segmented than unsegmented (0.3). If the source is segmented, then three distinct segments are considered (Table 3-2).

3.2.2.4 **Fault Dip and Geometry**. Fault dip defines the average dip of faults at depth within the seismogenic crust. The dip of faults beneath the anticlines in the Yakima Fold Belt are

generally not well constrained. Limited exposures of some of the faults associated with the Yakima Folds, such as the Frenchman Hills watergap and the Columbia Hills near Rock Creek (Grolier and Bingham, 1971; Swanson and others as cited in Reidel and others, 1989); interpretations of borehole stratigraphy (Reidel and others, 1989); and geometry of secondary faults in the Umtanum anticline (Price and Watkinson, 1989) suggest faults increase in dip with depth to about 45° to 70°. The dips of seismogenic reverse faults worldwide, derived from the pattern of aftershocks and from focal mechanisms, indicate that dips of between 30° to 60° are typical (Wells and Coppersmith, 1991; Coppersmith, 1991). Based on these observations, we allow for average dips of 30°, 45°, and 60°. Equal weight is given to each alternative for folds where there are no data. For structures where a published or otherwise recorded assessment of the dip has been made, the assigned weights reflect these available data. Data constraining fault dips are available for the Saddle Mountains, Umtanum Ridge, Frenchman Hills, Horse Heaven Hills, and folds associated with RAW. The assigned distributions of dip are assumed to apply to all segments for those folds that are potentially segmented.

The faults are assumed to have a generally southward dip and to daylight at the base of the northern limb of the folds at the locations shown on Figures 3-8 and 3-9.

3.2.2.5 Seismogenic Crustal Thickness and Downdip Width. The downdip width of faults within the seismogenic crust is an important parameter in assessing maximum magnitudes and earthquake recurrence rates (e.g., Coppersmith, 1991) and is determined by the seismogenic crustal thickness and the fault dip. The average crustal thickness is determined for each of the Yakima Fold sources using the crustal model presented above in Section 3.2.1 and on Figure 3-6, and is conditional on whether or not the fold is assumed to be coupled. For the coupled case in which faults at the surface are assumed to persist downdip into the crystalline basement, the crustal thickness is taken as the entire thickness of the seismogenic crust. The seismogenic crustal thickness is defined from the ground surface to the 95% cutoff in seismicity, a depth of about 21 km in the Columbia Basin. For the uncoupled case, where the folds and related faults are confined to the CRBG (layer A), the crustal thickness used to

calculate fault width is the average thickness of the basalts that lies beneath the mapped fold being characterized.

3.2.2.6 Maximum Magnitude. Different methods are used to assess maximum magnitudes for each fold depending on whether or not it is assumed to be coupled and whether or not it is assumed to be segmented. An example of this dependency is illustrated for the Umtanum Ridge-Gable Mountain fold system on Figure 3-10. In the case where a fold is assessed to be both coupled and segmented, a rupture area is estimated based on the product of the length of the segment and the downdip width. This rupture area, A, is empirically correlated with moment magnitude M by the relationship $M = Log_{10} A + 4.02$ (Coppersmith, 1991; Wells and Coppersmith, in press). Use of the relationship between rupture area and magnitude was preferred to the use of rupture-length magnitude relationships because it utilizes additional information in the assessment of the second dimension of rupture.

In the case where a fold is assessed to be coupled, but not segmented, the length of segments cannot be used to estimate maximum magnitudes. As discussed in Section 3.2.2.3, published segmentation characteristics are only available for Saddle Mountains (Reidel, 1984), Umtanum Ridge-Gable Mountain, and RAW (Power and others, 1981). Hence, in the cases where these three folds are assumed to not be segmented (i.e., along the "no" segmented branch of the logic tree) and in the case of all other folds for the coupled case, the lengths of segments are not used for estimating maximum magnitude. Instead, three alternative methods are used: (1) the total length of the fault is assumed to rupture and, together with the downdip width, defines a rupture area that is related to magnitude; (2) one-half the total length is assumed to rupture and a rupture area is derived and related to magnitude; or (3) the downdip width is directly correlated with earthquake magnitude using the empirical relationship $M = 4.18 + 2.11 * log$(rupture width in km), which was developed using worldwide rupture data (Wells and Coppersmith, in press). The total length method is given least weight (0.1) because rupture of the total length of a fault zone is extremely rare (e.g., Slemmons, 1982; Schwartz, 1988; Coppersmith, 1991); the half-length approach is given more weight (0.4) because fault zones typically rupture less than half their total length in individual events (e.g.,

Slemmons, 1982); and the fault width approach is given the highest weight (0.5) because it bypasses the rupture length issue altogether, which is probably appropriate for the unsegmented case.

In the cases where the folds are assumed to not be coupled, the assessment of maximum magnitude is made using two approaches regardless of whether or not the folds are assessed to be segmented. In the uncoupled model, the downdip dimensions of faults are restricted to the basalt section of the crust, which is less than 5 km thick. This fundamental constraint on downdip width is judged to be the most important constraint on maximum magnitude and the maximum magnitude methods are designed to directly take this into account. The two methods used are: an assessment of the average length to width aspect ratio for a given fault width; and a direct estimate of magnitude for a given width, using the width versus magnitude empirical relationship presented earlier. The aspect ratio data of Wells and Coppersmith (in press) for reverse faulting earthquakes indicate that length to width aspect ratios are less than 2.5 for rupture widths of about 5 to 10 kilometers. For this analysis, we adopt the aspect ratio of 2.5, use this to estimate the length associated with a given fault width, derive the associated rupture area, and calculate a magnitude for this rupture area using the empirical relationship discussed earlier. The aspect-ratio maximum magnitude method and the width method are both believed to be appropriate magnitude estimation methods for the uncoupled case and they are assigned equal weight.

The resulting maximum magnitude assessments incorporate the uncertainties in coupling, segmentation, fold geometries, and maximum magnitude methods. Discrete magnitude values are listed in Tables 3-2 and 3-3.

3.2.2.7 Slip Rate. Fault slip rate provides a fundamental constraint on the average rate of seismic moment release and earthquake recurrence. Slip rate holds the advantage of spanning a longer time period than the historical record, although there are uncertainties in measuring displacement and determining the ages of geologic units displaced. In the case of the Yakima Folds, additional uncertainty exists because the fold geometry and the rate of fold growth is

being used to infer the slip rate on the fault underlying the fold. Using techniques that have become common in seismic hazard analysis (e.g., Schwartz, 1988; Coppersmith, 1991), we assess slip rates for each of the folds and associated faults, calculate seismic moment rates based on the rates and geometries of the faults, and develop a recurrence relationship for all magnitudes up to the maximum using a magnitude distribution model. It is assumed that the slip rate is an indicator of the average rate of seismic moment release on a fault, acknowledging that some component of the slip rate may have occurred aseismically.

Because our analysis is intended to assess the potential for future earthquake activity, we typically are most interested in the slip rates during a geologically-recent period (e.g., late Quaternary - Holocene). If slip rates are averaged over a time period that is too long, changes in rates resulting from temporal clustering of slip events (Sharp, 1980; Wallace, 1987; Swan, 1988) or regional changes in tectonics are averaged out. In the case of the Yakima Folds, the Quaternary record is usually absent and we typically do not have information that constrains the slip rates or fold development since the deposition of the Elephant Mountain Member 10.5 million years ago (Ma) or the Ringold Formation deposited 3.5 to 8.0 Ma. Although this is a long period, the time history of fold development suggests that no major changes in tectonics have occurred in the past 10 million years (Reidel, 1984; Reidel and others, 1989; Reidel and others, in press).

The basalt stratigraphy of the Columbia River Basalt Group stratigraphy and the timing and amount of deformation of these units provide a basis for estimating the average rate of deformation during and subsequent to the deposition of the basalt flows (Reidel, 1984; Reidel and others, 1989). The detailed study of the Saddle Mountains fold, one of the most pronounced folds in the Yakima Fold Belt (see DOE, 1988), provides valuable information regarding the time history of development of the Yakima Fold Belt (Reidel, 1984). Reidel concluded that the period from 17 to about 10.5 million years ago was a distinctly more active period of fold deformation than the period from 10.5 Ma to the present. Specifically, Reidel found that the rate of fold development during 17-10.5 Ma accounts for approximately 80% of the total strain, while the period from 10.5 Ma to the present accounts for the remaining

20%. This temporal concentration of activity during the middle Miocene, followed by a waning of activity in the upper Miocene, is consistent with most published tectonic models for the Yakima Fold Belt. Reidel also found that the rate of fold development for the Saddle Mountains has remained relatively constant at about 0.04 mm/yr since 10.5 Ma on the basis of a comparison of the structural relief on the Elephant Mountain Member (10.5 Ma) exposed in the Saddle Mountains, structural relief on the Ringold Formation (5.0 to 3.4 Ma), and the present structural relief of the Saddle Mountains. Furthermore, studies conducted on other folds in the Yakima Fold Belt (e.g., Hagood, 1986; Reidel and others, 1989, and in press) indicate similar rates and timing of CRBG deformation suggesting contemporaneous development of the entire fold belt.

Slip rates for the folds are estimated on a fold-by-fold basis by dividing the amount of fold deformation by the time period over which it occurred. The age of geologic units having measured fold deformation is different for different folds. This calculation was made assuming that the fold deformation followed the time history of fold development interpreted for Saddle Mountains. Figure 3-12a shows the interpreted time history of deformation of Saddle Mountains (Reidel, 1984; Reidel and others, 1989). As discussed above, the interpreted history indicates a period of rapid fold development followed by a long period of steady deformation continuing to the present. For purposes of seismic hazard estimation, we are interested in the most recent deformation rate, represented by the post-10.5 Ma rate. Thus, it is important to determine the fraction of the total deformation that has occurred post 10.5 Ma. Figure 3-12b shows the relationship between the age of total deformation and the fraction of the total deformation that is assumed to have occurred post 10.5 Ma, interpreted from the deformation history shown on Figure 3-12a. This relationship was used to compute the slip rate for the fold in the following manner. If the age of the total deformation is assessed to be 10.5 Ma, then the total deformation is divided by 10.5 Ma to obtain the slip rate. If the age of the deformation is assessed to be older than 10.5 Ma, then the relationship shown on Figure 3-12b is used to estimate the fraction of the total deformation that has occurred post 10.5 Ma, and this amount of deformation is divided by 10.5 Ma to obtain the slip rate.

As shown on Figure 3-10, uncertainty in estimating the slip rate for the folds is modeled by addressing separately the uncertainty in the time period over which the total deformation occurred (the "age" node of the logic tree) and the uncertainty in method used to obtain an estimate of the total deformation (the "technique" node of the logic tree). The age node deals with the time period over which the observed slip is assumed to have occurred and is based on assessments of the age of the basalt flows that are represented in the uplift. For some of the folds, the total amount of deformation can be assigned to a basalt flow of a particular age. In other cases it is possible to estimate the amount of fold deformation, but the age of the basalt unit involved in the total deformation cannot be assigned with certainty. For example, in the Grand Ronde Basalt over 100 basalt flows were erupted over a 1-2 million-year period, yet the age dates for the flows have an error of ±0.5 to 1.0 million years (Reidel and others, 1989b). In these cases alternative ages are assigned representing the range of ages for the basalt flows that are deformed.

Slip rates are assessed for each fault using two types of displacement data associated with the fold structures: a vertical displacement measured as structural relief, and a horizontal displacement measured in the forelimb region of the fold. These data are used to derive fault slip estimates using the simple single-fault evolutionary model for the development of the folds shown on Figure 3-13. According to this model, the Yakima Folds develop initially as fault-propagation folds. During this stage of development, the observed structural relief is produced that represents vertical tectonic displacement resulting entirely from slip on the fault ramp underlying the fold structure. It is assumed that slip is conserved across the flat/ramp transition at the base of the ramp and onto the detachment beneath and behind of the fold. Structural relief, and hence ramp slip, is therefore a measure of the horizontal component of slip (i.e., shortening) required to produce the observed structural relief. Some of the folds (e.g., Umtanum Ridge-Gable Mountain and Saddle Mountains) have further evolved into a fault-bend fold stage by propagation of the fault ramp onto a horizontal upper detachment or flat. Slip on the upper ramp does not contribute to structural relief on the fold because it occurs after the ramp has developed assuming that the folds are underlain by a single ramp. Fault slip or total shortening for these folds is therefore simply the sum of the shortening

GEOMATRIX

calculated from structural relief and the horizontal displacement measured on the upper flat (Reidel, 1984).

Interpretation of this style of faulting for the Yakima Folds is consistent with the structural analysis of the Umtanum Ridge anticline (Price and Watkinson, 1989) and field observations of other folds in the Columbia Plateau (Reidel, 1984; pers. comm.). The displacement and age data for each of the fold structures and the fault slip derived from these data are listed in Table 3-4. The vertical displacement is the total structural relief measured directly from the appropriate 1:24,000-scale geologic map using the difference in elevation of the youngest basalt flow exposed on the ridge crest and in outcrop at the base of the fold (in some cases subsurface well data were used to constrain the lower elevation). The horizontal displacement used for those folds that have developed an upper flat is the maximum horizontal offset assigned to the structure on the basis of observations in field at the few locations where erosion has exposed the upper flat located forward of the fault ramp (Reidel and others, in press).

It is uncertain whether it is appropriate to include the estimation of horizontal slip in estimating total fault slip for both the structure as a whole and for distribution of the horizontal slip along strike; the availability and quality of such data vary with the fold. Therefore, for each source an assessment is made of whether the total estimated fault slip is to be derived from the vertical strain data only, or from a combination of the vertical and horizontal strain data. This assessment is indicated as slip rate "technique" on Figure 3-10. For example, in the segmented case of the Umtanum Ridge-Gable Mountain structure, observations indicate the ramp has broken through to an upper flat at the west end of the eastern segment, near Priest Rapids Dam (Price and Watkinson, 1989). We therefore assign a likelihood of 0.7 that both the vertical and horizontal strains represent the total slip or shortening for that segment (the Central segment). The probability decreases for segments farther away from the Priest Rapids Dam area to reflect both the uncertainty and the decrease in observed deformation. Lesser preference (0.3) is given to the use of the vertical strain only. In the unsegmented case, the averaged slip rate is used for the fold as a whole.

3.2.2.8 Magnitude Distribution and _b_-Value. The magnitude distribution model specifies the relative frequency of earthquakes of various magnitudes and, as discussed in Section 2, we allow for two alternative models when using slip rates to constrain recurrence rates: the characteristic and exponential models. The assessment of the relative preference for these models varies with whether the folds are assumed to be coupled or uncoupled (Figure 3-10). In the coupled case, the folds are modeled as reverse faults occurring from the surface throughout the depth of the seismogenic crust. The characteristic earthquake model was developed to specifically account for the recurrence behavior of individual _faults_, rather than the behavior of _regions_ (Youngs and Coppersmith, 1985a, b; Coppersmith, 1991). Therefore, because we are characterizing the behavior of individual faults in the coupled case, we assign a considerably higher weight (0.8) to the characteristic earthquake model than the exponential model (0.2). In the uncoupled case, we are also characterizing faults, but their dimensions are very limited and there may be multiple faults in the folds. The worldwide geologic observations that give support to the characteristic earthquake model (e.g., Schwartz, 1988) have not yet been confirmed on small faults with limited earthquake potential. In light of this uncertainty, we assign equal weights to the characteristic and exponential magnitude distribution models for the uncoupled case.

The slope of the recurrence curve, or the _b_-value, specifies the exponential portion of the recurrence relationship for each fault. The earthquakes that can be spatially associated with the folds are too few to obtain a reliable estimate of the _b_-value, requiring use of regional estimates. The shallow seismicity is dominated by the abundant occurrences of small-magnitude events within the basalts away from the folds and exhibits a steep _b_-value typical of swarm activity, while the deeper seismicity exhibits a _b_-value more typical of earthquakes associated with crustal faulting. We assume that seismicity occurring on faults associated with the folds should behave similarly to seismicity occurring in the basement because both are assumed to occur on crustal faults of significant dimension. A maximum likelihood fit to the data with focal depths greater than 5 km yields a _b_-value of 0.99 ($\pm$0.11) and this value and range is used in the analysis to characterize seismicity occurring on the fold sources.

3.2.2.9 <u>Comparison of Observed and Predicted Recurrence Rates for Folds</u>. Figure 3-14 compares the observed earthquake frequencies within the Yakima Fold Belt to those predicted using the seismic source characterization assuming the folds are coupled. Shown for the observed seismicity are the rates for all independent events and for events with focal depths greater than 5 km. . The latter represents the seismicity rate without consideration of the abundant, very shallow seismicity. . This comparison indicates that the source parameters developed on the basis of estimated slip rates provide a reasonable estimate of the observed seismicity, neglecting the shallow basalt.

Figure 3-15 compares the observed earthquake frequencies within the Columbia River basalt (upper 5 km) with the predicted rates for the Yakima Fold Belt assuming that the folds are not coupled. The comparison indicates that the predicted rates for shallow activity occurring on the folds are somewhat lower than the observed rate of shallow basalt seismicity, which is to be expected because most of the shallow basalt seismicity occurs away from the folds (Figure 3-8).

3.2.3 Columbia River Basalt Group Source

The instrumental seismicity record shows clear evidence of small to moderate magnitude earthquakes occurring in the Columbia River basalts. Most of these events are not spatially associated with the Yakima Folds axes or orientation, or other structures, thus making their causative structures difficult to interpret. In the hazard analysis, the Columbia River basalt source is assessed to be active (with probability of 1.0) and alternative models for its spatial distribution are included. This source is explicitly separate from the Yakima Fold sources, which have some probability of being active or inactive. The elements of the logic tree for this source (Figure 3-16) are the spatial distribution of seismicity, maximum magnitude, earthquake recurrence, and magnitude distribution. These are discussed below.

3.2.3.1 <u>Spatial Distribution</u>. Instrumental epicenters of earthquakes occurring within the Columbia River basalts (upper 5 kilometers) do not show clear associations with the axes of major folds of the Yakima Fold Belt (Figure 3-8). We therefore consider the basalt source to

be an areal source zone, and we include three alternative models for its spatial distribution (Figure 3-16). In all cases we assume that the maximum width of the basaltic source is 5 km, reflecting the depth extent of shallow seismicity as well as the thickness of the Columbia River basalts within the central part of the Pasco Basin, as interpreted from deep boreholes and geophysical data (Glover and others, 1985). The spatial distribution of shallow seismicity is shown on Figures 3-17 and 3-18 in terms of the largest event within clusters and noncluster events, respectively. In the "uniform" model, the spatial distribution of basaltic seismicity is assumed to be random within the zone outlined on Figures 3-17 and 3-18. This model implies that, given a sufficiently long period of time, the spatial distribution of seismicity would eventually be uniform throughout the shallow crust. The "concentrated zone" model distinguishes an arcuate zone of more concentrated seismicity that roughly parallels the boundary of the Pasco Basin. This zone contains 80 percent of the seismicity within the uniform seismicity zone. The "smoothed observed" model assumes that the spatial distribution of future seismicity will mirror that of the observed seismicity. Figure 3-19 shows the distribution of distance from Sites A and C to cluster and noncluster earthquakes. As can be seen on the figure, these two distributions are generally similar in shape, indicating that non-cluster earthquakes occur more frequently in the vicinity of clusters than elsewhere. The smoothed observed model thus identifies source zones that generally encircle the zones of seismicity that have been observed within the instrumental seismicity record, such as those observed at Wooded Island and between Saddle Mountains and Frenchman Hills.

The concentrated zone model is preferred slightly over the "uniform" because it acknowledges the general differences in the spatial distribution of seismicity, yet it does not strongly rely on the rather short 20-year seismicity record to completely constrain source locations (the smoothed observed model). The smoothed observed distribution is given the lowest weight because it assumes the very restricted viewpoint of complete spatial stationarity.

Note that the subsequent assessments of maximum magnitude and recurrence-related parameters are the same regardless of the spatial distribution model.

3.2.3.2 <u>Maximum Magnitude</u>. The maximum magnitude for the shallow basaltic seismic source is assessed based on a consideration of the historical seismicity and maximum dimensions of rupture on faults within the basalts. The largest earthquake that occurred within the Columbia River basalts during the historical record was a magnitude 4.3 event in 1973 near Royal Slope. This magnitude provides the minimum size of the maximum event, but because the historical record is relatively short, we do not consider the magnitude 4.3 event to provide a strong constraint on estimates of maximum magnitude.

The largest earthquake recorded within the Columbia Plateau was the 1936 Milton-Freewater earthquake. The magnitude of this event has been assessed as M_S 5.7 (Washington Public Power Supply System, 1985). Given that crystalline basement is located at a depth of 3 to 4 km in the epicentral region, it is very unlikely that this event occurred within the CRBG and it was not considered in assessing the CRBG maximum magnitude.

As discussed previously, the CRBG source is assumed to be distinctly separate from the Yakima Fold sources. Hence, faults giving rise to seismicity within the basalts are not those that are modeled as the causative structures associated with folding. Instead, the earthquake process within the basalt source occurs without the development of significant amounts of cumulative, observable folding or faulting. This process may be one of small-scale fault displacements, perhaps with faulting occurring within one or more basalt flows, separated by sedimentary interbeds that are not sufficiently competent to behave in a brittle manner. The maximum scale of fault surfaces involved in this process would be on the order of a few kilometers and displacements on the order of centimeters. Based on this model for seismogenisis within the basalts, a maximum magnitude distribution is developed that ranges from 4½ to 5½, as shown on Figure 3-16.

3.2.3.3 <u>Recurrence Parameters</u>. In all three alternatives for the spatial distribution of seismic sources, the seismic source is an areal source zone and not a fault. We therefore consider the truncated exponential magnitude distribution model to be appropriate to describe the distribution of various magnitudes in the earthquake recurrence relationship. Both the

number of events having magnitude greater than M 5 and the b-values given in the logic tree (Figure 3-16) are derived directly from the instrumental seismicity data using the maximum likelihood formulation of Weichert (1980). The distributions on parameters were calculated by assigning a range of seismicity rates and b-values and computing the relative likelihood of observing the historical seismicity given the specified recurrence parameters. The weights shown on the logic tree reflect values at the midpoint of the distribution for cumulative frequency. As discussed above in Section 3.1.5, the correlation between $N(m^0)$ and b were accounted for in developing the parameter distributions and the weights on b change as a function of $N(m^0)$.

3.2.4 Basement Sources

Figure 3-20 presents the seismic source logic tree for the deep seismic sources within crystalline basement. The basement seismic sources in the site vicinity are those that exist within the crystalline crust beneath the relatively low-velocity sub-basalt sediments (Figures 3-6 and 3-7). The occurrence of seismicity within this zone confirms that it is seismogenic, although the causative structures giving rise to earthquakes in the basement are not known. The first node of the basement source logic tree (Figure 3-20) represents alternative models to explain the basement seismic source. These models are herein referred to as the failed rift model, the basement block model and the random model, and the seismic source characteristics for each of these models are discussed below. The failed rift model and the basement block model represent interpretations of the crustal structure of the Columbia Plateau in the vicinity of the Yakima Folds. Although they may represent reasonable interpretations of the evolution of the crust, they do not appear to be represented in the present-day pattern of seismicity, and there are no compelling arguments for their adoption as the explanation of present day seismicity. Therefore, these two models are assigned a relatively low weight (0.1 each) that they represent models explaining the occurrence of present day seismicity. The remaining weight is assigned to the random model.

3.2.4.1 Failed Rift Model. In the failed rift model, we consider the tectonic model proposed by Catchings and Mooney (1988), whereby the basement crustal structure of the region is

interpreted to be a failed intra-continental rift that exists beneath the Columbia River basalts and the sub-basalt sediments. This interpretation is based on a crustal cross-sectional velocity model developed along a single seismic refraction line through the southern Columbia Basin and analogies to other intra-continental rifts. Ludwin and others (1992) superimpose earthquake hypocenters along the Catchings and Mooney transect (see Figure 3-7) and suggest that the seismicity data support the velocity cross-section, with the earthquakes occurring in the basalts and in the underlying basement.

The viability of the reactivated rift model depends to a large extent on the orientation of the rift. Because only a single seismic refraction line crosses the inferred rift structure, its orientation in the present stress field is not known. The orientation of the graben structures to the north of the Columbia Plateau (which are likely to be related to the inferred rift in some manner) have variable strikes ranging from northwest to north (Tabor and others, 1984). Examination of rift systems worldwide shows that they are typically composed of one or more grabens and the strikes of individual grabens can be quite variable (Cloos, 1939, as cited in Laubscher, 1981). Therefore, the orientation of the grabens north of the Columbia Plateau does not necessarily constrain the strike of the rift beneath the Plateau. Figure 3-21 superimposes the location of the refraction profile (Figure 3-7) on the gravity contours from Weston Geophysical (1981). The heavy dashed lines in the figure indicate the inferred northwest-southeast orientation of the rift along an elongation in the gravity contours and an elongation in the contours of subbasalt sediment thickness (Figure 3-22). This orientation is consistent with rift reactivation by strike-slip faulting in a north-south compressive stress regime. If the orientation of the hypothesized rift is north-south, along the general grain of the gravity contours shown on Figure 2-21, then reactivation of the system is much less likely for the following reasons. In-situ stress measurements indicate that the maximum principal stress direction is north-south and the minimum principal stress direction is vertical (Kim and others, 1986). These results, together with the focal mechanism data for the deeper events are incompatible with reactivation of a north-south rift by east-west extension.

The spatial distribution of deep seismicity (Figure 3-23) does not clearly define a northwest-trending basement structure and indicates that there is not an elevated rate of seismicity within the boundary of the inferred rift. More importantly, the available focal mechanism for deep earthquakes, summarized in DOE (1988) all show reverse faulting on generally east-west fault planes, rather than strike slip motion. The uncertainty in rift orientation, the evidence for reverse rather than strike-slip faulting, and the lack of a signature in the seismicity are the primary reasons that the failed rift model is given low weight (0.1) relative to a more general model of random seismicity in the basement (0.8). In addition, it is supported by a continuous sediment package across the Cascade Range that demonstrates no geologic evidence for the western rift boundary (Reidel and others, in press).

In the case where the rift is assumed to be operative and the block and random basement models are not, the seismic sources considered are the rift zone itself and the adjacent basement (Figures 3-22 and 3-33).

3.2.4.1.1 Rift Zone Width. If the rift zone is considered to be reactivated within the present tectonic regime, two alternative models are considered for the rift zone geometry: a "narrow" model in which the boundaries of the source zone are specified by the inward-most faults of the rift zone, and a "wide" model in which the boundaries are specified by the limits of the region within which 50% necking of the crystalline crust has occurred. Both of the models reflect the observation of other reactivated rifts that show that the central parts of the rift have the most significant amounts of extension and are the most likely locations for reactivated normal faults (Ziegler and others, 1986). We slightly favor the narrow model because detailed studies of some failed rift systems, such as the Viking Graben in Norway, suggest that most of the seismicity occurs within the central or axial parts of the rift system (Ringdal and others, 1982). The extent of these zones is shown on Figure 3-23.

3.2.4.1.2 Crustal Thickness. The "crustal thickness" node of the logic tree (Figure 3-19) refers to the downdip thickness of the seismogenic crystalline basement, as defined by the distribution of hypocenters and the crustal model (Figure 3-7). As discussed previously in

Section 3.2.2.6, the base of the seismogenic crust in the region as defined by the 95% cut-off in seismicity, is approximately 21 km. This depth is assumed to be the bottom of the basement source. Interpretations of geophysical data (Rohay and others, 1985; Catchings and Mooney, 1988) suggest that the depth to the top of basement is about 8 to 9 km in the central Columbia Plateau. From these observations, we conclude that the approximate seismogenic thickness of the basement source is about 12 to 13 km, indicated as 12.5 km in the logic tree (Figure 3-20).

3.2.4.1.3 Maximum Magnitude. The assessment of the maximum magnitude for the rift zone is difficult because the zone is not exposed, and there have not been any large-magnitude events in the historical record. The largest historical earthquakes in the region have magnitude estimates based on intensity data. The estimated magnitudes for these events are about 5 to 5.5. The largest instrumental earthquake in the region is the M_s 5.7 1936 Milton-Freewater earthquake. Analysis of this event (Foxall and others, 1981) suggests that it was a strike-slip event and was most likely associated with the Hite fault zone to the southeast of the Columbia Plateau.

In the absence of large earthquakes in the historical record, maximum earthquake magnitudes for the rift model were estimated based on the expected dimensions of fault rupture. Lengths of rift-related faults are not known, but we can infer lengths based on the assessed downdip widths. The faults in other well-known rift zones are typically high-angle normal faults (Ziegler and others, 1986), and, assuming the faults are being reactivated in the present tectonic regime, they probably remain high-angle faults. Assuming that the downdip width of any particular fault of the zone is 12 to 13 km (the full width of the seismogenic crystalline crustal layer), we can use the expected aspect ratio to estimate the length of rupture and, thereby, the area of rupture. Compilations of observed rupture length to rupture width aspect ratios for historical ruptures (e.g., Purcaru and Berkhemer, 1982; Wells and Coppersmith, in press) indicate that aspect ratios vary as a function the sense of slip on the fault.

Strike-slip ruptures tend to have higher aspect ratios than dip-slip ruptures and generally range from 2:1 to 5:1, with some cases of aspect ratios of 10:1 or higher. Reverse-slip ruptures generally show aspect ratios of about 2:1 or less. Using this information and assuming a downdip rupture width of a rift zone fault of 12 to 13 km, then the maximum length of rupture is estimated to range from about 16 km to as much as 100 km (i.e., aspect ratios of 2:1 to 10:1). The resulting rupture areas are used with rupture area-magnitude relationships of Wells and Coppersmith (in press) to estimate magnitudes that range from about 6 to 7. Use of the empirical relationship between rupture width and magnitude (see Section 3.2.2.6) results in similar magnitudes. Because the rift structure may contain fairly coherent structures that can produce larger earthquakes, the maximum magnitude distribution is assessed to be between magnitude 6.5 and 7.0. Outside of the rift, the basement structures are likely to be smaller and maximum magnitudes in the 6 to 6.5 range are judged to be most credible and are given highest weight (Figure 3-20), although we allow for the possibility of magnitudes as large as 7.

3.2.4.1.4 Slip Rate and Earthquake Recurrence. In the case where the rift model is assumed, the recurrence rate for the basement adjacent to the rift is assessed from the observed basement seismicity data directly. For the rift zone itself, recurrence is estimated based on an assessment of the cumulative rate of slip on faults within the rift zone. The slip rate is then converted to a seismic moment rate assuming characteristic and exponential magnitude distribution models.

The slip rate for the rift is assessed based on the assumption that the total rate of shortening across the Yakima Fold Belt, as measured at the surface, is equivalent to the total slip rate across the rift zone at depth. This assumption is based on the inference that the north-south compressive stresses that exist in the Columbia River basalts in the upper 5 km of the crust also exist within the crystalline basement rocks at depths of about 12 to 21 km. We assume that the compressive style of deformation (reverse faulting on east-west trends in the basalts; dextral strike-slip faulting on northwest trends in the basement) is compatible, and that the rate

of deformation derived from rates of shortening within the basalts reflects the rate of shortening within the crystalline basement.

As discussed previously in Section 3.2.2.7, slip rates have been assessed for each of the folds of the Yakima Fold Belt.. To estimate the rate for the rift zone, we sum the total rate of shortening inferred form the individual fold slip rate assessments along three north-south cross-sections at longitude 119°W, 119.5°W, and 120°W perpendicular to the major folds of the central Columbia Plateau using the data presented in Reidel and others (in press). Assuming that this rate of north-south shortening occurs at depth within the crystalline basement and is expressed as dextral strike-slip faulting along a fault zone having a northwest orientation, we arrive at slip rate estimates of in the range of 0.24 to 0.68 mm/yr. These are represented by a range of equal weighted values in the logic tree (Figure 3-20). Because we have no information on the slip rate on individual faults, the slip rates are for the entire rift zone and are used to estimate the average recurrence rate across the entire zone. Other investigators (Mann and Meyer, 1993, Pezzopane and Weldon, in review) have suggested dextral shear slip rates for the region in the range of 0.2 to 1 mm/yr, which is consistent with the values obtained in this study from the geologic data. Prescott and Savage (1984) analyzed geodetic measurements from a regional trilateration array and found that the region was compressing in a north-south direction at 0.016 microstrain/yr. These measured strain rates only marginally exceed their estimated errors of 0.013 microstrain/yr. For the purpose of comparison, these strain rates are approximately equivalent to a total shortening rate of 2 ± 1 mm/yr across the Yakima Fold Belt, and are inconsistent with geological estimates.

Figure 3-24 shows a comparison between the observed rate of earthquake occurrence in the basement and that predicted using the failed rift model based of the estimated slip rates. As can be seen from the figure, the predicted mean rate of seismicity is somewhat larger than the observed rate of seismicity, but the observed seismicity rate falls within the uncertainty band for the predicted rate.

3.2.4.2 Basement Block Model. An alternative model for the basement seismic source is considered that recognizes a region of depressed or "down-dropped" crystalline crust shown diagrammatically on Figure 3-25. The basement is divided into two blocks or regions, an inner source zone representing the down-dropped area, and an outer source zone. The inner source zone is distinguished by generally deeper crystalline crust and increased levels of observed seismicity relative to the outer source zone. The two zones are separated by block boundaries that are also source zone boundaries (described below). The seismicity rates for the crustal regions located within and outside of the basement block are determined from the observed seismicity. Maximum magnitudes are assumed to be similar to those assessed for the basement source outside of the rift model.

The block boundaries could potentially represent pre-existing faults that might be re-activated. The two potential fault sources are termed basement faults "A" and "B". Basement fault A is the eastern boundary to the inner source zone. It is interpreted to lie along the Ice Harbor Dike Swarm, a possible major crustal discontinuity that marks the transition from shallow, stable cratonic basement to the east to a subsided region to the west (Reidel and others, in press). They consider this feature to be a long-lived major crustal boundary that may have originated as a suture zone separating stable North American craton from accreted terrain on the west. An alternative interpretation for the location of this structure is provided by regional seismic refraction data (Rohay and others, 1985; Glover, 1985) (see Figures 3-21 and 3-22).

Basement fault B forms the northern boundary of the inner source zone, separating the region of deeper, subsided crystalline crust from shallower, more stable basement to the north. Fault B is located on the basis of seismic refraction data that indicate a down-to-the-south step in basement between the Frenchman Hills and Saddle Mountains (Rohay and others, 1985; Glover, 1985; Catchings and Mooney, 1988). The probability that faults A and B are seismogenic is assessed to be 0.5, representing a maximum state of uncertainty, because there is little evidence either for or against activity. There is no correlation of deep seismicity with these structures and the subsidence observed geologically is difficult to reconcile with the present tectonic stress field.

If faults A and B are considered active, earthquake recurrence rates are assessed using the subsidence rate in the Columbia basin, estimated to be approximately 0.003 mm/yr (Reidel, 1989). Because the boundary faults have significant length, the maximum magnitude distribution is assumed to be the same as that assessed for the rift structure.

3.2.4.3 Random Basement Model. A third model is considered for the basement seismic source that assumes a random occurrence of earthquakes throughout the region. This model assumes that neither the rift model nor the block model provides a proper representation of the seismic sources in the basement. By assuming that seismicity occurs randomly within an areal source zone, the model implies that the causative structures giving rise to seismicity are unknown. Because of the low level of confidence that either of the two structural models provide a proper representation of the current basement tectonic deformation, the random model is given the highest weight.

The maximum magnitude distribution for the random basement model is assumed to be the same as that for the basement sources outside the rift, because they are derived primarily from the thickness of the seismogenic crystalline basement, which does not vary by model. The recurrence rate is derived directly from the observed rate of seismicity.

3.2.5 Predicted Regional Seismicity Rates

The seismic source model developed above consists of three sources of earthquakes, random seismicity occurring in the CRBG, seismicity occurring in the crystalline basement rocks, and potential seismicity generated by faults associated with the Yakima folds. Each of the sources is characterized independently from the others. The CRBG and basement sources rely primarily on the observed seismicity to develop the earthquake recurrence parameters, and together account for all of the observed seismicity. The Yakima fold sources utilize crustal deformation rates to estimate earthquake recurrence rates, and represent an additional source of seismicity. Thus, the model is somewhat conservative, in that the earthquakes in the recorded catalog that may have been generated by faults associated with the Yakima folds have been used to characterize the seismicity rates of the other two sources.

Figure 3-26 shows a comparison between the observed rate of seismicity and the seismicity rate predicted by the complete seismic source model. Shown on the left (a) are the predicted seismicity rates for the three types of sources and shown on the right (b) is the uncertainty estimates for earthquake frequency resulting from the distributions of input parameters defined in the logic trees. The predicted seismicity rate is about 50 percent higher than the observed seismicity rate in the magnitude 3 to 5 range. However, there is large overlap in the uncertainty bands for both the predicted and observed rates, such that the mean rates for both predicted and observed rates lie within the 90-percent confidence intervals of the other.

The predicted recurrence relationship for events occurring on the Yakima folds (Figure 3-26b) indicates an annual frequency of events of magnitude ≥ 6 of $2 \cdot 10^{-4}$, or one every 5,000 years. Given the proposed tectonic model for faulting associated with the Yakima folds (fold and thrust belt within a compressive regime), it is not clear that the deformation associated with these events would always clearly manifest itself in the exposed surface geology (e.g. blind thrusting earthquakes like the M 6.5 1983 Coalinga earthquake are often associated with subtle fold growth and no surface faulting). However, there are a number of locations where recent faulting has been documented in the area. Reidel and others (in press) list 21 locations at which Quaternary-Holocene faulting has been either documented (their Table 4) or suggested (their Table 5). Field evidence at several sites suggests multiple displacement histories over the life of the fault. For example, the central fault on Gable Mountain has had periods of activity from the Miocene to post 13,000 years before present. The Mill Creek thrust fault on Toppenish Ridge shows as much as several meters of movement since the Quaternary, suggestive of several events (Reidel, in press).

On the basis of the comparison shown on Figure 3-26, it is judged that the seismicity model provides a good representation of the regional seismicity, both recorded historically and in the geology.

3.3 SEISMIC HAZARD SOURCE MODEL FOR CASCADIA SOURCES

The Cascadia subduction zone lies along the west coast of North America from Cape Mendocino in northern California to mid Vancouver Island. Studies of subduction zones worldwide have shown that subduction zone earthquakes are related to two separate and distinct processes: stresses within the subducting slab (usually downdip-tension due to slab-pull forces), and compressional stresses at the interface between the two plates. Experience has shown that these two domains act as independent seismic sources from the standpoint of source locations, maximum magnitudes, and earthquake recurrence. We therefore treat these two subduction zone-related sources separately. The characterization of the plate interface source and the intraslab source is based on the model presented in seismic hazard analyses for the Bull Run Dam sites (Cornforth and Geomatrix, 1992) and the Humboldt Bay, California bridges (Geomatrix, 1993). The main points of these models are briefly summarized below.

The characterization of the plate interface source includes assessments of: the probability of activity, segmentation of the interface, constraints on the downdip width of the seismogenic interface, maximum magnitude, plate convergence rates, seismic coupling, paleoseismic evidence of earthquake recurrence, and alternative recurrence models. Based on the latest research, the plate interface is believed to lie offshore (see Figure 3-27). The model used considered the width of the interface to be uncertain, varying from 60 to 100 km. At its widest point, the interface lies at a distance of approximately 350 km from the Hanford sites. Based on consideration of various alternative segmentation models for the interface, the maximum magnitude distribution ranges from M 8 to 9, with preferred values near M 8½. Estimates for the frequency of occurrence of the largest events were based on plate convergence rates and paleoseismic data and range from a few hundred to a few thousand years, with a preference for values near 500 years.

The intraslab source represents seismicity occurring within the subducting Juan de Fuca plate. The intraslab source is characterized by its: geometry (based on a number of data sets), maximum magnitude, and recurrence rate. Figure 3-28 shows the spatial distribution of

intraslab seismicity and the boundary of the intraslab source used in the analysis. Earthquake recurrence rates were based on the recorded seismicity. The maximum magnitude distribution ranged from 7 to 7.5, representative of the largest intraslab events observed worldwide. Uncertainties in all of the Cascadia source characteristics are quantified and incorporated into the Hanford seismic hazard analysis.

TABLE 3-1
ASSESSMENT OF PROBABILITY OF ACTIVITY AND
COUPLING FOR YAKIMA FOLDS SEISMIC SOURCES

Fold	Probability of Activity	Probability of Coupling
Umtanum-Gable Mountain	0.25	0.15
Rattlesnake-Wallula	0.25	0.05 Strike Slip 0.30 Reverse
Manastash Ridge	0.25	0.15
Saddle Mountains	0.50	0.60
Horse Heaven Hills NW	0.25	0.15
Horse Heaven Hills NE	0.25	0.70
Rattlesnake Hills	0.25	0.15
Yakima Ridge	0.25	0.15
Frenchmen Hills	0.25	0.15
Toppenish Ridge	0.60	0.70
Hog Ranch	0.10	0.50

TABLE 3-2
SOURCE PARAMETERS FOR ASSESSING MAXIMUM MAGNITUDE
FOR COUPLED YAKIMA FOLDS SEISMIC SOURCES

Fold	Segmented	Segment	Total Length (km)	Rupture Length (km)	Dip	Maximum Magnitude
Umtanum-Gable Mountain	no(0.4)	-	141	141(0.1)	30°(0.2)	7.8
					45°(0.4)	7.6
					60°(0.4)	7.6
				70.5(0.4)	30°(0.2)	7.5
					45°(0.4)	7.3
					60°(0.4)	7.3
				width(0.5)	30°(0.2)	7.6
					45°(0.4)	7.3
					60°(0.4)	7.1
	yes(0.6)	SE Anticline	11	11(1.0)	30°(0.2)	6.7
					45°(0.4)	6.5
					60°(0.4)	6.5
		Gable Mtn	25	25(1.0)	30°(0.2)	7.0
					45°(0.4)	6.9
					60°(0.4)	6.8
		Umtanum East	32	32(1.0)	30°(0.2)	7.2
					45°(0.4)	7.0
					60°(0.4)	6.9
		Umtanum Central	30	30(1.0)	30°(0.2)	7.1
					45°(0.4)	7.0
					60°(0.4)	6.9
		Umtanum West	43	43(1.0)	30°(0.2)	7.3
					45°(0.4)	7.1
					60°(0.4)	7.0
Rattlesnake-Wallula Strike Slip	no(1.0)	-	115	115(0.1)	90°(1.0)	7.4
				57.5(0.4)	90°(1.0)	7.1
				width(0.5)	90°(1.0)	7.0
Rattlesnake-Wallula Reverse	no(0.3)	-	115	115(0.1)	30°(0.2)	7.7
					45°(0.4)	7.6
					60°(0.4)	7.5
				57.5(0.4)	30°(0.2)	7.4
					45°(0.4)	7.3
					60°(0.4)	7.2
				width(0.5)	30°(0.2)	7.6
					45°(0.4)	7.3
					60°(0.4)	7.1
	yes(0.7)	Wallula	45	45(1.0)	30°(0.2)	7.3
					45°(0.4)	7.2
					60°(0.4)	7.1

GEOMATRIX

TABLE 3-2 (continued)
SOURCE PARAMETERS FOR ASSESSING MAXIMUM MAGNITUDE
FOR COUPLED YAKIMA FOLDS SEISMIC SOURCES

Fold	Segmented	Segment	Total Length (km)	Rupture Length (km)	Dip	Maximum Magnitude
		Rattlesnake-Wallula	50	50(1.0)	30°(0.2)	7.3
					45°(0.4)	7.2
					60°(0.4)	7.1
		Rattlesnake Mtn	20	20(1.0)	30°(0.2)	6.9
					45°(0.4)	6.8
					60°(0.4)	6.7
Manastash Ridge	no(1.0)	-	80	80(0.1)	30°(0.33)	7.6
					45°(0.33)	7.4
					60°(0.33)	7.3
				40(0.4)	30°(0.33)	7.3
					45°(0.33)	7.1
					60°(0.33)	7.0
				width(0.5)	30°(0.33)	7.6
					45°(0.33)	7.3
					60°(0.33)	7.1
Saddle Mtns	no(0.4)	-	116	116(0.1)	30°(0.1)	7.7
					45°(0.3)	7.6
					60°(0.6)	7.5
				58(0.4)	30°(0.1)	7.4
					45°(0.3)	7.3
					60°(0.6)	7.2
				width(0.5)	30°(0.1)	7.6
					45°(0.3)	7.3
					60°(0.6)	7.1
	yes(0.6)	McDonald Spr.	26	26(1.0)	30°(0.1)	7.1
					45°(0.3)	6.9
					60°(0.6)	6.8
		Sentinel Gap	24	24(1.0)	30°(0.1)	7.0
					45°(0.3)	6.9
					60°(0.6)	6.8
		Smyrna Bench	19	19(1.0)	30°(0.1)	6.9
					45°(0.3)	6.8
					60°(0.6)	6.7
		Saddle Gap	28	28(1.0)	30°(0.1)	7.1
					45°(0.3)	6.9
					60°(0.6)	6.9
		Eagle Lakes	19	19(1.0)	30°(0.1)	6.9
					45°(0.3)	6.8
					60°(0.6)	6.7

GEOMATRIX

TABLE 3-2 (continued)
SOURCE PARAMETERS FOR ASSESSING MAXIMUM MAGNITUDE
FOR COUPLED YAKIMA FOLDS SEISMIC SOURCES

Fold	Segmented	Segment	Total Length (km)	Rupture Length (km)	Dip	Maximum Magnitude
Horse Heaven Hills NW	no(1.0)	-	70	70(0.1)	30°(0.2)	7.5
					45°(0.4)	7.3
					60°(0.4)	7.3
				35(0.4)	30°(0.2)	7.2
					45°(0.4)	7.0
					60°(0.4)	7.0
				width(0.5)	30°(0.2)	7.6
					45°(0.4)	7.3
					60°(0.4)	7.1
Horse Heaven Hills NE	no(0.2)	-	170	170(0.1)	30°(0.25)	7.9
					45°(0.5)	7.7
					60°(0.25)	7.6
				85(0.4)	30°(0.25)	7.6
					45°(0.5)	7.4
					60°(0.25)	7.3
				width(0.5)	30°(0.25)	7.6
					45°(0.5)	7.3
					60°(0.25)	7.1
	yes(0.8)	West	100	100(1.0)	30°(0.25)	7.6
					45°(0.5)	7.5
					60°(0.25)	7.4
		East	70	70(1.0)	30°(0.25)	7.5
					45°(0.5)	7.3
					60°(0.25)	7.3
Rattlesnake Hills	no(1.0)	-	72	72(0.1)	30°(0.2)	7.5
					45°(0.4)	7.4
					60°(0.4)	7.3
				36(0.4)	30°(0.2)	7.2
					45°(0.4)	7.1
					60°(0.4)	7.0
				width(0.5)	30°(0.2)	7.6
					45°(0.4)	7.3
					60°(0.4)	7.1

TABLE 3-2 (continued)
SOURCE PARAMETERS FOR ASSESSING MAXIMUM MAGNITUDE
FOR COUPLED YAKIMA FOLDS SEISMIC SOURCES

Fold	Segmented	Segment	Total Length (km)	Rupture Length (km)	Dip	Maximum Magnitude
Yakima Ridge	no(1.0)	-	79	79(0.1)	30°(0.33)	7.5
					45°(0.33)	7.4
					60°(0.33)	7.3
				39.5(0.4)	30°(0.33)	7.2
					45°(0.33)	7.1
					60°(0.33)	7.0
				width(0.5)	30°(0.33)	7.6
					45°(0.33)	7.3
					60°(0.33)	7.1
Frenchmen Hills	no(1.0)	-	78	78(0.1)	30°(0.25)	7.5
					45°(0.5)	7.4
					60°(0.25)	7.3
				39(0.4)	30°(0.25)	7.2
					45°(0.5)	7.1
					60°(0.25)	7.0
				width(0.5)	30°(0.25)	7.6
					45°(0.5)	7.3
					60°(0.25)	7.1
Toppenish Ridge	no(1.0)	-	50	50(0.1)	30°(0.33)	7.3
					45°(0.33)	7.2
					60°(0.33)	7.1
				25(0.4)	30°(0.33)	7.0
					45°(0.33)	6.9
					60°(0.33)	6.8
				width(0.5)	30°(0.33)	7.6
					45°(0.33)	7.3
					60°(0.33)	7.1
Hog Ranch	no(1.0)	-	150	150(0.1)	60°(0.4)	7.6
					75°(0.4)	7.5
					90°(0.2)	7.5
				75(0.4)	60°(0.4)	7.3
					75°(0.4)	7.2
					90°(0.2)	7.2
				width(0.5)	60°(0.4)	7.1
					75°(0.4)	7.0
					90°(0.2)	7.0

GEOMATRIX

TABLE 3-3
SOURCE PARAMETERS FOR ASSESSING MAXIMUM MAGNITUDE
FOR UNCOUPLED YAKIMA FOLDS SEISMIC SOURCES

Fold	Segmented	Segment	Depth (km)	Technique	Dip	Maximum Magnitude
Umtanum-Gable	no(0.4)	--	4	asp ra(0.5)	30°(0.2)	6.2
					45°(0.4)	5.9
					60°(0.4)	5.8
				width(0.5)	30°(0.2)	6.1
					45°(0.4)	5.8
					60°(0.4)	5.6
	yes(0.6)	SE Anticline	4	asp ra(0.5)	30°(0.2)	6.2
					45°(0.4)	5.9
					60°(0.4)	5.8
				width(0.5)	30°(0.2)	6.1
					45°(0.4)	5.8
					60°(0.4)	5.6
		Gable Mtn	4	asp ra(0.5)	30°(0.2)	6.2
					45°(0.4)	5.9
					60°(0.4)	5.8
				width(0.5)	30°(0.2)	6.1
					45°(0.4)	5.8
					60°(0.4)	5.6
		Umtanum East	4	asp ra(0.5)	30°(0.2)	6.2
					45°(0.4)	•5.9
					60°(0.4)	5.8
				width(0.5)	30°(0.2)	6.1
					45°(0.4)	5.8
					60°(0.4)	5.6
		Umtanum Central	3.5	asp ra(0.5)	30°(0.2)	6.1
					45°(0.4)	5.8
					60°(0.4)	5.6
				width(0.5)	30°(0.2)	6.0
					45°(0.4)	5.7
					60°(0.4)	5.5
		Umtanum West	3	asp ra(0.5)	30°(0.2)·	6.0
					45°(0.4)	5.7
					60°(0.4)	5.5
				width(0.5)	30°(0.2)	5.8
					45°(0.4)	5.5
					60°(0.4)	5.3
Rattlesnake-Wallula Reverse	no(0.3)	-	4	asp ra(0.5)	30°(0.2)	6.2
					45°(0.4)	5.9
					60°(0.4)	5.8
				width(0.5)	30°(0.2)	6.1

TABLE 3-3 (continued)
SOURCE PARAMETERS FOR ASSESSING MAXIMUM MAGNITUDE
FOR UNCOUPLED YAKIMA FOLDS SEISMIC SOURCES

Fold	Segmented	Segment	Depth (km)	Technique	Dip	Maximum Magnitude
					45°(0.4)	5.8
					60°(0.4)	5.6
	yes(0.7)	Wallula	3	asp ra(0.5)	30°(0.2)	6.0
					45°(0.4)	5.7
					60°(0.4)	5.5
				width(0.5)	30°(0.2)	5.8
					45°(0.4)	5.5
					60°(0.4)	5.3
		Rattlesnake-Wallula	4	asp ra(0.5)	30°(0.2)	6.2
					45°(0.4)	5.9
					60°(0.4)	5.8
				width(0.5)	30°(0.2)	6.1
					45°(0.4)	5.8
					60°(0.4)	5.6
		Rattlesnake Mtn	5	asp ra(0.5)	30°(0.2)	6.4
					45°(0.4)	6.1
					60°(0.4)	5.9
				width(0.5)	30°(0.2)	6.3
					45°(0.4)	6.0
					60°(0.4)	5.8
Manastash Ridge	no(1.0)	-	1.5	asp ra(0.5)	30°(0.33)	5.4
					45°(0.33)	5.1
					60°(0.33)	4.9
				width(0.5)	30°(0.33)	5.2
					45°(0.33)	4.9
					60°(0.33)	4.7
Saddle Mtns	no(0.4)	-	3	asp ra(0.5)	30°(0.1)	6.0
					45°(0.3)	5.7
					60°(0.6)	5.5
				width(0.5)	30°(0.1)	5.8
					45°(0.3)	5.5
					60°(0.6)	5.3
	yes(0.6)	McDonald Spr.	2.5	asp ra(0.5)	30°(0.1)	5.8
					45°(0.3)	5.5
					60°(0.6)	5.3
				width(0.5)	30°(0.1)	5.7
					45°(0.3)	5.3
					60°(0.6)	5.2
		Sentinel Gap	2.5	asp ra(0.5)	30°(0.1)	5.8
					45°(0.3)	5.5

TABLE 3-3 (continued)
SOURCE PARAMETERS FOR ASSESSING MAXIMUM MAGNITUDE
FOR UNCOUPLED YAKIMA FOLDS SEISMIC SOURCES

Fold	Segmented	Segment	Depth (km)	Technique	Dip	Maximum Magnitude
					60°(0.6)	5.3
				width(0.5)	30°(0.1)	5.7
					45°(0.3)	5.3
					60°(0.6)	5.2
		Smyrna Bench	3	asp ra(0.5)	30°(0.1)	6.0
					45°(0.3)	5.7
					60°(0.6)	5.5
				width(0.5)	30°(0.1)	5.8
					45°(0.3)	5.5
					60°(0.6)	5.3
		Saddle Gap	3.5	asp ra(0.5)	30°(0.1)	6.1
					45°(0.3)	5.8
					60°(0.6)	5.6
				width(0.5)	30°(0.1)	6.0
					45°(0.3)	5.7
					60°(0.6)	5.5
		Eagle Lakes	3.5	asp ra(0.5)	30°(0.1)	6.1
					45°(0.3)	5.8
					60°(0.6)	5.6
				width(0.5)	30°(0.1)	6.0
					45°(0.3)	5.7
					60°(0.6)	5.5
Horse Heaven Hills NW	no(1.0)	-	4	asp ra(0.5)	30°(0.2)	6.2
					45°(0.4)	5.9
					60°(0.4)	5.8
				width(0.5)	30°(0.2)	6.1
					45°(0.4)	5.8
					60°(0.4)	5.6
Horse Heaven Hills NE	no(0.2)	-	5	asp ra(0.5)	30°(0.25)	6.4
					45°(0.5)	6.1
					60°(0.25)	5.9
				width(0.5)	30°(0.25)	6.3
					45°(0.5)	6.0
					60°(0.25)	5.8
	yes(0.8)	West	5	asp ra(0.5)	30°(0.25)	6.4
					45°(0.5)	6.1
					60°(0.25)	5.9
				width(0.5)	30°(0.25)	6.3
					45°(0.5)	6.0
					60°(0.25)	5.8

TABLE 3-3 (continued)
SOURCE PARAMETERS FOR ASSESSING MAXIMUM MAGNITUDE
FOR UNCOUPLED YAKIMA FOLDS SEISMIC SOURCES

Fold	Segmented	Segment	Depth (km)	Technique	Dip	Maximum Magnitude
		East	4.5	asp ra(0.5)	30°(0.25)	6.3
					45°(0.5)	6.0
					60°(0.25)	5.9
				width(0.5)	30°(0.25)	6.2
					45°(0.5)	5.9
					60°(0.25)	5.7
Rattlesnake Hills	no(1.0)	-	2.5	asp ra(0.5)	30°(0.2)	5.8
					45°(0.4)	5.5
					60°(0.4)	5.3
				width(0.5)	30°(0.2)	5.7
					45°(0.4)	5.3
					60°(0.4)	5.2
Yakima Ridge	no(1.0)	-	1.5	asp ra(0.5)	30°(0.33)	5.4
					45°(0.33)	5.1
					60°(0.33)	4.9
				width(0.5)	30°(0.33)	5.2
					45°(0.33)	4.9
					60°(0.33)	4.7
Frenchmen Hills	no(1.0)	-	2.5	asp ra(0.5)	30°(0.25)	5.8
					45°(0.5)	5.5
					60°(0.25)	5.3
				width(0.5)	30°(0.25)	5.7
					45°(0.5)	5.3
					60°(0.25)	5.2
Toppenish Ridge	no(1.0)	-	3	asp ra(0.5)	30°(0.33)	6.0
					45°(0.33)	5.7
					60°(0.33)	5.5
				width(0.5)	30°(0.33)	5.8
					45°(0.33)	5.5
					60°(0.33)	5.3
Hog Ranch	no(1.0)	-	3.5	asp ra(0.5)	60°(0.4)	5.6
					75°(0.4)	5.5
					90°(0.2)	5.5
				width(0.5)	60°(0.4)	5.5
					75°(0.4)	5.4
					90°(0.2)	5.3

TABLE 3-4
SLIP RATE ASSESSMENT FOR YAKIMA FOLDS

Fold	Method	Offset (m) Vert.	Horz.	Age (Ma)	Fault Slip Rate (mm/yr) 30° Dip	45° Dip	60° Dip
Umtanum Ridge	V(0.5)	417	-	10.5(0.5)	0.079	0.056	0.046
Gable Mtn.		417	-	14.5(0.5)	0.050	0.035	0.029
	V+H(0.5)	417	433	10.5(0.5)	0.121	0.097	0.087
		417	433	14.5(0.5)	0.075	0.061	0.054
SE Anticline	V(0.7)	102	-	10.5(1.0)	0.019	0.014	0.011
	V+H(0.3)	102	300	10.5(1.0)	0.048	0.042	0.040
Gable Mtn.	V(0.7)	305	-	10.5(1.0)	0.058	0.041	0.034
	V+H(0.3)	305	300	10.5(1.0)	0.087	0.070	0.062
Umtanum East	V(0.3)	530	-	10.5(0.5)	0.101	0.071	0.058
Estimate A		530	-	14.5(0.5)	0.063	0.045	0.036
(0.7)	V+H(0.7)	530	1100	10.5(0.5)	0.206	0.176	0.163
		530	1100	14.5(0.5)	0.129	0.110	0.102
Estimate B	V(0.6)	305	-	10.5(1.0)	0.058	0.041	0.034
(0.3)	V+H(0.4)	305	300	10.5(1.0)	0.087	0.070	0.062
Umtanum	V(0.3)	762	-	14.0(1.0)	0.098	0.069	0.057
Central	V+H(0.7)	762	300	14.0(1.0)	0.117	0.089	0.076
Umtanum West	V(0.6)	500	-	14.5(0.5)	0.060	0.042	0.034
		500	-	16.0(0.5)	0.033	0.024	0.019
	V+H(0.4)	500	300	14.5(0.5)	0.077	0.060	0.052
		500	300	16.0(0.5)	0.043	0.034	0.029
RAW (90° dip) Strike slip	cumulative shortening	-	-		0.08(0.2)	0.14(0.6)	0.20(0.2)
RAW	V(1.0)	365	-	10.5(1.0)	0.070	0.049	0.040
Wallula	V(1.0)	152	-	10.5(1.0)	0.029	0.020	0.017
Rattlesnake-Wallula	V(1.0)	323	-	10.5(1.0)	0.062	0.044	0.036
Rattlesnake Mtn.	V(1.0)	640	-	10.5(1.0)	0.122	0.086	0.070
Manastash	V(0.6)	300	-	14.5(0.5)	0.036	0.025	0.021
Ridge		300	-	16.0(0.5)	0.020	0.014	0.012
	V+H(0.4)	300	1000	14.5(0.5)	0.095	0.085	0.080
		300	1000	16.0(0.5)	0.053	0.048	0.045
Saddle Mtns.	V(0.6)	405	-	10.5(0.5)	0.077	0.055	0.045
		405	-	14.0(0.5)	0.052	0.037	0.030
	V+H(0.4)	405	640	10.5(0.5)	0.138	0.116	0.105
		405	640	14.0(0.5)	0.093	0.078	0.071

GEOMATRIX

TABLE 3-4 (continued)
SLIP RATE ASSESSMENT FOR YAKIMA FOLDS

| Fold	Method	Offset (m) Vert.	Horz.	Age (Ma)	Fault Slip Rate (mm/yr) 30° Dip	45° Dip	60° Dip
McDonald Sprs.	V(0.6)	549	-	14.0(1.0)	0.071	0.050	0.041
	V+H(0.4)	549	1000	14.0(1.0)	0.135	0.114	0.105
Sentinel Gap	V(0.6)	420	-	10.5(1.0)	0.080	0.057	0.046
	V+H(0.4)	420	1000	10.5(1.0)	0.175	0.152	0.141
Smyrna Bench	V(0.6)	628	-	13.0(1.0)	0.093	0.066	0.054
	V+H(0.4)	628	700	13.0(1.0)	0.144	0.117	0.105
Saddle Gap	V(0.6)	366	-	12.0(1.0)	0.061	0.043	0.035
	V+H(0.4)	366	400	12.0(1.0)	0.094	0.076	0.068
Eagle Lakes	V(0.6)	61	-	10.5(1.0)	0.012	0.008	0.007
	V+H(0.4)	61	100	10.5(1.0)	0.021	0.018	0.016
Horse Heaven Hills NW	V(1.0)	323	-	10.5(1.0)	0.062	0.044	0.036
Horse Heaven Hills NE	V(1.0)	346	-	10.5(1.0)	0.066	0.047	0.038
Horse Heaven Hills NE-E	V(1.0)	323	-	10.5(1.0)	0.062	0.044	0.036
Horse Heaven Hills NE-W	V(1.0)	368	-	10.5(1.0)	0.070	0.050	0.040
Rattlesnake Hills	V(1.0)	762	-	10.5(1.0)	0.145	0.103	0.084
Yakima Ridge	V(1.0)	500	-	10.5(0.5)	0.095	0.067	0.055
		500	-	16.0(0.5)	0.033	0.024	0.019
Frenchmen Hills	V(0.3)	200	-	10.5(0.5)	0.038	0.027	0.022
		200	-	16.0(0.5)	0.013	0.009	0.008
	V+H(0.7)	200	300	10.5(0.5)	0.067	0.056	0.051
		200	300	16.0(0.5)	0.023	0.019	0.018
Toppenish Ridge	V(1.0)	500	-	10.5(0.5)	0.095	0.067	0.055
		500	-	16.0(0.5)	0.033	0.024	0.019
Columbia Hills	V(0.5)	365	-	10.5(0.5)	0.070	0.049	0.040
		365	-	16.0(0.5)	0.024	0.017	0.014
	V+H(0.5)	365	1000	10.5(0.5)	0.165	0.144	0.135
		365	1000	16.0(0.5)	0.058	0.051	0.048
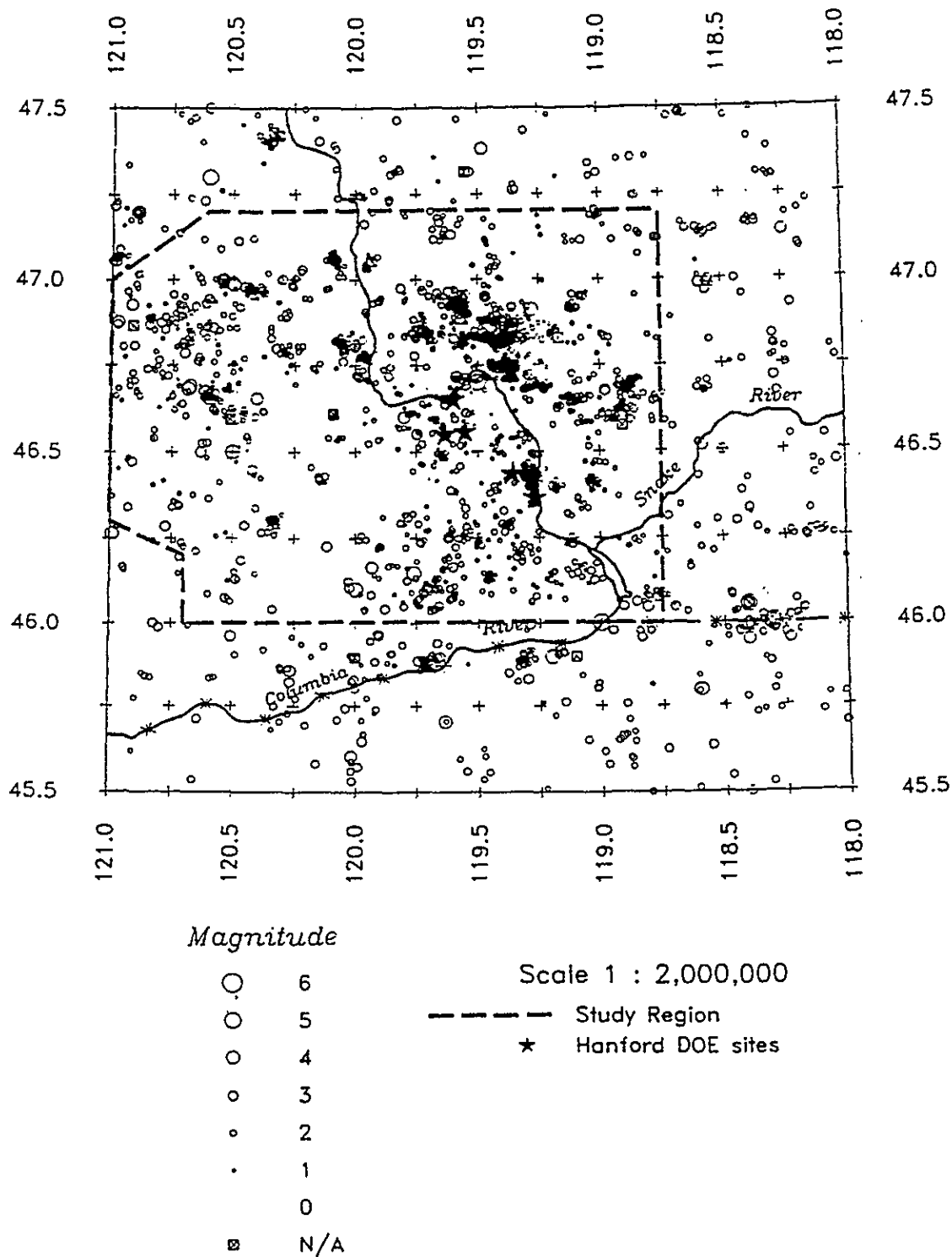
Figure 3-1   Seismicity of the site region for the period 1850 to April, 1991. Shown
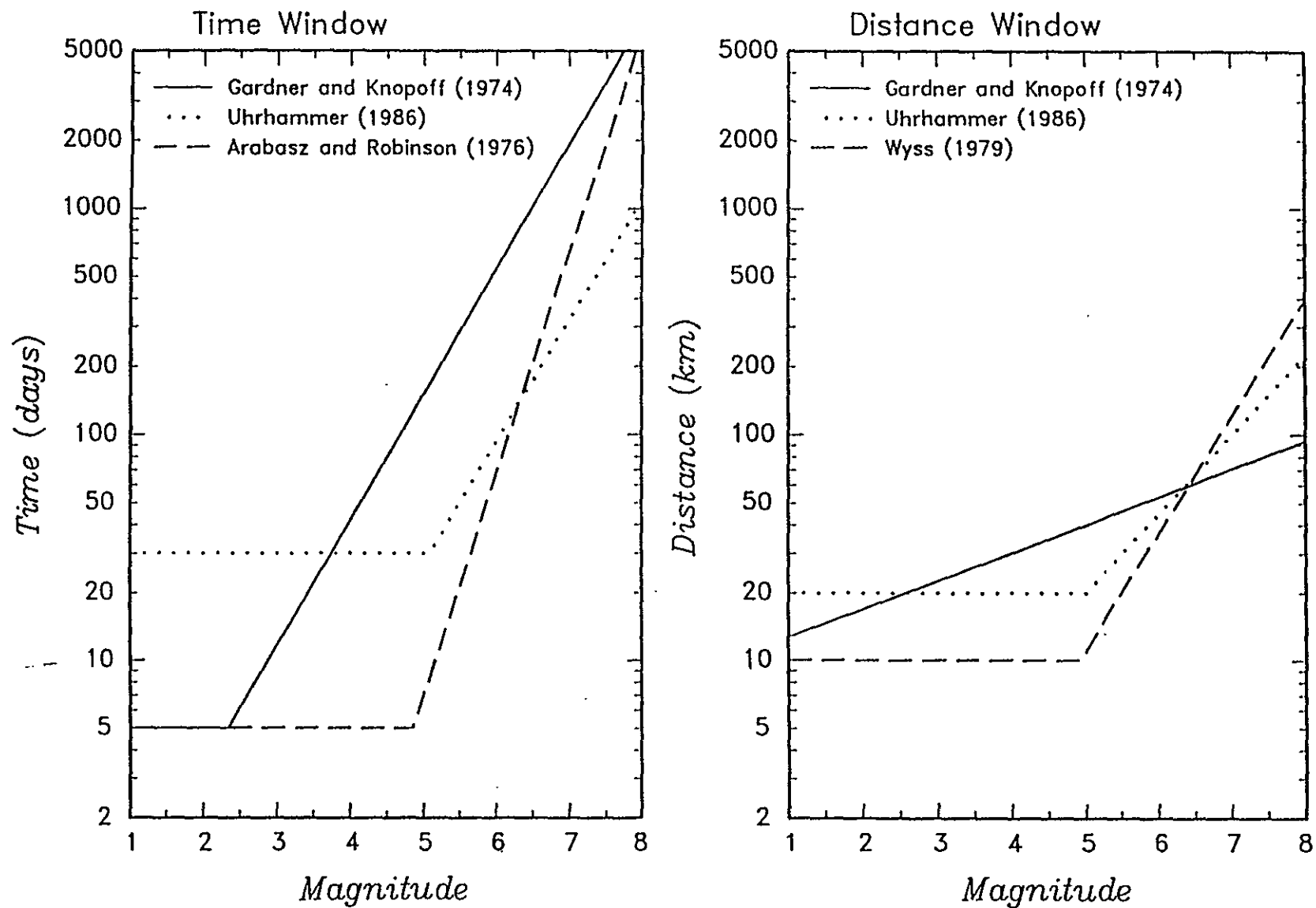also is the general region of the Yakima Fold Belt examined in this study.

Time Window

Time Window

- Gardner and Knopoff (1974)
- ··· Uhrhammer (1986)
- — Arabasz and Robinson (1976)

y-axis: Time (days) — 5000, 2000, 1000, 500, 200, 100, 50, 20, 10, 5, 2

x-axis: Magnitude — 1 to 8

Distance Window

- Gardner and Knopoff (1974)
- ···· Uhrhammer (1986)
- — Wyss (1979)

y-axis: Distance (km) — 5000, 2000, 1000, 500, 200, 100, 50, 20, 10, 5, 2

x-axis: Magnitude — 1 to 8

Figure 3-2   Empirical time and distance window criteria for identifying aftershock sequences.
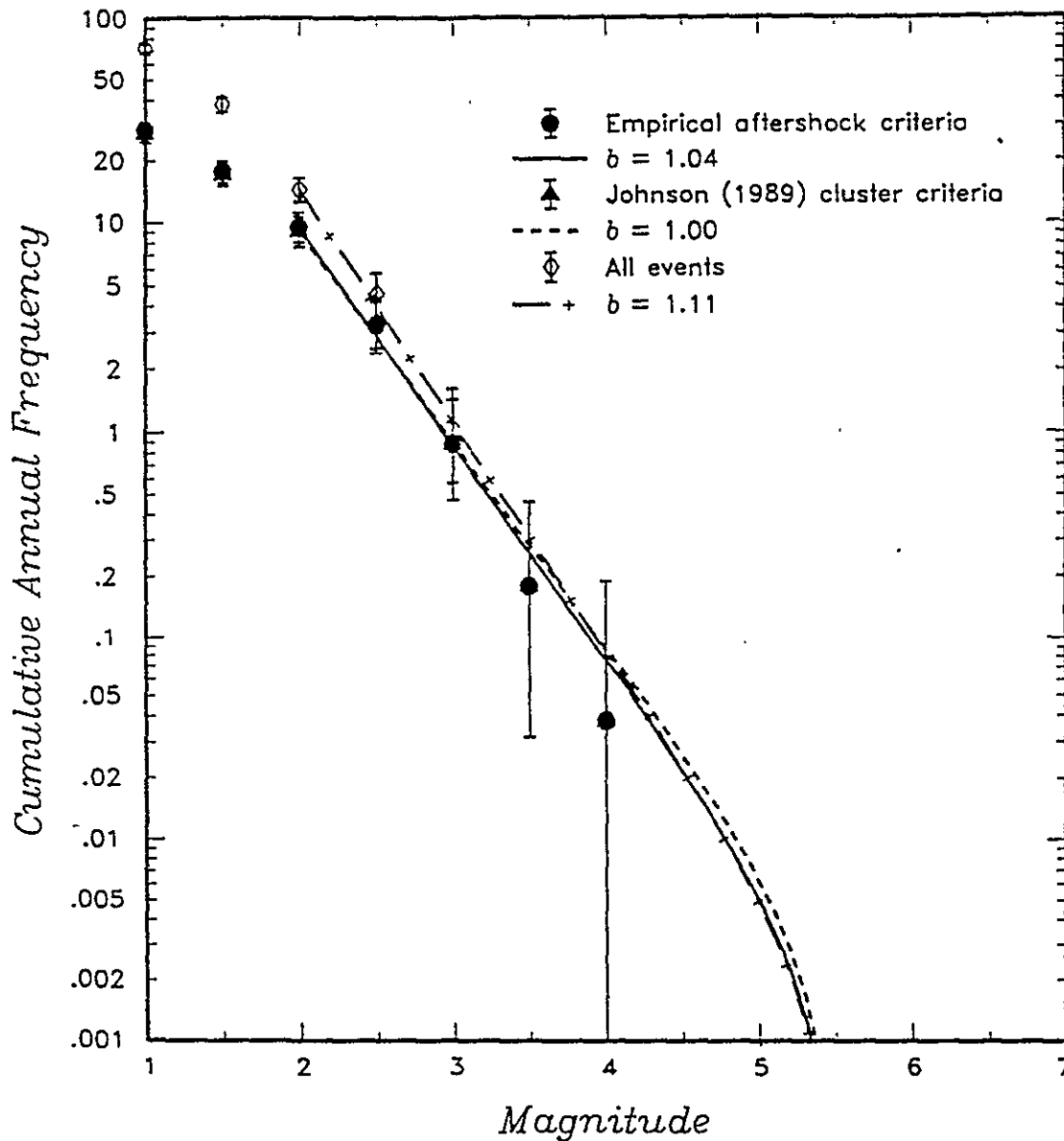
Figure 3-3. Comparison of recurrence rates for independent earthquakes in site region identified using the empirical aftershock criteria shown in Figure 3-2 with that based on independent events identified using Johnson's (1989a) cluster criteria. Also shown are rates for all events. Lines show fitted recurrence relationships with indicated b-values. Rates are for the time period of 1970/01/01-1991/04/01.
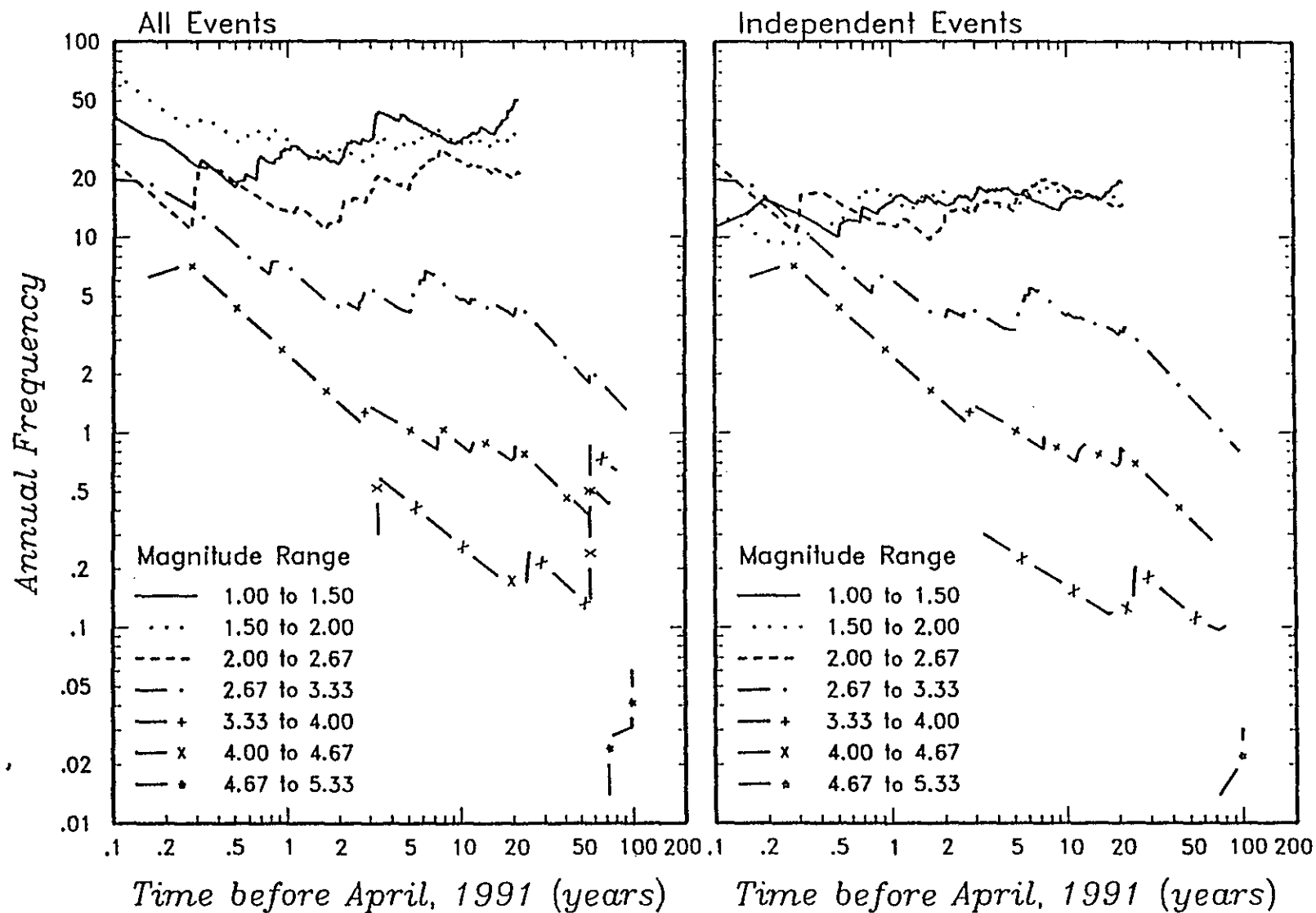
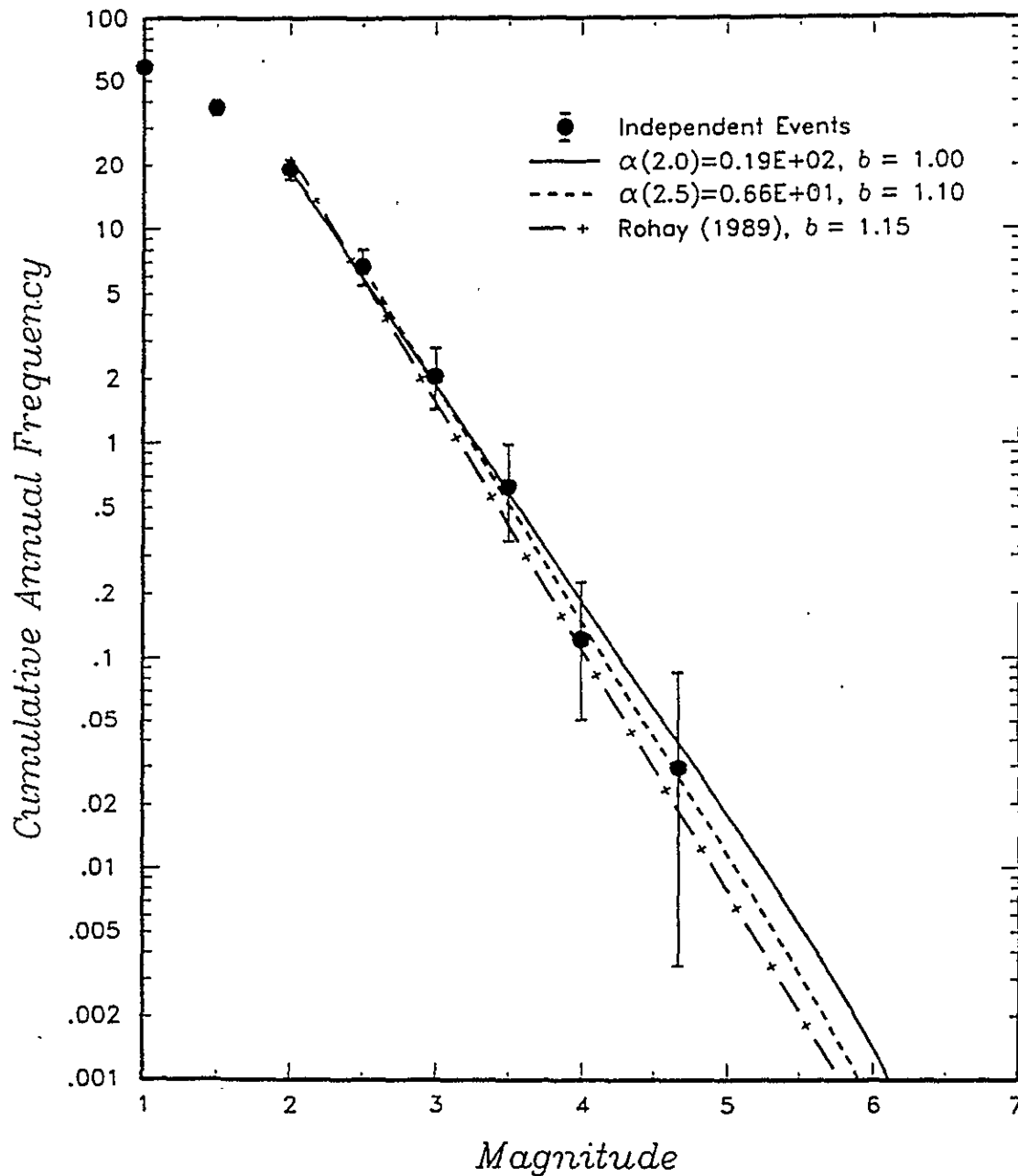Figure 3-4   Earthquake frequency versus time for Yakima Fold Belt study region.

Figure 3-5   Comparison of computed cumulative earthquake frequencies for the
Yakima fold belt region for time period of 1850 to April, 1991 with the
earthquake frequencies obtained by Rohay (1989). Solid and short dashed
lines shows maximum likelihood fit to independent event data for
minimum magnitudes of 2.0 and 2.5, respectively. The vertical error bars
indicate 90-percent confidence intervals on the observed earthquake
frequencies.

GEOMATRIX

Location Map
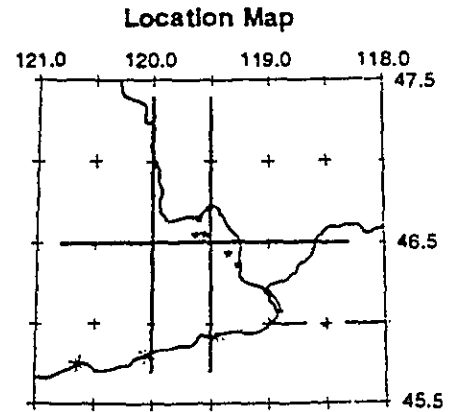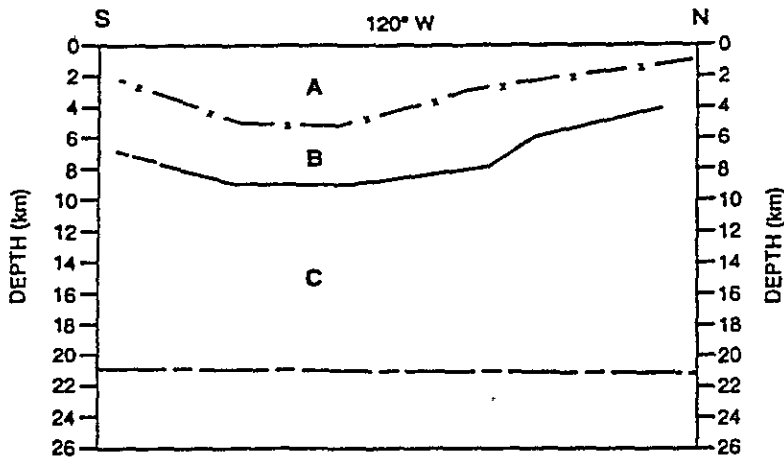
EXPLANATION

Geophysical Horizons

—·—·— Base Columbia River
Basalt Group (Glover,
1985)

——— Top crystalline basement
(Rohay and others,
1985)

— — — 95% cuttoff in seismicity

Geologic Units

A Columbia River Basalt
Group

B Sub-basalt sediments
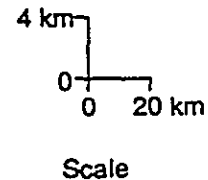
C Crystalline basement
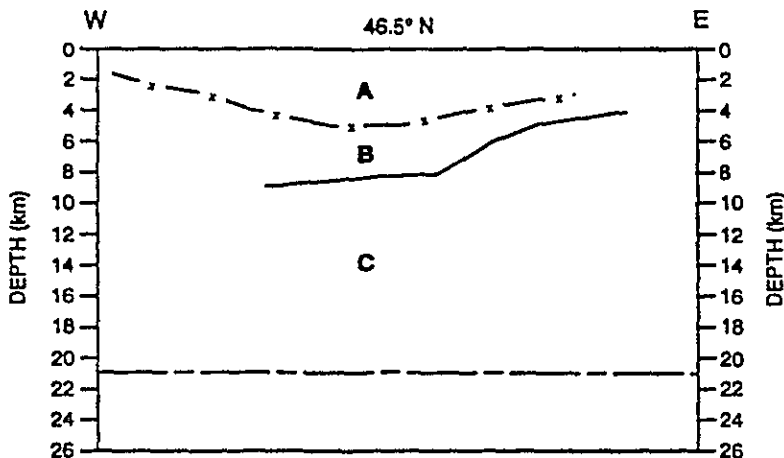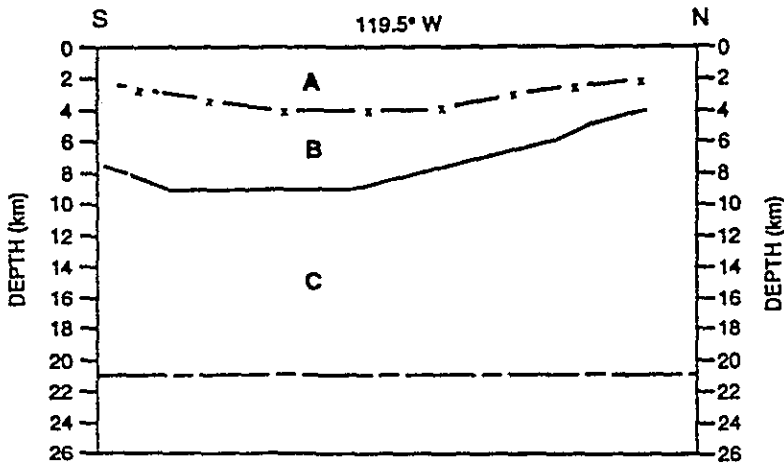
4 km

0

0   20 km

Scale

Figure 3-6 Cross sections through the upper portion of the Columbia Plateau crust showing
details of crustal layering in the Pasco Basin. (Note Layer D lies below cross
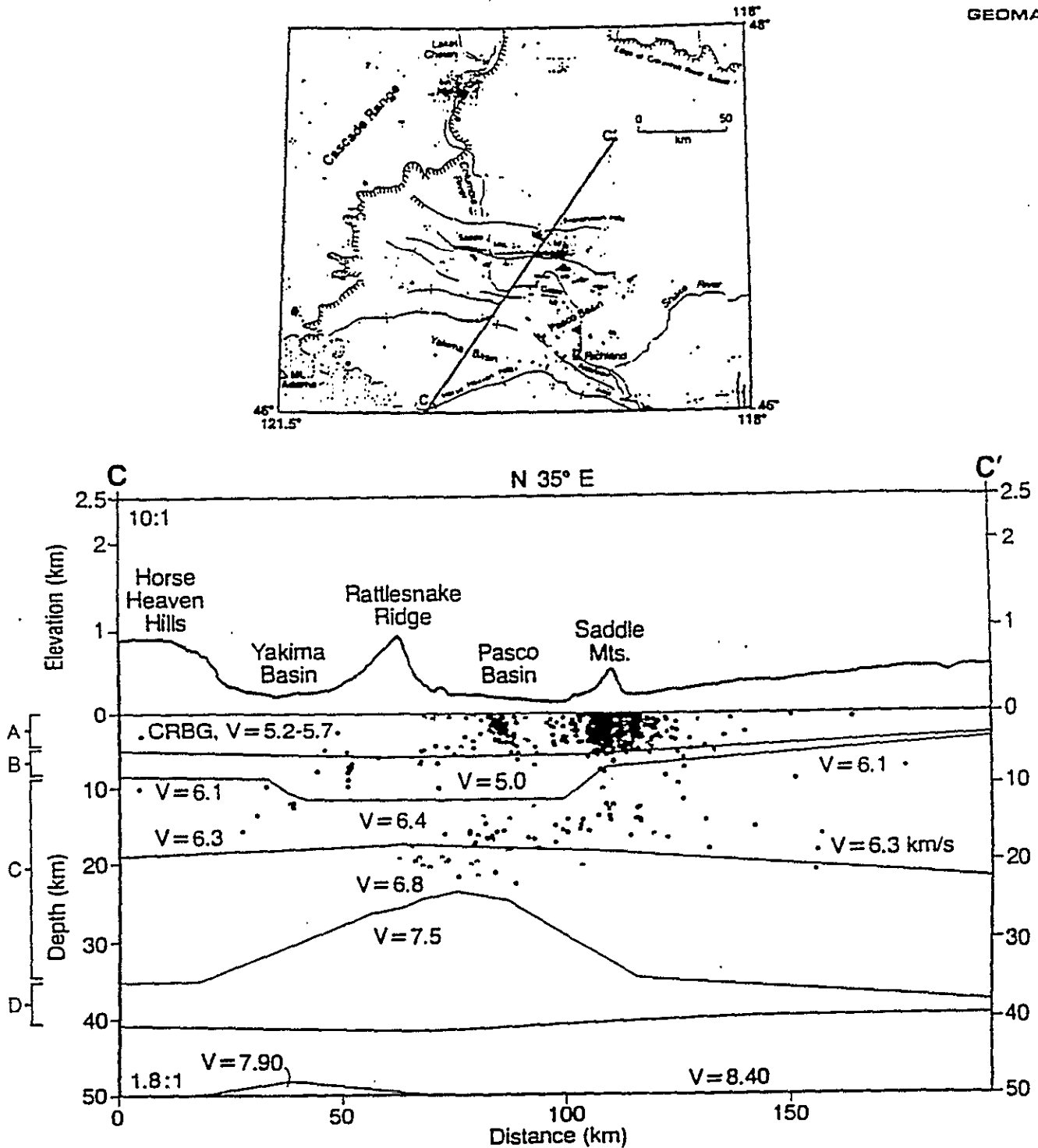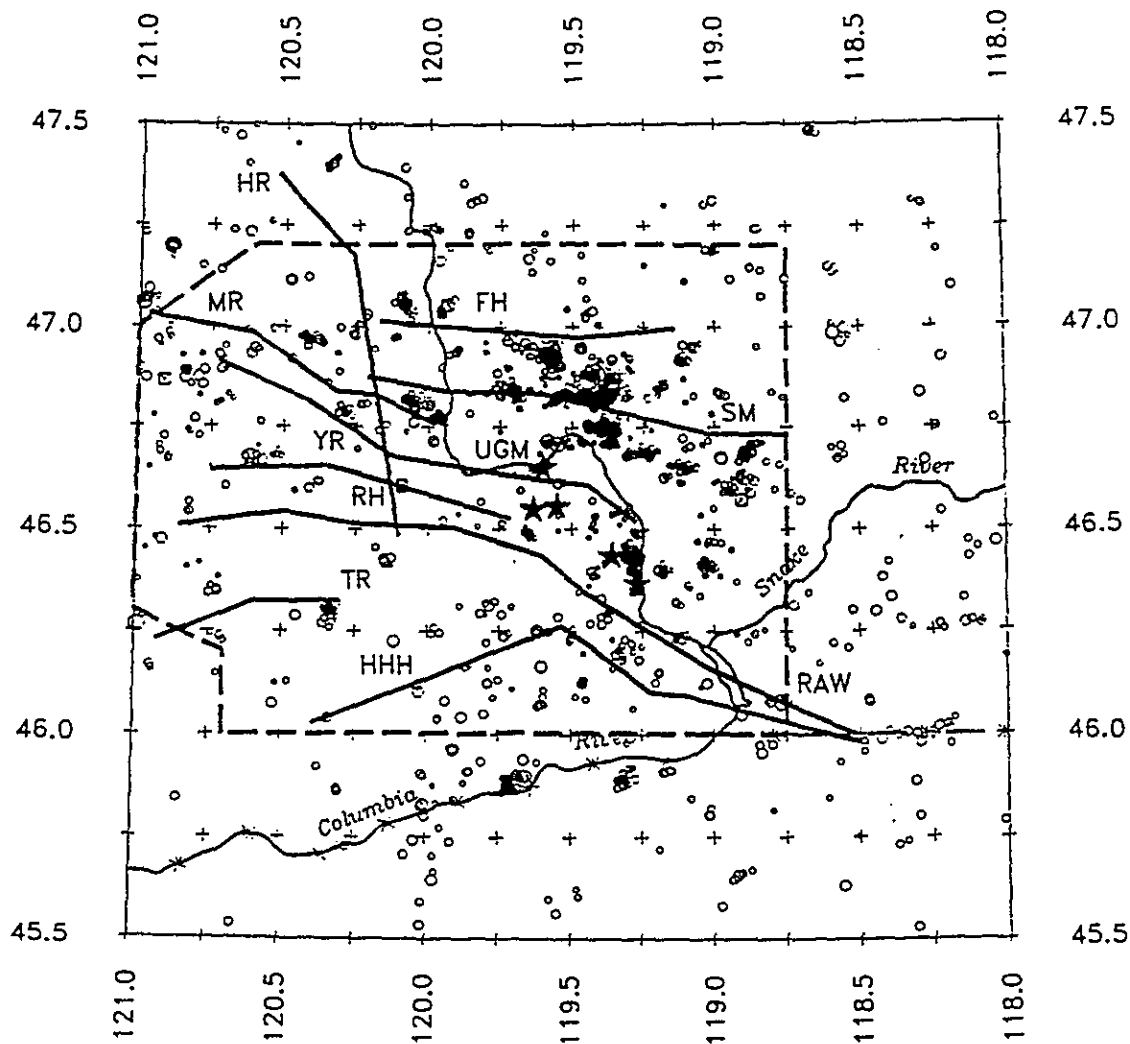sections.)

GEOMATRIX

Figure 3-7   Crustal cross section through Columbia Plateau showing location of inferred rift and distribution of recorded seismicity (from Ludwin and others, 1992). Crustal layers are identified on left vertical axis).

GEOMATRIX

Depth <= 5 km

Magnitude

○	5
○	4
○	3
○	2
·	1
	0
⌀	N/A

Scale 1 : 2,000,000

- - - - Study Region
★ Hanford DOE sites
——— Yakima Folds

FH — Frenchman Hills   RH — Rattlesnake Hills
MR — Manastash Ridge   RAW — Rattlesnake—Wallula
SM — Saddle Mountains   TR — Toppenish Ridge
UGM — Umtanum—Gable Mtn   HHH — Horse Heaven Hills
YR — Yakima Ridge   HR — Hog Ranch

Figure 3-8   Location of major Yakima folds considered as potential seismic sources in the coupled model. Superimposed is the spatial distribution of seismicity for the time period 01/1970-04/1991 occurring primarily within the Columbia River Basalts (focal depth ≤ 5 km).

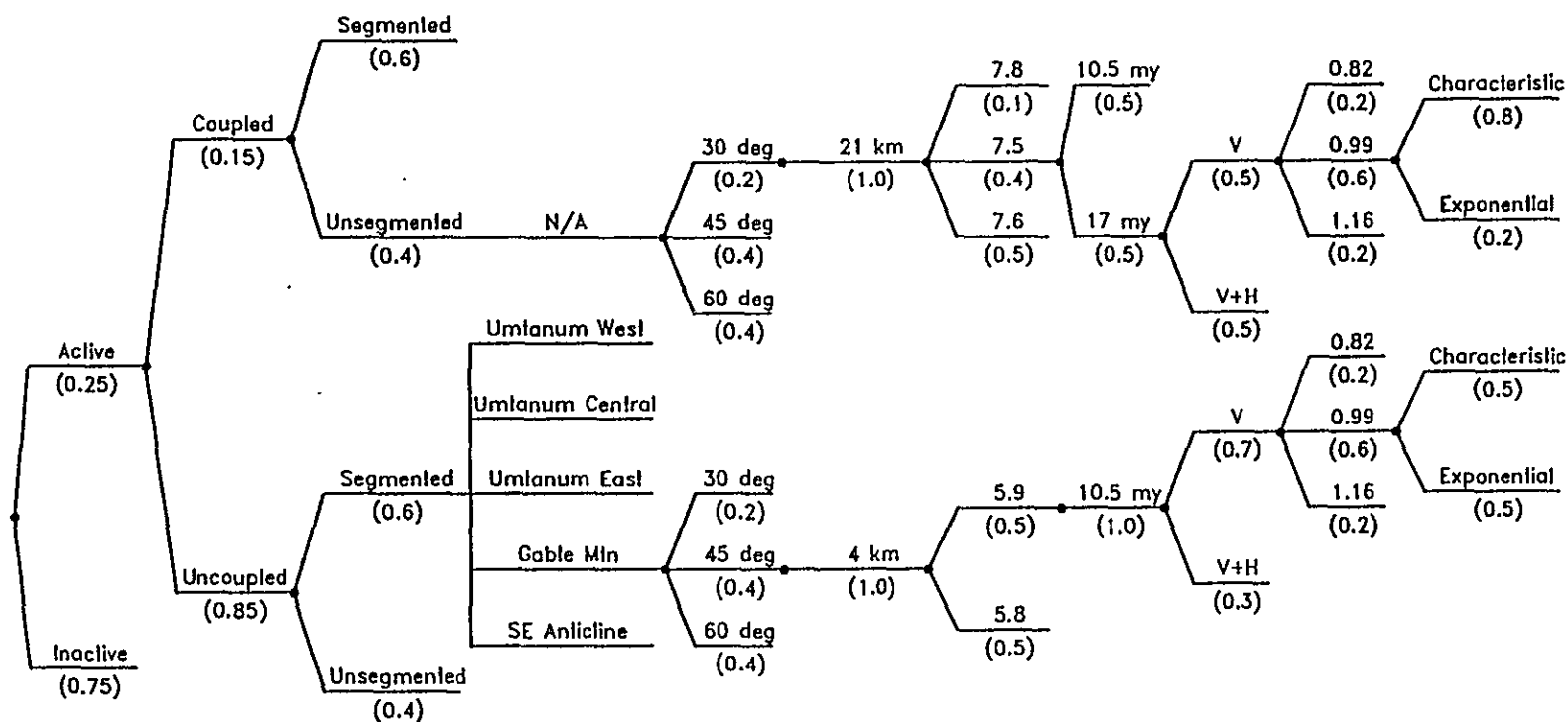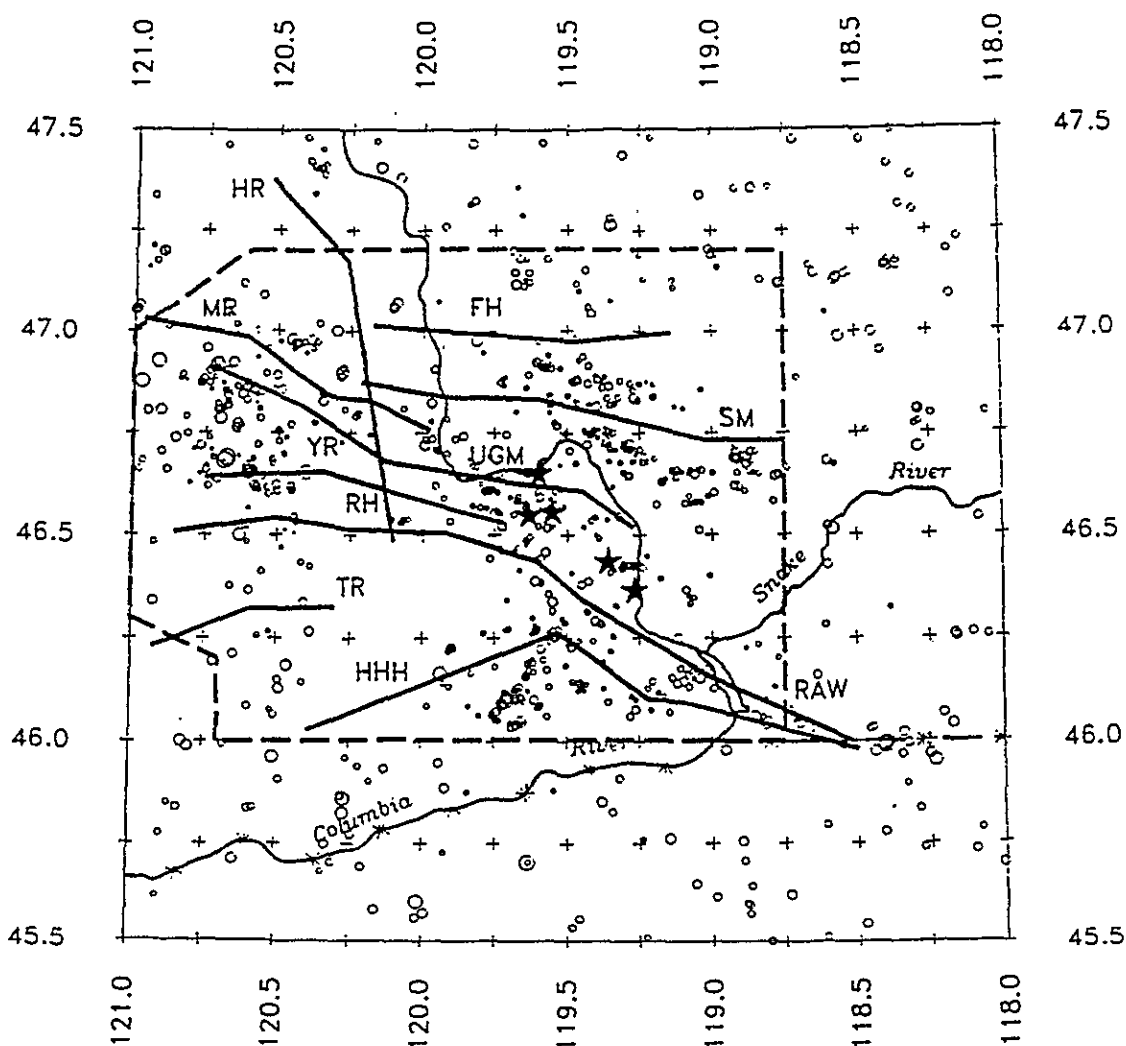| Activity	Coupling	Segmentation	Segments	Dip	Seismogenic Depth	Maximum Magnitude	Age	Technique	b-Value	Magnitude Distribution

Figure 3-10   Logic tree for Umtanum Ridge-Gable Mountain seismic source.

Figure 3-9   Location of major Yakima folds considered as potential seismic sources in the coupled model. Superimposed is the spatial distribution of seismicity for the time period of 01/1970-04/1990 occurring primarily within the crystalline basement (focal depth > 5 km).
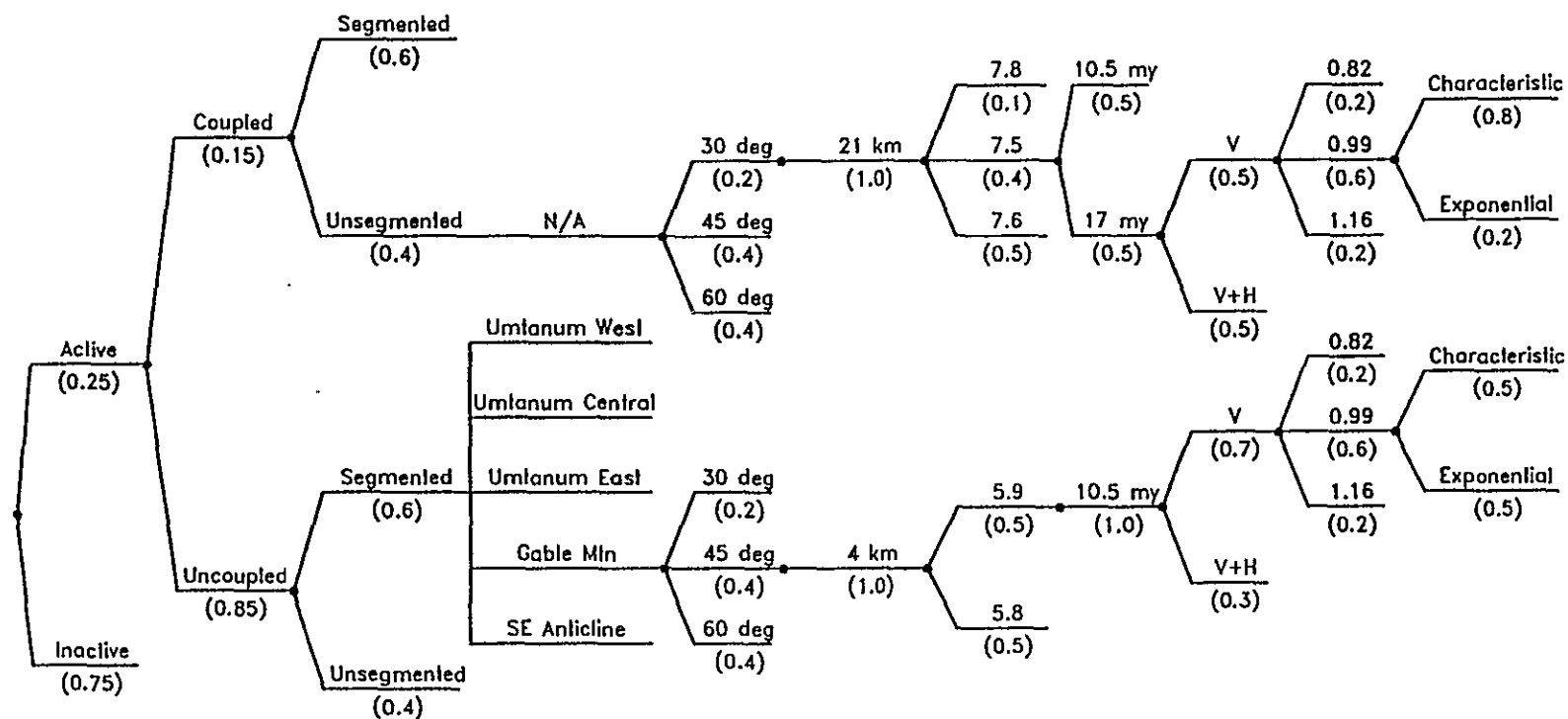
Figure 3-10   Logic tree for Umtanum Ridge-Gable Mountain seismic source.
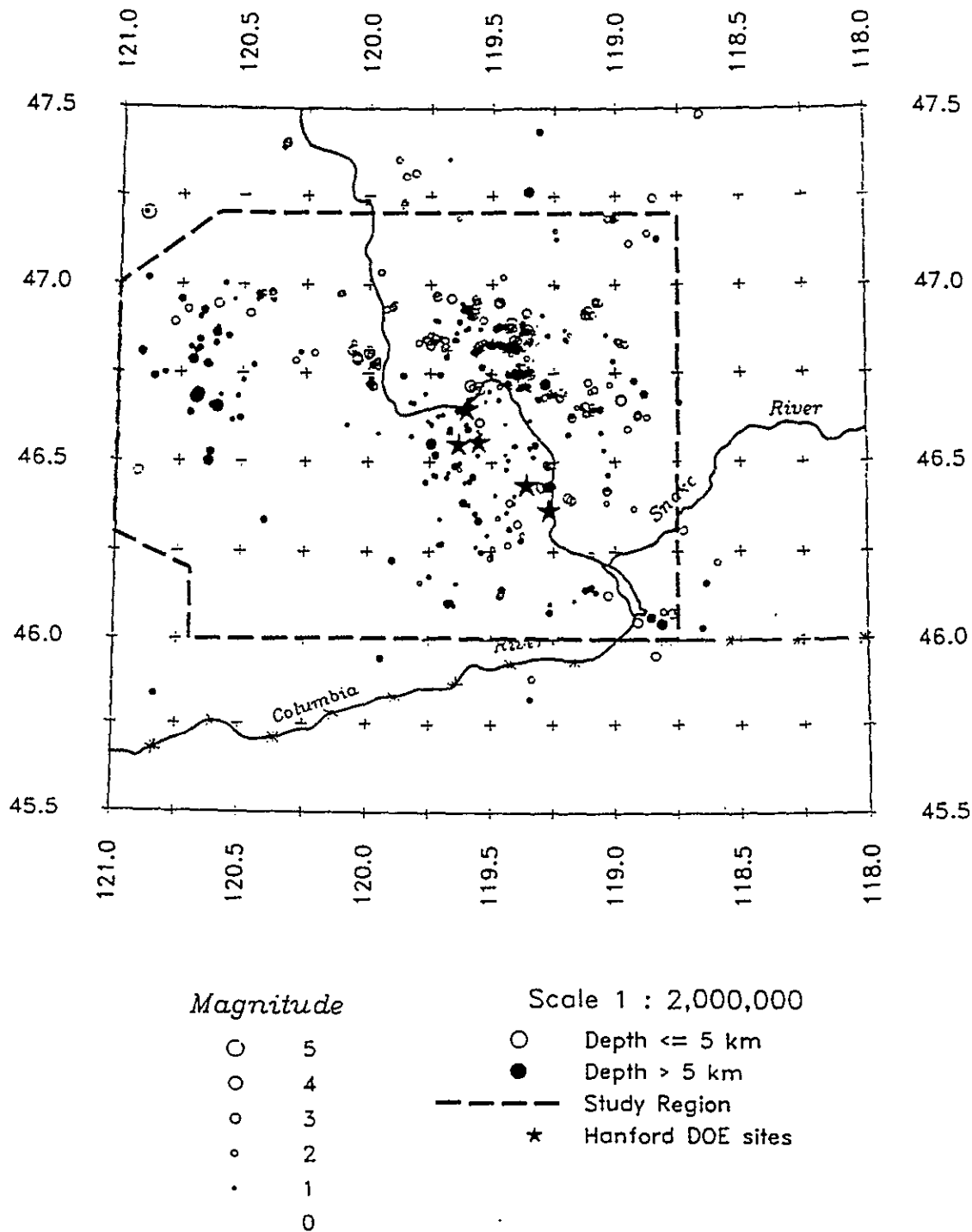
Figure 3-11 Spatial distribution of shallow and deep seismicity for earthquakes with well located hypocenters (standard error of location |≤ 1.0 km).

(a)

(b)

Figure 3-12 (a) Time history of deformation of Saddle Mountains (from Reidel and others, 1989). (b) Fraction of observed total deformation occurring post-10.5 Ma as a function of age of total deformation inferred from (a).
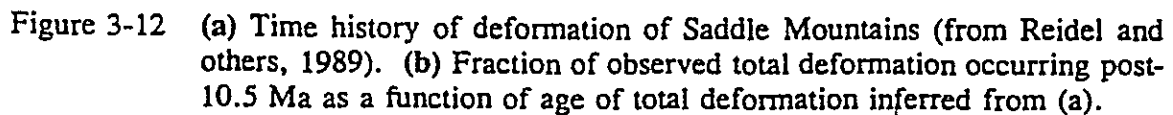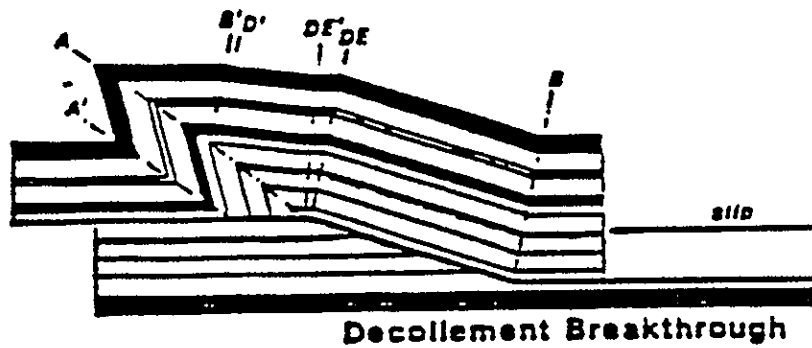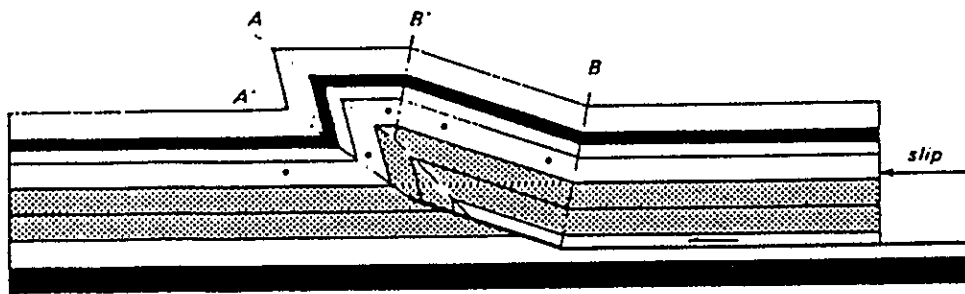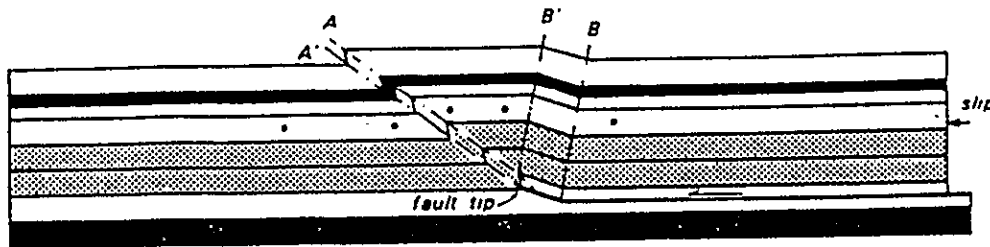
Figure 3-13   Evolution of fault-propagation fold into fault-bend fold by decollement breakthrough (modified from Suppe, 1988).

GEOMATRIX
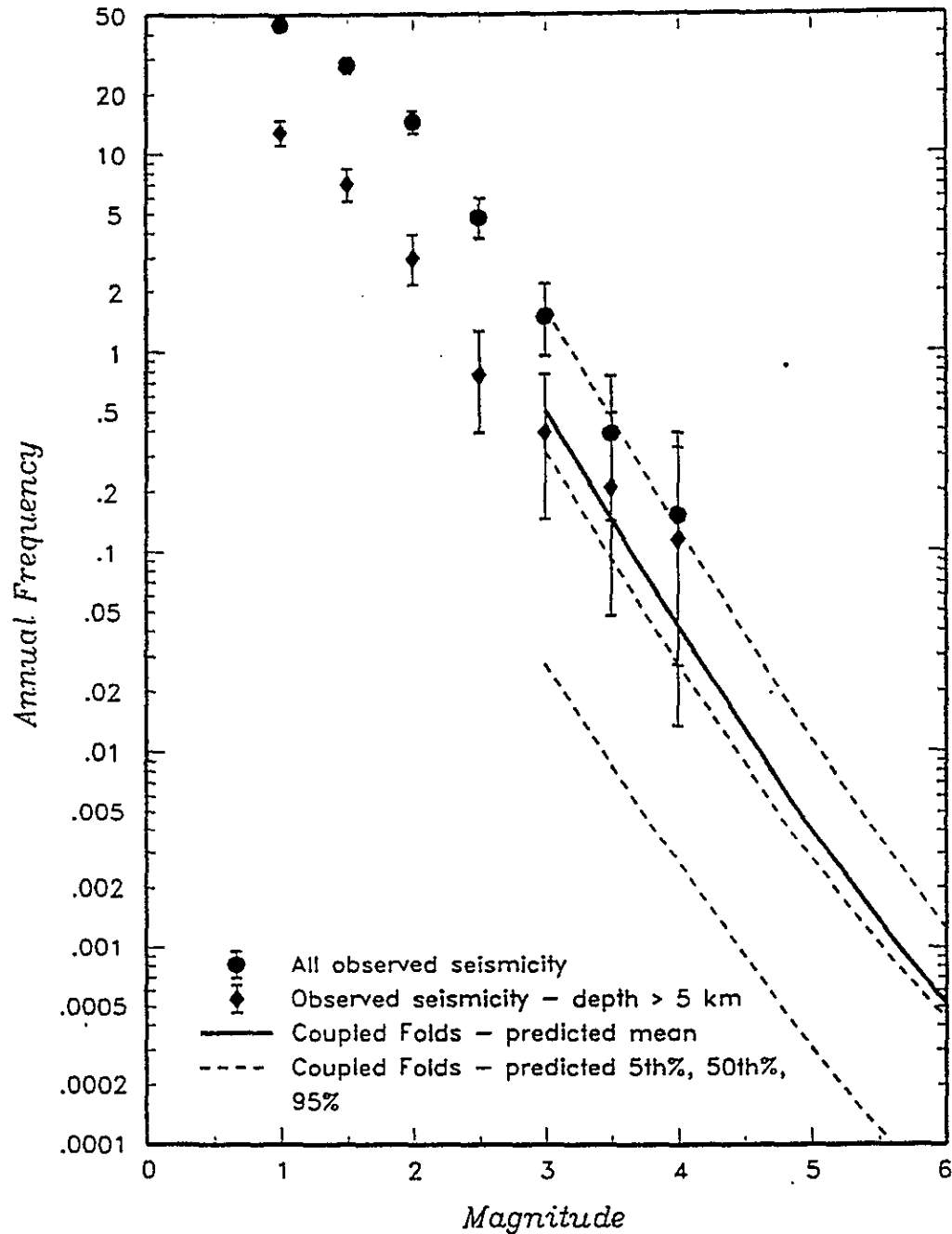
Figure 3-14 Comparison of observed seismicity for the central Yakima Fold Belt region with that predicted using the coupled fold model source parameters. The solid line represents the mean frequency of earthquakes predicted using the coupled models for the individual folds. The vertical error bars indicate 90-percent confidence intervals on the observed earthquake frequencies.

GEOMATRIX
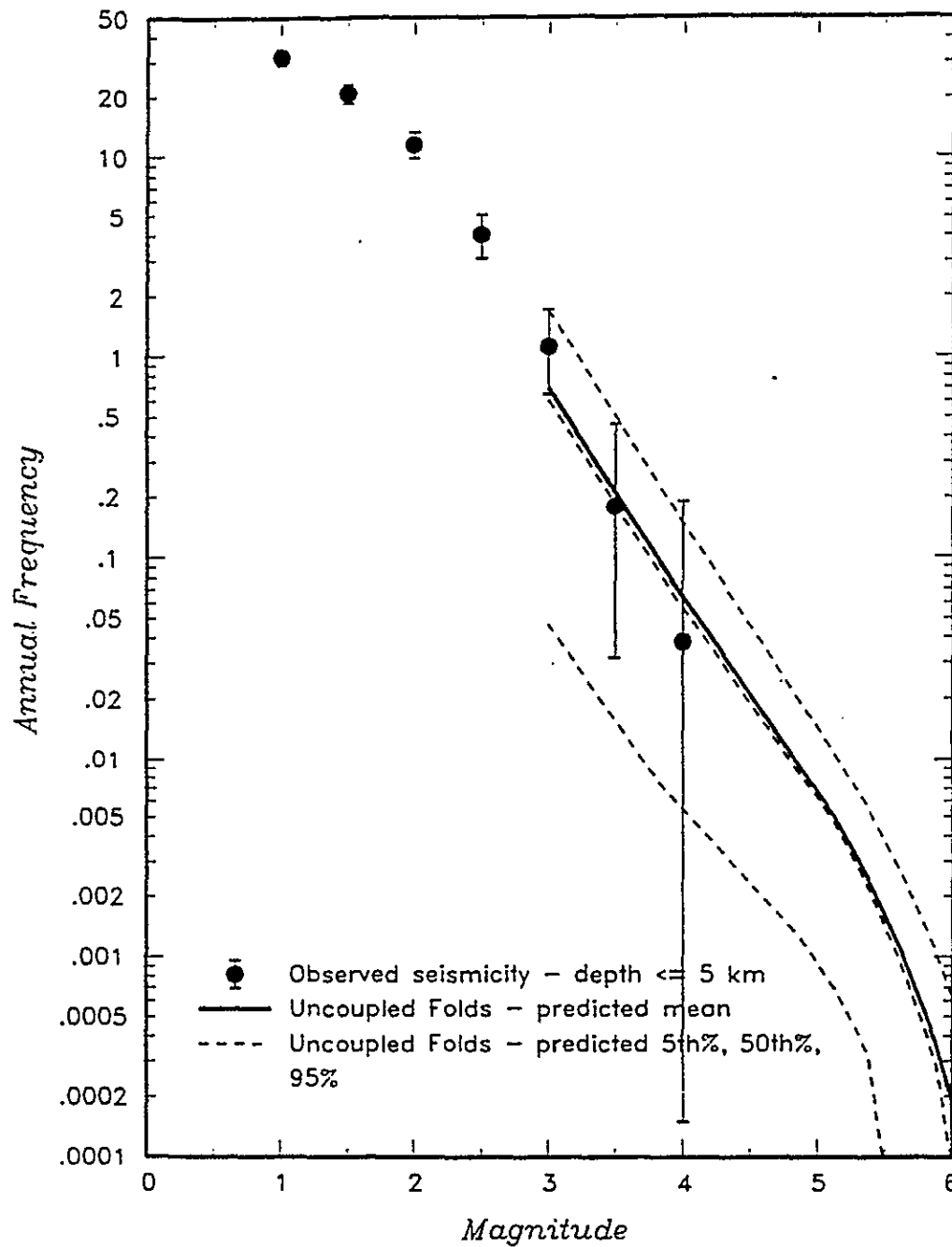
Figure 3-15 Comparison of observed shallow seismicity for the central Yakima Fold Belt region with that predicted using the uncoupled fold model source parameters. The heavy solid line represents the mean frequency of earthquakes predicted using the uncoupled models for the individual folds.

Spatial Distribution	Maximum Magnitude	N(m>5) (events/year)	b-Value	Magnitude Distribution

Uniform
(0.4)

4.5
(0.05)

0.0189
(0.026)

0.88
(0.048)

4.75
(0.25)

0.0122
(0.245)

0.94
(0.236)

Concentrated Zone
(0.5)

5.0
(0.35)

0.0079
(0.49)

1.01
(0.388)

Exponential
(1.0)

5.25
(0.25)

0.0051
(0.218)

1.07
(0.253)

5.5
(0.1)

0.0033
(0.021)

1.14
(0.075)

Smoothed observed
(0.1)
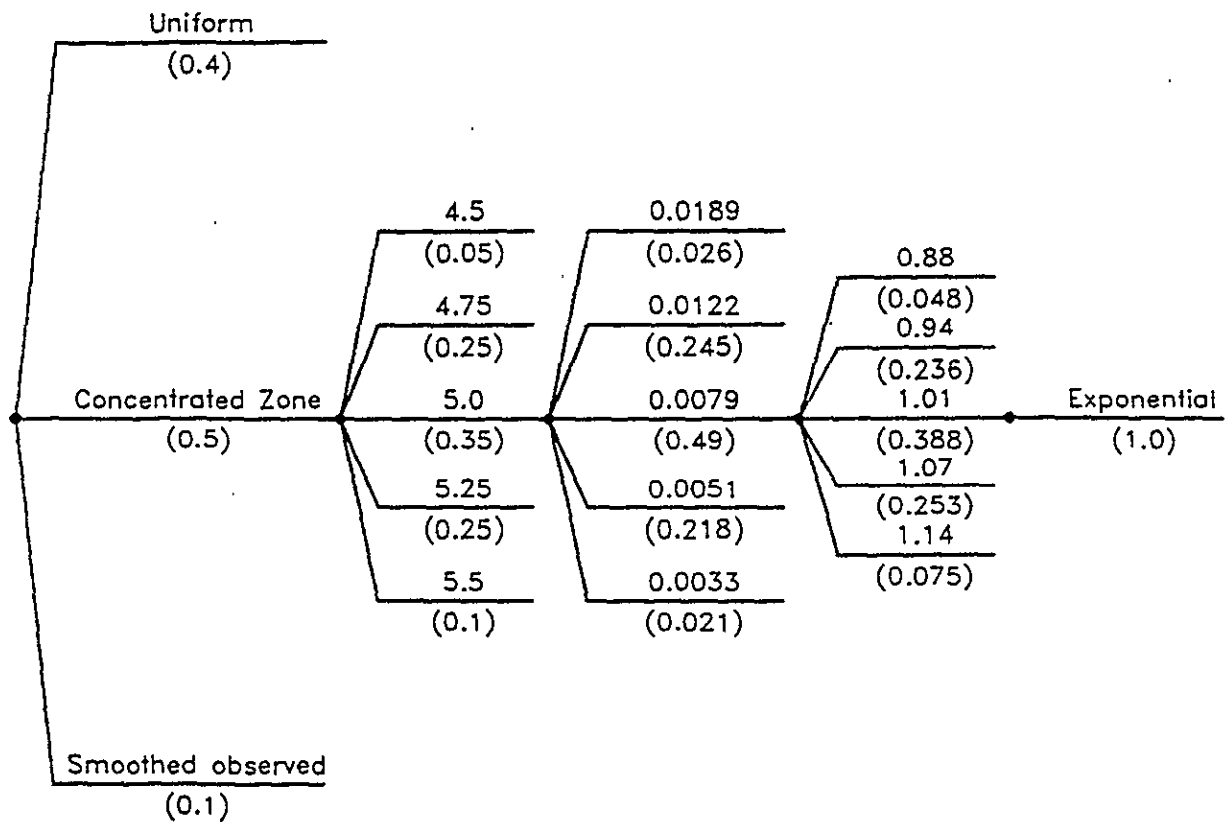
Figure 3-16   Logic tree for Columbia River Basalt seismic source.

Clusters

Magnitude

O	5
O	4
o	3
○	2
·	1

Scale 1 : 2,000,000

— — — — Study Region

★ Hanford DOE sites

● ● ● ● ● Uniform seismicity zone

— + — + Concentrated seismicity zone
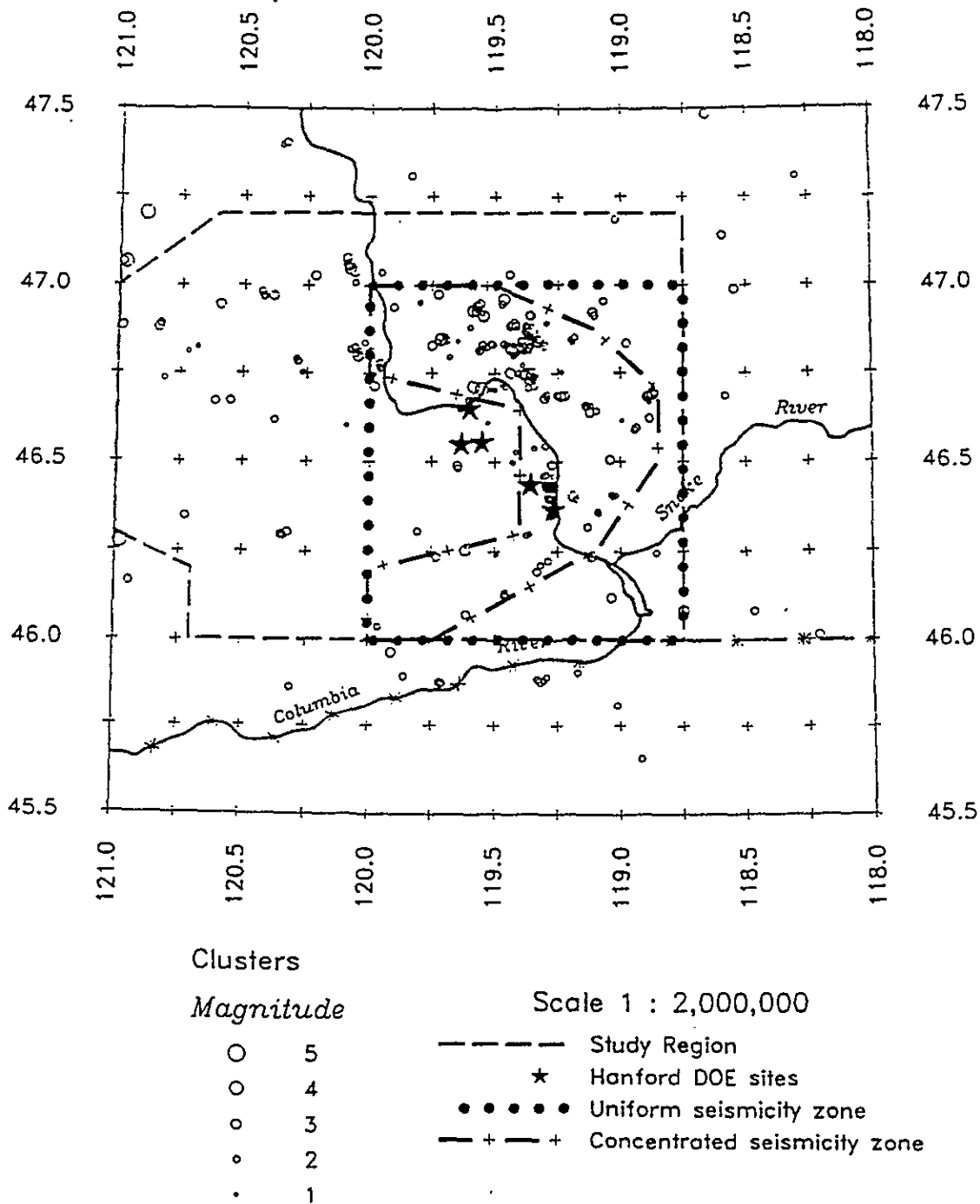
Figure 3-17   Spatial distribution of clusters (defined using the criteria of Johnson, 1989) within the shallow basalts. Also shown are the boundaries of the uniform seismicity zone and the concentrated seismicity zone.
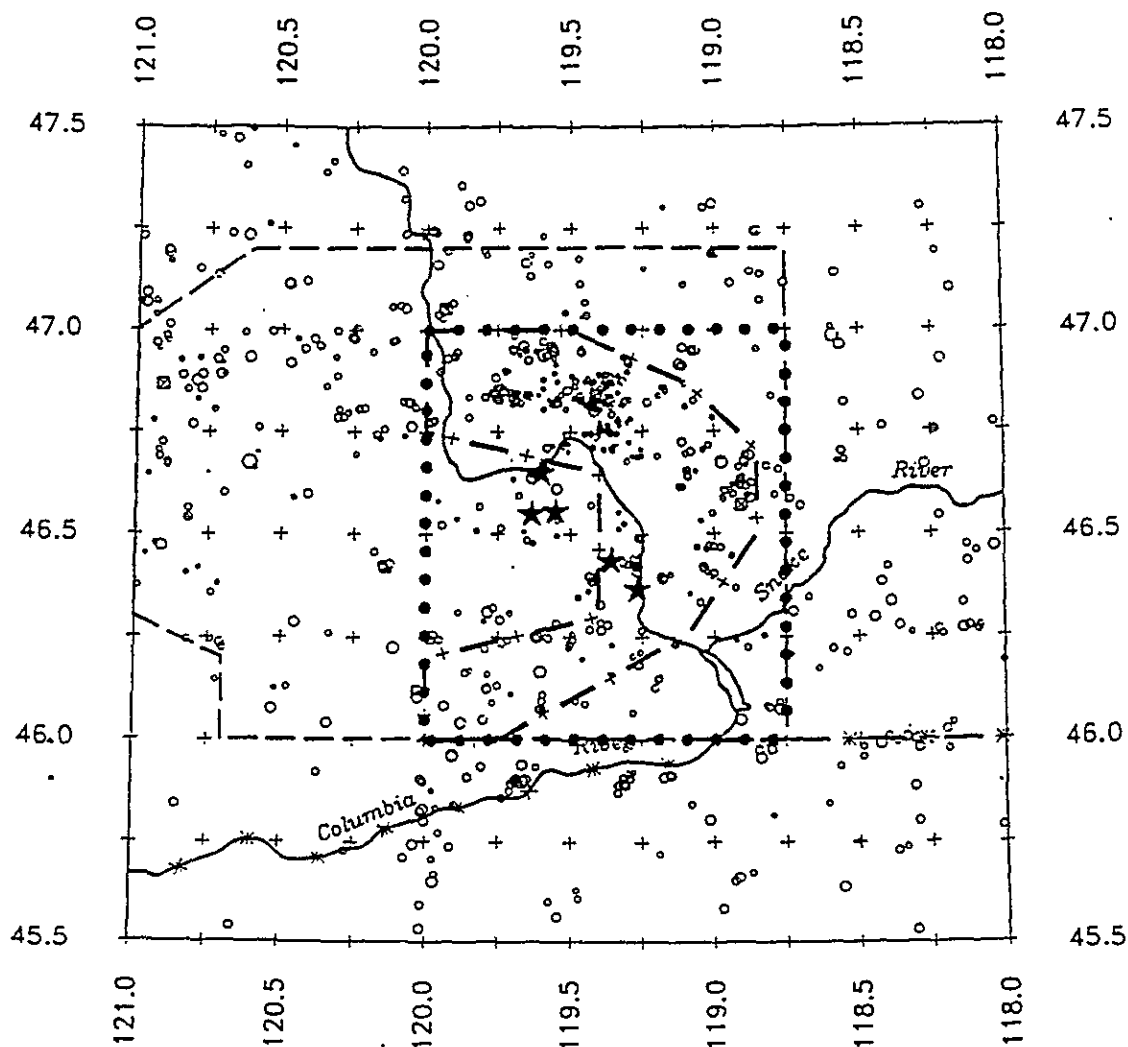
Single Events

Magnitude

		Scale 1 : 2,000,000
○	4	— — — — Study Region
○	3	★ Hanford DOE sites
○	2	●●●●● Uniform seismicity zone
·	1	— + — + Concentrated seismicity zone
	0	
⊠	N/A	

Figure 3-18   Spatial distribution of non-cluster earthquakes within the shallow basalts. Also shown are the boundaries of the uniform seismicity zone and the concentrated seismicity zone.
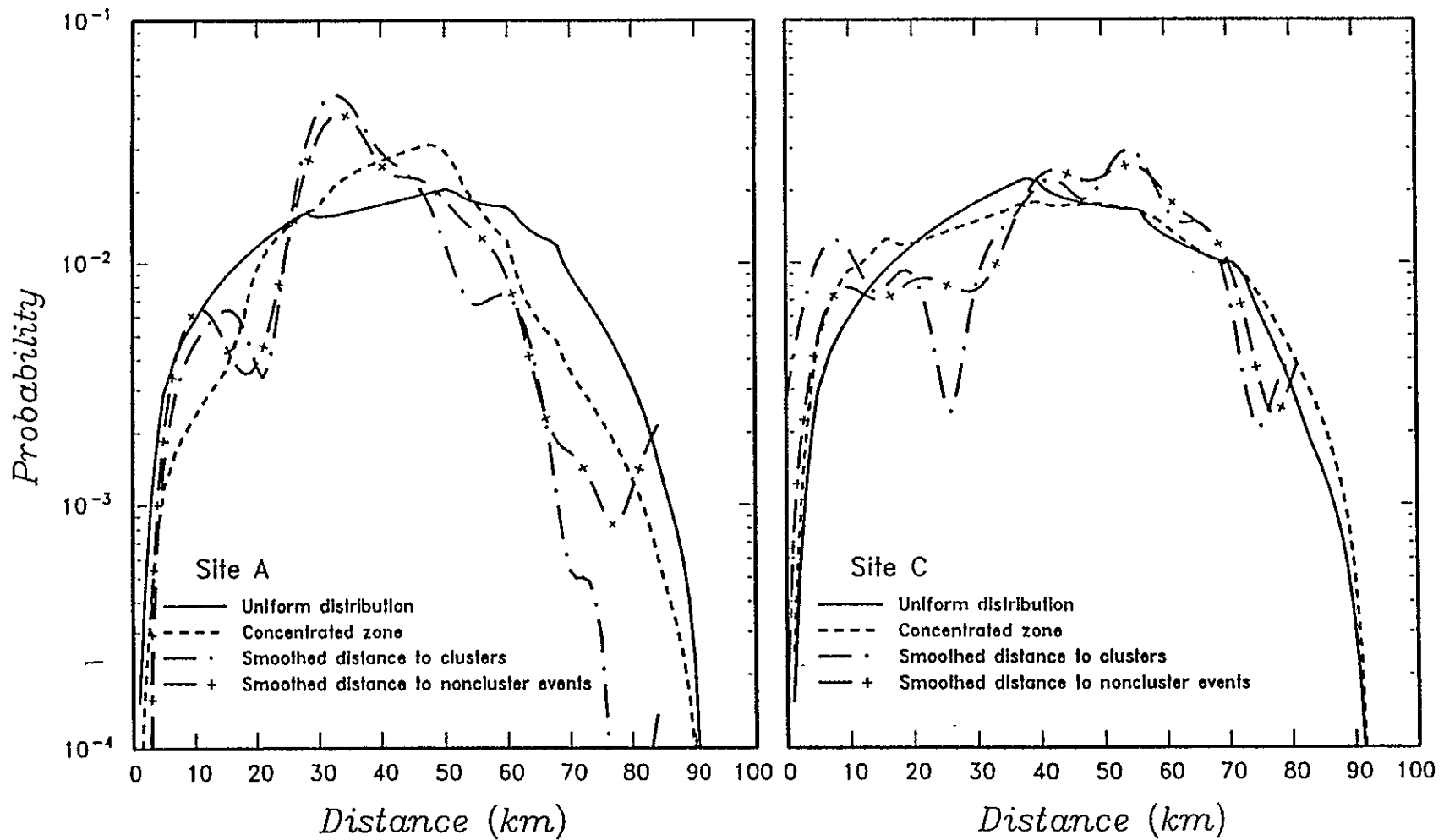
Figure 3-19 Distribution of distance to earthquakes within the shallow basalts to Sites A and C. Shown are the distributions assuming a random location within a uniform zone of seismicity, a concentrated zone, and smoothed distributions of the distances to observed cluster and non-cluster locations.

Tectonic Model	Sources	Activity	Rift Zone Geometry	Crustal Thickness (km)	Maximum Magnitude	Slip Rate/ N(m>3.75) (mm or events/year)	b-Value	Magnitude Distribution

Failed Rift (0.1)

Rift zone — Active (1.0)
Narrow (0.6)
Wide (0.4) — 12.5 (1.0)
6.5 (0.5)
7 (0.5)
0.23 (0.5)
0.29 (0.5)
0.80 (0.2)
0.95 (0.6)
1.10 (0.2)
Exponential (0.2)
Characteristic (0.8)

Adj Basement — Active (1.0) — N/A — 12.5 (1.0)
6 (0.4)
6.5 (0.5)
7 (0.1)
0.161 (0.028)
0.103 (0.258)
0.065 (0.489)
0.041 (0.205)
0.026 (0.02)
0.67 (0.038)
0.80 (0.229)
0.92 (0.388)
1.04 (0.259)
1.17 (0.086)
Exponential (1.0)

Block (0.1)

Basement — Active (1.0)
Faults A & B — Active (0.5) / Inactive (0.5)

Random (0.8)

Basement — Active (1.0) — N/A — 12.5 (1.0)
6 (0.4)
6.5 (0.5)
7 (0.1)
0.152 (0.027)
0.093 (0.255)
0.057 (0.489)
0.035 (0.208)
0.021 (0.021)
0.72 (0.04)
0.83 (0.231)
0.95 (0.388)
1.06 (0.258)
1.18 (0.083)
Exponential (1.0)

Figure 3-20   Logic tree for crystalline basement sources.

EXPLANATION

SP-3 Seismic refraction line and shot point locations of Catchings and Mooney (1985, 1988)

2 —— Residual Bouger gravity anomaly (contour interval equals 2 milligals)

★ Hanford DOE sites

▬ ▬ ▬ ▬ Inferred location of northwest-southeast trending rift margins from integration of CLEW lineament and seismic refraction data by Catchings and Mooney (1988)
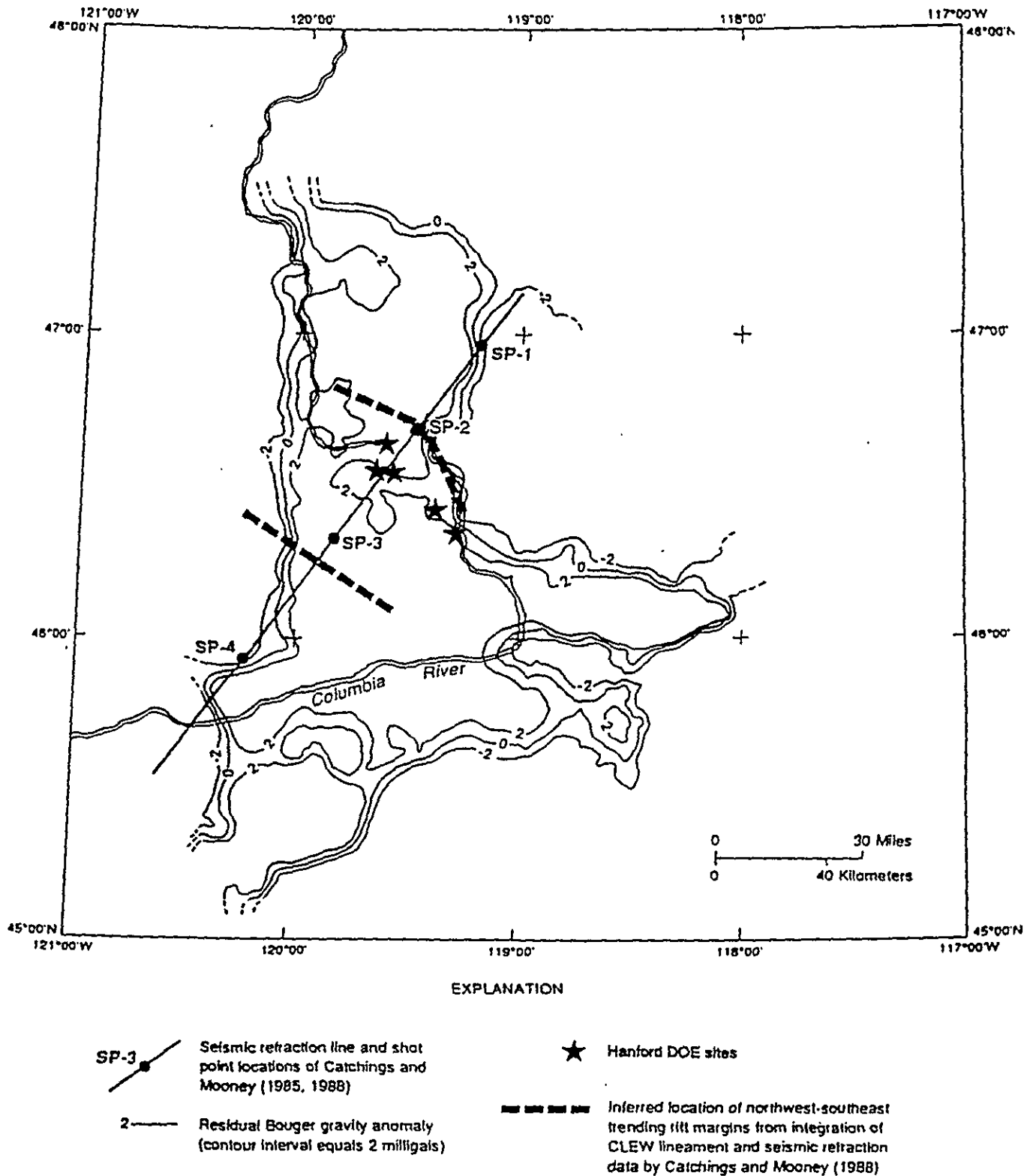
Figure 3-21 Superposition of refraction profile from Catchings and Mooney (1988) on gravity modeling from Weston Geophysical (1981). Heavy dashed lines show hypothesized rift orientation.

EXPLANATION

Saddle Mountains and Toppenish Ridge thrust faults; dashed where approximate; dotted where concealed; teeth on upper plate

Undifferentiated faults; dashed where approximate; teeth on upper plate

Anticline; dashed where approximate

Wide rift model

Narrow rift model

★   Hanford DOE sites

1000 ——— Thickness contours on sub-basalt sediments in meters (from Campbell, 1989)

Figure 3-22   Isopach of subbasalt sediment thickness.   Shown is the location of the inferred northwest-southeast oriented rift and the two folds with inferred Quaternary active faults.
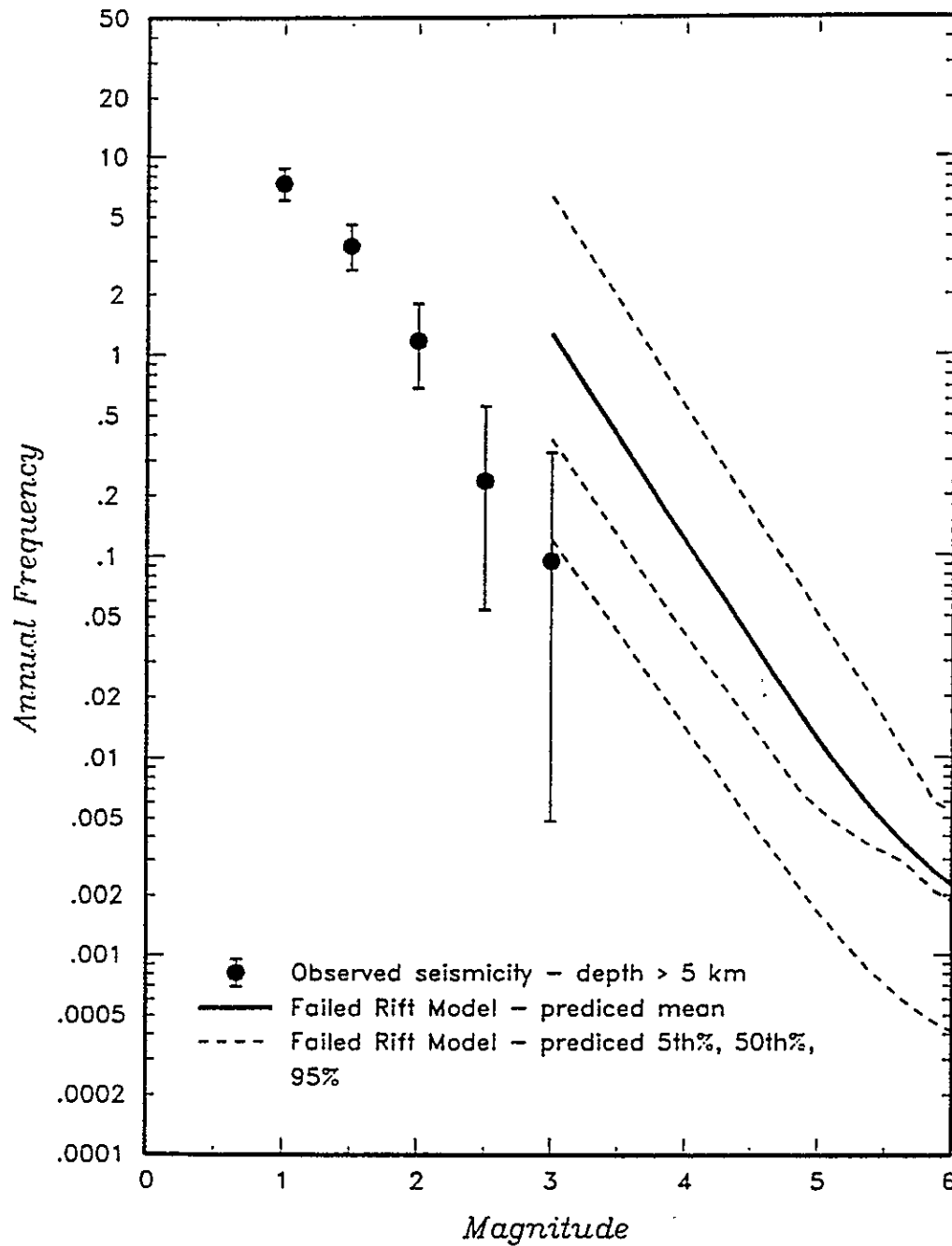
Figure 3-24   Comparison of observed seismicity for crystalline basement within region of inferred rift (depth greater than 5 km) with that predicted using the source parameters for the rift zone.

GEOMATRIX

Depth > 5 km

Magnitude

Scale 1 : 2,000,000

O	5
O	4
o	3
o	2
·	1
	0

★   Hanford DOE sites
● ● ● ● ●   Deep seismicity zone
— — — —   Basement Block
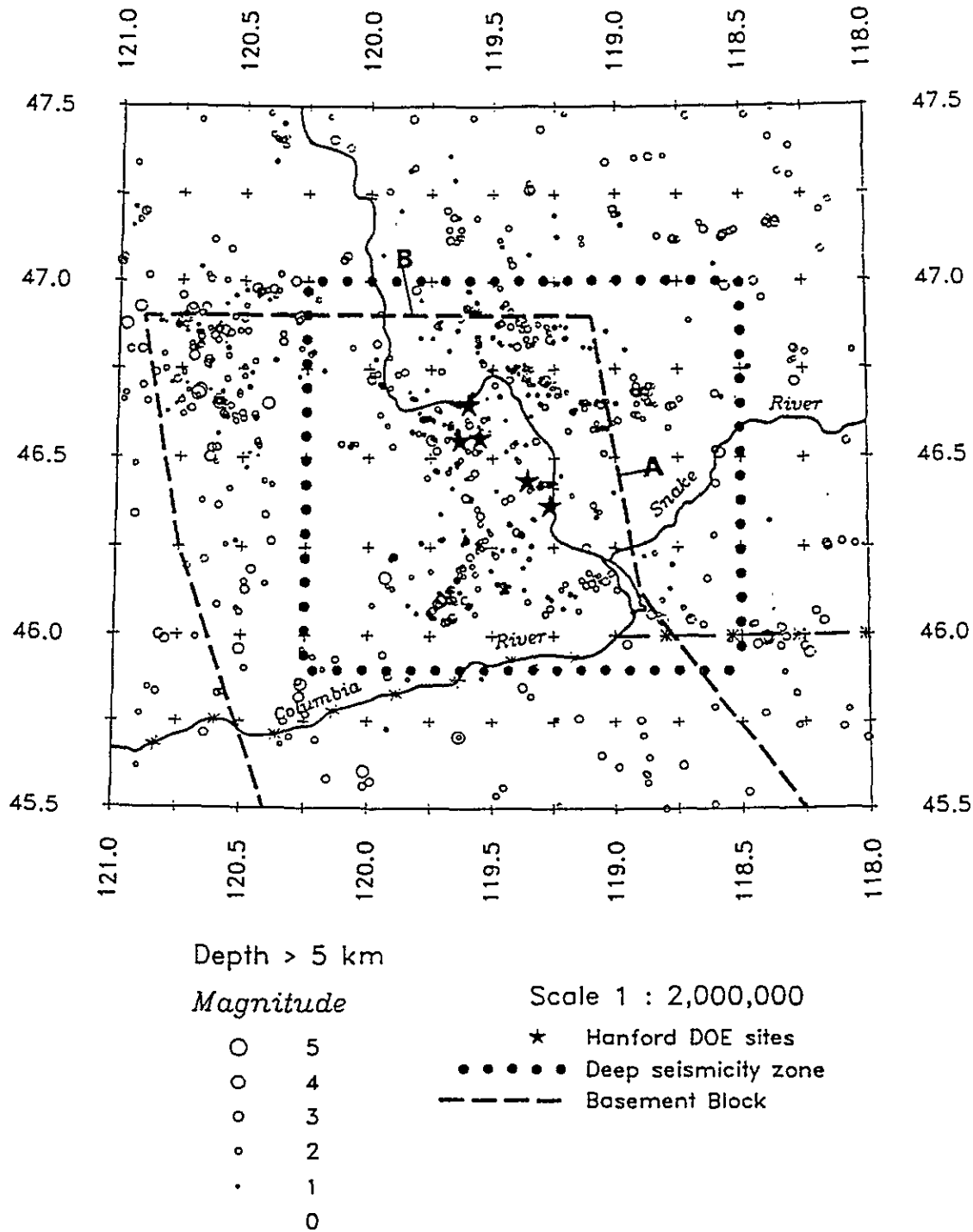
Figure 3-25   Spatial distribution of seismicity occurring within the crystalline basement compared with basement block structure.
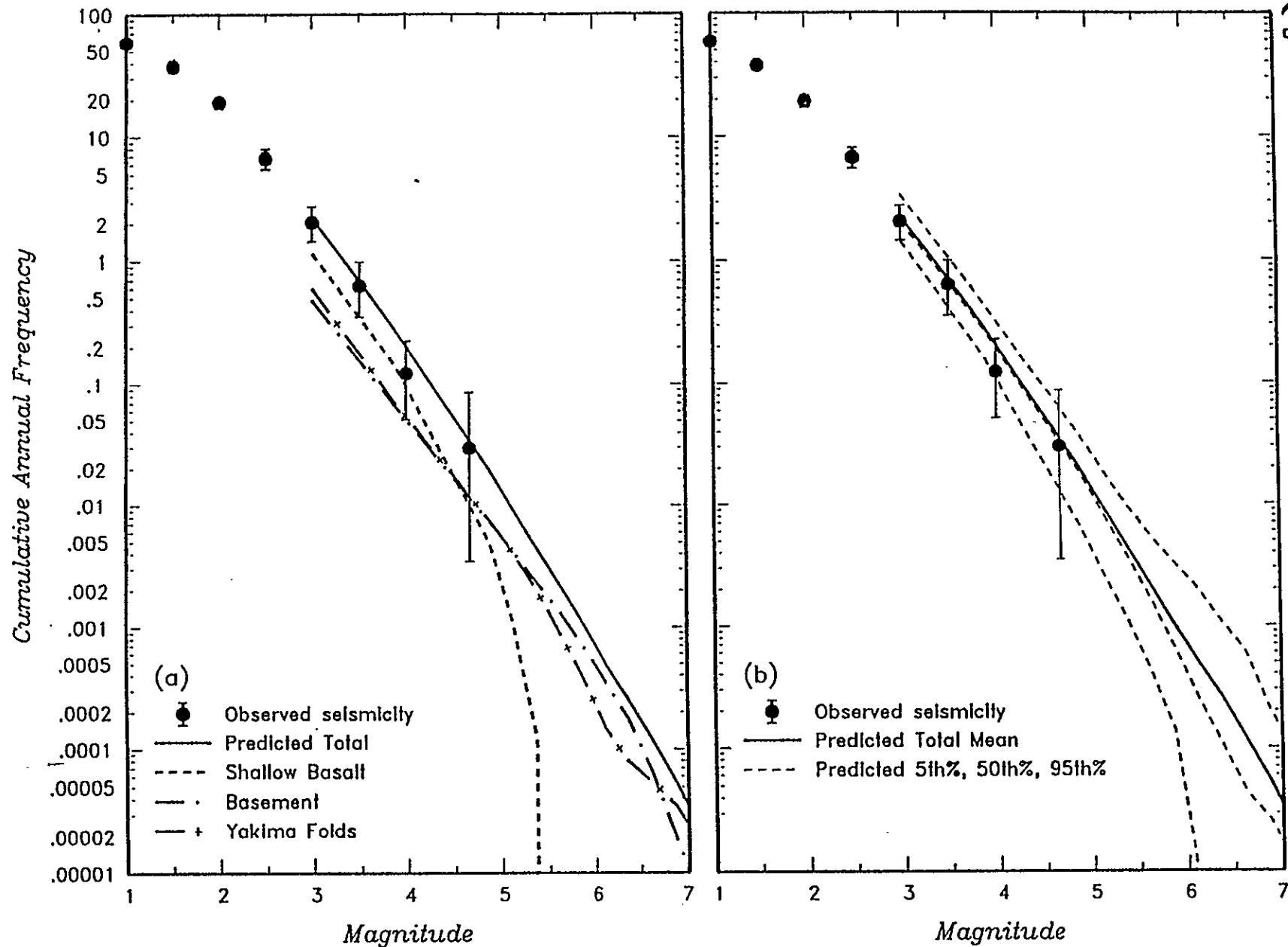
Figure 3-26 Comparison of observed earthquake frequencies for the study region (see Figure 3-1) for the time period of 1850 to April, 1991 with seismicity predicted by the seismic source model developed for this study. (a) Shows the contributions to the total predicted recurrence from the three source types and (b) shows the uncertainty intervals for the predicted recurrence.
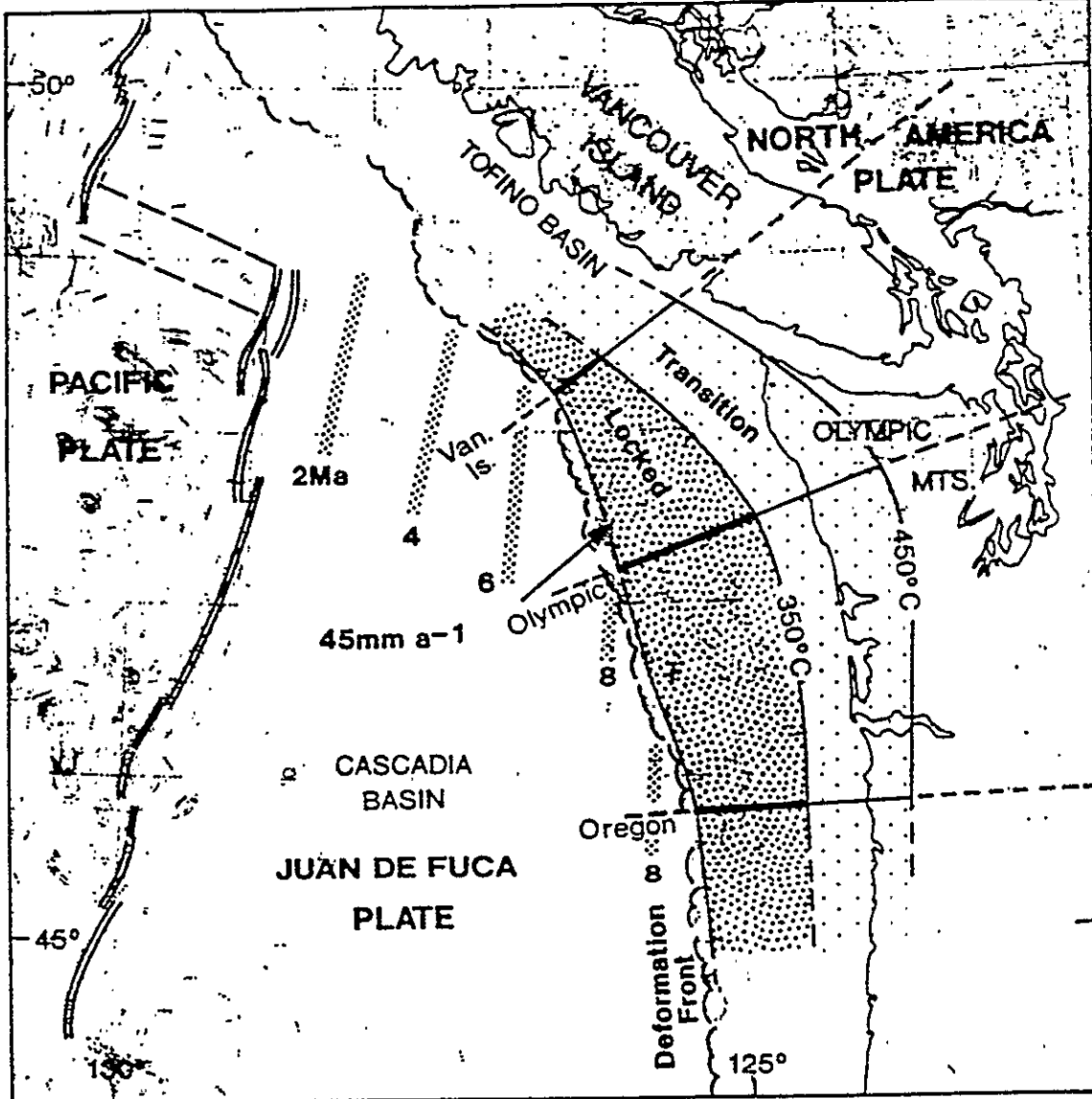
Figure 3-27   Cascadia margin area showing the locations of the three model profiles with the computed limits of stick-slip "locked" and stable sliding "transition" zones for the subduction thrust plate. The recognized uncertainties give error limits of about ±30 km in the landward boundaries of the locked and transition zones (Hyndman and Wang, 1993).

GEOMATRIX

Magnitude

5 ○
4 ○
3 ○
2 ○
1 .

○ 1971–1992

Scale 1:7,000,000
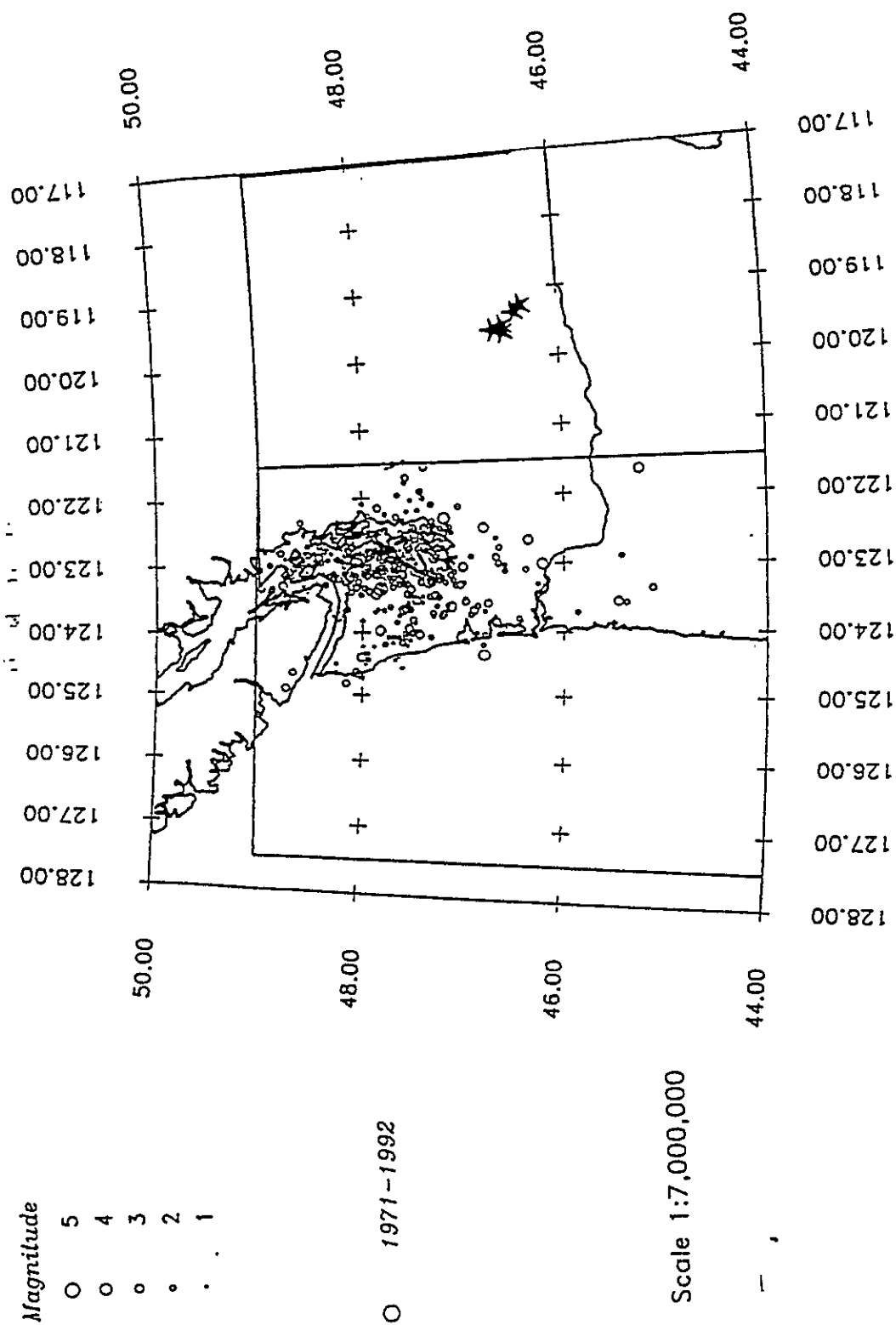
Figure 3-28   Location of Juan de Fuca plate seismicity and the intraslab source.

4.0 ATTENUATION RELATIONSHIPS

4.1 SELECTION OF APPROPRIATE RELATIONSHIPS

Strong ground motions produced by earthquakes are influenced by the characteristics of the earthquake source, the crustal wave propagation path, and the local site geology. At present, no strong motion data have been recorded in the study region with which one can evaluate these characteristics. Therefore, empirical attenuation models from regions considered to have similar characteristics have been used to evaluate the ground motion hazard.

The source and travel path characteristics of a region are a function of the general tectonic environment. The Hanford site lies at the eastern edge of the plate boundary between North America and the Pacific and Juan de Fuca plates. The limited data from earthquakes occurring to the west of the site in northern Oregon, indicated that the source characteristics, as measured by the relationship between local magnitude, M_L and seismic moment are similar to those of California earthquakes (see Section 3.1.2). Regional measurement of the effects of scattering and absorption along the crustal travel path of seismic waves (parameterized by Q) indicate that the attenuation of seismic waves may be somewhat less in eastern Washington than in California (Singh and Herrmann, 1983). However, studies conducted by the University of Washington (1986) found Q values for eastern Washington comparable or lower to those reported in California. Studies by Campbell (1987) have shown that the tectonic environment (extensional versus compressional stress regime) has little effect on California strong motion data. Indeed, empirical ground motion models developed from shallow crustal earthquake data recorded in the active areas of the Mediterranean Basin also are similar to those developed from California strong motion data (Ambraseys and Bommer, 1991). Youngs and others (1987) have also shown that the influence of difference in crustal path characteristics between those of California and those of Utah, which exhibits less attenuation (higher Q) than eastern Washington, has little impact on seismic hazards in regions where the hazard is due primarily to nearby sources. On this basis, it was judged that empirical strong motion models based primarily on California strong motion data would be appropriate to represent the effects of source and travel path for eastern Washington earthquakes.

The Hanford DOE sites are underlain by stiff to very stiff alluvial soils overlying the Columbia River basalts. Depth to basalt varies in the range of 200 to 600 ft. The alluvial soils consist of Holocene loess, and Pleistocene and Holocene sands and gravels underlain by the Ringold formation, which consists of dense gravels and gravelly silts and clays. Locally the Ringold unit is cemented and exhibits shear wave velocities in excess of 4,000 ft/sec. As part of the studies conducted for the WNP-2 commercial nuclear power plant located on the Hanford Reservation, Washington Public Power Supply System (1985) performed comparative site response studies using the soil velocity profile at the WNP-2 site and typical firm alluvial soil profiles representative of California strong motion recording sites. The conclusion of that analysis was that the empirical strong motion data from firm alluvial sites in California was appropriate for use at Hanford. This conclusion was adopted for this study. Studies are currently underway to support this assumption for the specific profiles at the five DOE sites listed in Section 1.

Power and others (1981) developed attenuation relationships for the application to the Hanford region based on regression analyses of reverse faulting strong motion data, primarily from California. That work was extended to include both strike slip and reverse faulting earthquakes recorded on soil and rock sites and has been published by Sadigh and others (1986). The Sadigh and others relationships are considered to supersede those developed by Power and others (1981). To represent the uncertainty in modeling ground motions in the region, additional attenuation relationships were used as discussed below.

4.2 RELATIONSHIPS FOR SHALLOW CRUSTAL EARTHQUAKES

Three sets of attenuation relationships were selected for use in characterizing the ground motions at the Hanford DOE sites: Joyner and Boore (1982), Sadigh and others (1986), and Campbell (1993). The relationships developed by Sadigh and others (1986) and Campbell (1993) represent the latest efforts of researchers to analyze the available recorded strong motion data on soil sites, and those of Campbell (1993) developed out of work performed for the seismic safety review of the Diablo Canyon Nuclear Power Plant. The relationships developed by Sadigh and others (1986) were found to be consistent with recently recorded

strong motion data, including data recorded during the 1989 Loma Prieta earthquake. The
Sadigh and others (1986) relationships incorporate magnitude-dependent values of the standard
error in peak ground motion values. These standard error relationships were modified to
incorporate the standard error estimates provided in Youngs and others (1990, in review).
The relationships developed by Campbell (1993) are based primarily on recordings on soil
sites from well studied earthquakes. The relationships developed by Joyner and Boore (1982)
are less current than the other two, but they are a standard by which many other relationships
are evaluated, and they represent an alternative approach to modeling the empirical data.

Figure 4-1 compares the three sets of median peak horizontal acceleration relationships for
magnitude 5, 6, and 7 earthquakes. The comparisons shown are in terms of surface distance
to a vertical reverse fault. The relationships developed by Joyner and Boore (1982) and
Sadigh and others (1986) are in terms of moment magnitude, M. The relationships developed
by Campbell (1993) use M_L for magnitudes less than 6 and M_S for magnitudes greater than 6.
These measures can be considered essentially equivalent to M in terms of both the original
definition of M (Hanks and Kanamori, 1979) and the uniform moment magnitude scale used
in this study (see Section 3.1.2). As can be seen, all three relationships yield similar
estimates, except at close distances to the fault.

Part of the differences at close source-to-site distances is due to the different distance measures
used by the three sets of relationships. Joyner and Boore (1982) use closest distance to the
surface projection of the earthquake rupture. Sadigh and others (1986) use the closest distance
to the fault rupture plane. Campbell (1993) uses the closest distance to the fault rupture plane
at a depth where high frequency seismic waves can be generated (typically at depths of 2 to
4 km). The curves shown on Figure 4-1 for the Campbell (1993) relationship have been
adjusted to reflect the closest distance to the surface trace of a vertical fault, assuming a 3-km
depth for the minimum depth of seismogenic rupture. Use of the three relationships provides
a measure of the uncertainty in modeling earthquake ground motions in the near field.

Campbell (1993) includes a term to account for the effect of depth to basement rock (interpreted to be rock with a compression wave velocity in excess of 5 km/sec) on ground motions. Based on the crustal model presented in Rohay and Malone (1983) the depth to basement rock is approximately 0.6 km in the vicinity of the sites analyzed in this study. However, the site conditions for the recordings analyzed by Campbell did not include those representative of Hanford, that is a hard rock (basalt) layer over softer sedimentary rock. An alternative interpretation could be made the Campbell's depth term should refer to the depth to crystalline basement rocks. In this case, the value should be 8 km. Both depth terms were considered in computing the hazard.

Figure 4-2 compares the median 5%-damped response spectra predicted by the three sets of relationships for magnitude 5, 6, and 7 events at a distance of 15 km. The response spectra were developed by considering that peak acceleration represents spectral acceleration at a frequency of 30 Hz (period of 0.033 seconds). The three sets of spectral acceleration attenuation relationships show more variability than the peak acceleration relationships, reflecting differences in the form of the attenuation model and consideration of additional parameters. For example, the Campbell (1993) relationship considers the effect of depth to basement on long period motions, with greater depths leading to higher long period motion. The use of a shallow depth to basement for the Hanford sites (~0.6 km) leads to generally lower long period motions than obtained by the other two relationships, which do not account for this effect. If a deep depth to basement (8 km) is used, then the Campbell (1993) relationship predicts long period ground motion levels similar to the other two relationships.

Figure 4-3 compares the estimates of the standard error in the natural log of peak ground motion used by each of the three relationships. As noted above, the standard error for the Sadigh and others (1986) relationships vary with earthquake magnitude.

The weighting applied to the three sets of relationships was: 0.4 for Sadigh and others (1986), 0.4 for Campbell (1993), and 0.2 for Joyner and Boore (1982). The Sadigh and others (1986) and Campbell (1993) relationships were weighed equally because they incorporate most of the

latest strong ground motion data and represent some of the latest efforts to model strong ground motions The Joyner and Boore (1982) relationships were given lower weight for two reasons. First, the formulation employed assumes that the energy release occurs at an average depth of about 5 to 8 km. This is appropriated for most California earthquakes, but does not represent the conditions at Hanford. In this study the shallow crustal earthquakes are likely to be either occurring at depths less than 5 km with the Columbia River Basalts, or at depths of 8 to 21 km in the crystalline basement rocks. The other two attenuation relationships utilize a more direct measure of the distance to rupture which accounts for the different depths of the two sources. Second, the Joyner and Boore (1982) relationships do not account for the effect of fault-rupture type, which has been found to be a significant parameter in more recent studies. In applying the Campbell (1993) relationship, depth terms of 0.6 and 8 km were used. The two results were given equal weight in the combined analysis.

4.3 RELATIONSHIPS FOR SUBDUCTION ZONE EARTHQUAKES

The most up-to-date attenuation relationship developed for estimating ground motions on firm soil sites from subduction zone earthquakes is that developed by Crouse (1991). Crouse's relationship is based on regression analysis of strong motion data recorded in Mexico, South America, Alaska, and Japan. Figure 4-4 compares the peak acceleration attenuation relationship of Crouse (1991) with that for shallow crustal earthquakes. As indicated, subduction zone earthquakes produce significantly larger ground motions at large distances than do crustal earthquakes. Crouse (1991) also developed relationships for spectral ordinates. He did not develop a relationship for 0.3 sec and period. Coefficients for this period were interpolated from those of the adjacent periods to maintain a smooth spectral shape. Crouse 91991) includes a term to account for focal depth of the earthquakes. A depth of 25 km was used for interface earthquakes and a depth of 55 km was used for the intraslab earthquakes.
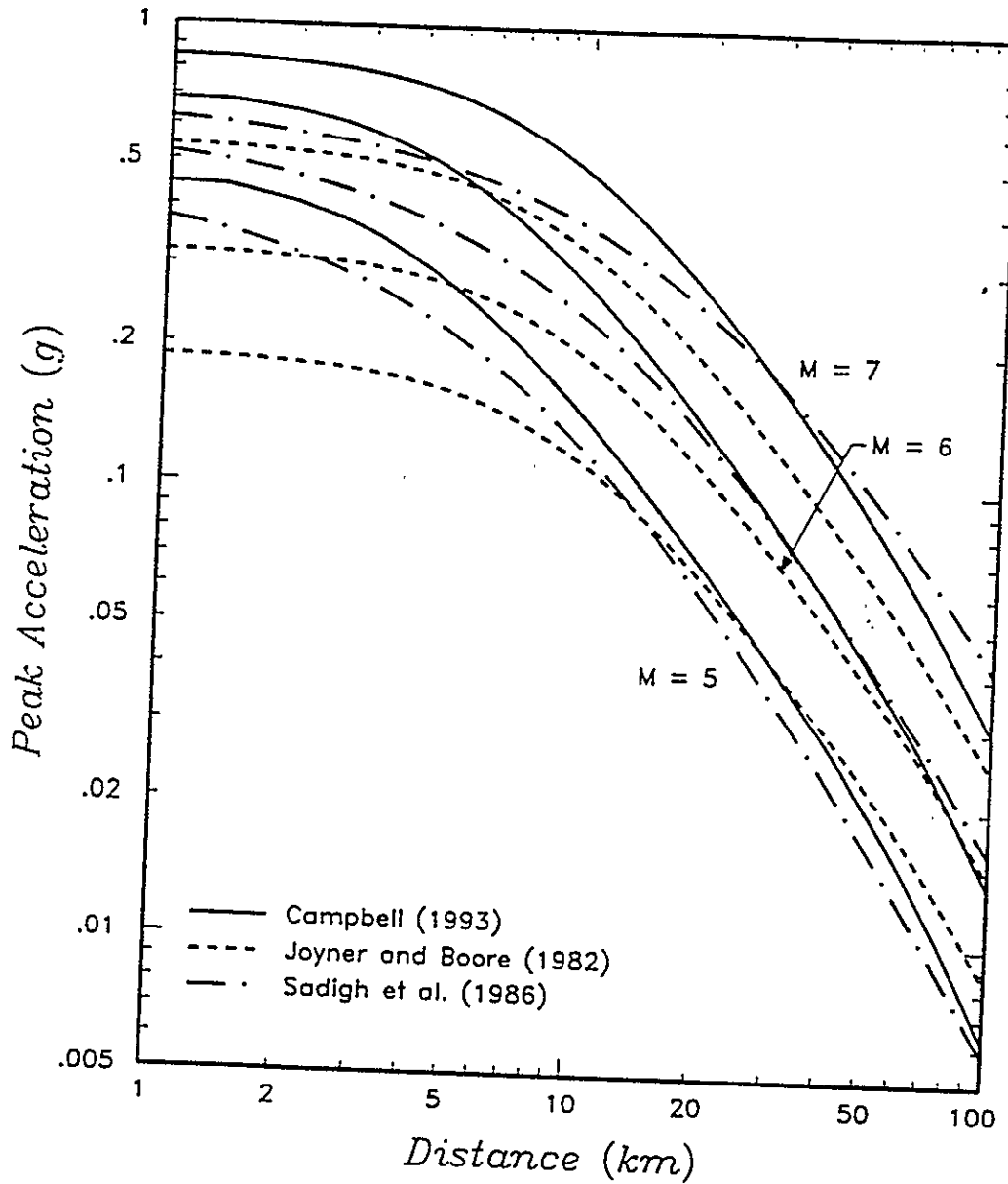
GEOMATRI

Figure 4-1   Comparison of empirical peak attenuation and acceleration relationships used in analysis.
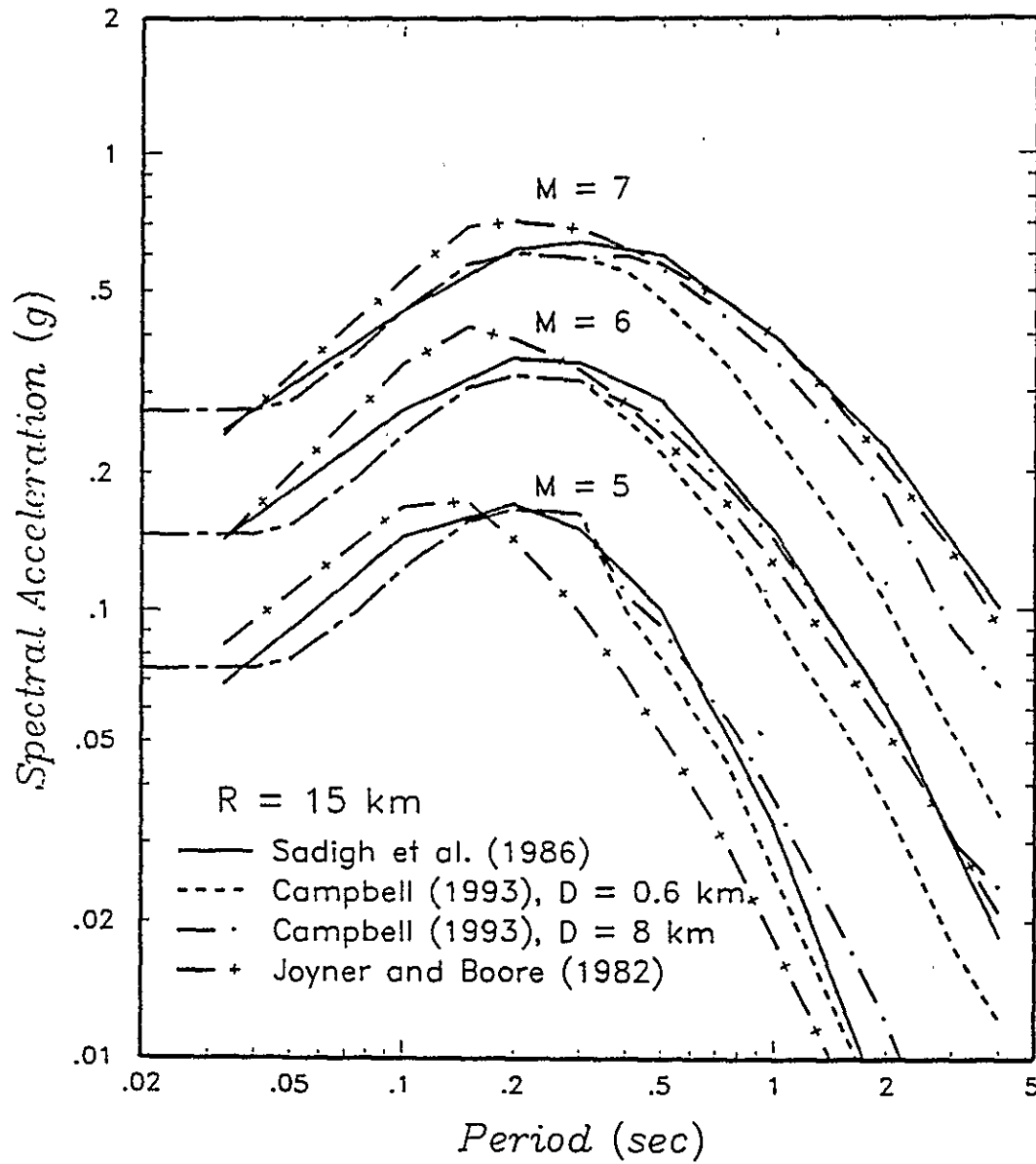
Figure 4-2   Comparison of 5-percent damped response spectra predicted using the attenuation relationships used in this study.
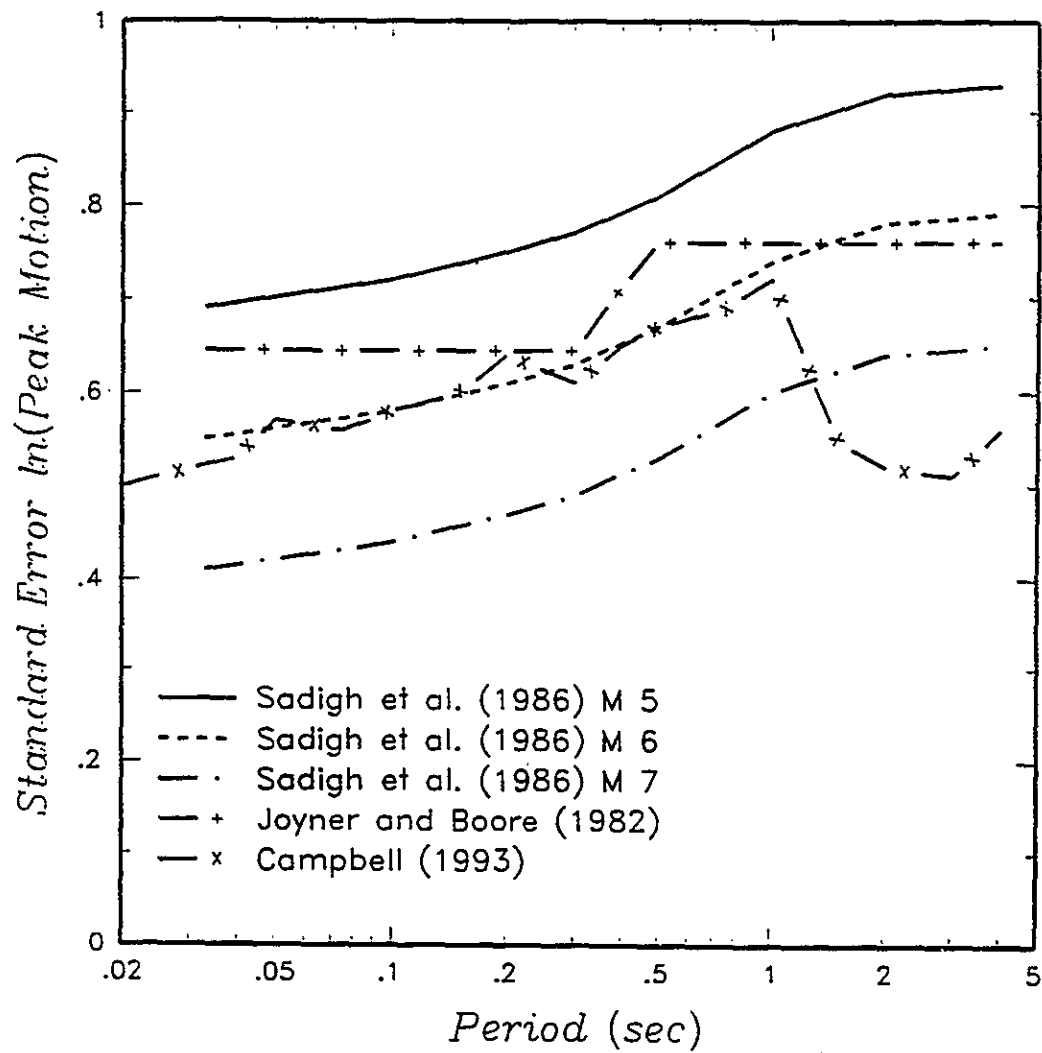
Figure 4-3   Comparison of the standard error in the natural log of peak ground motion
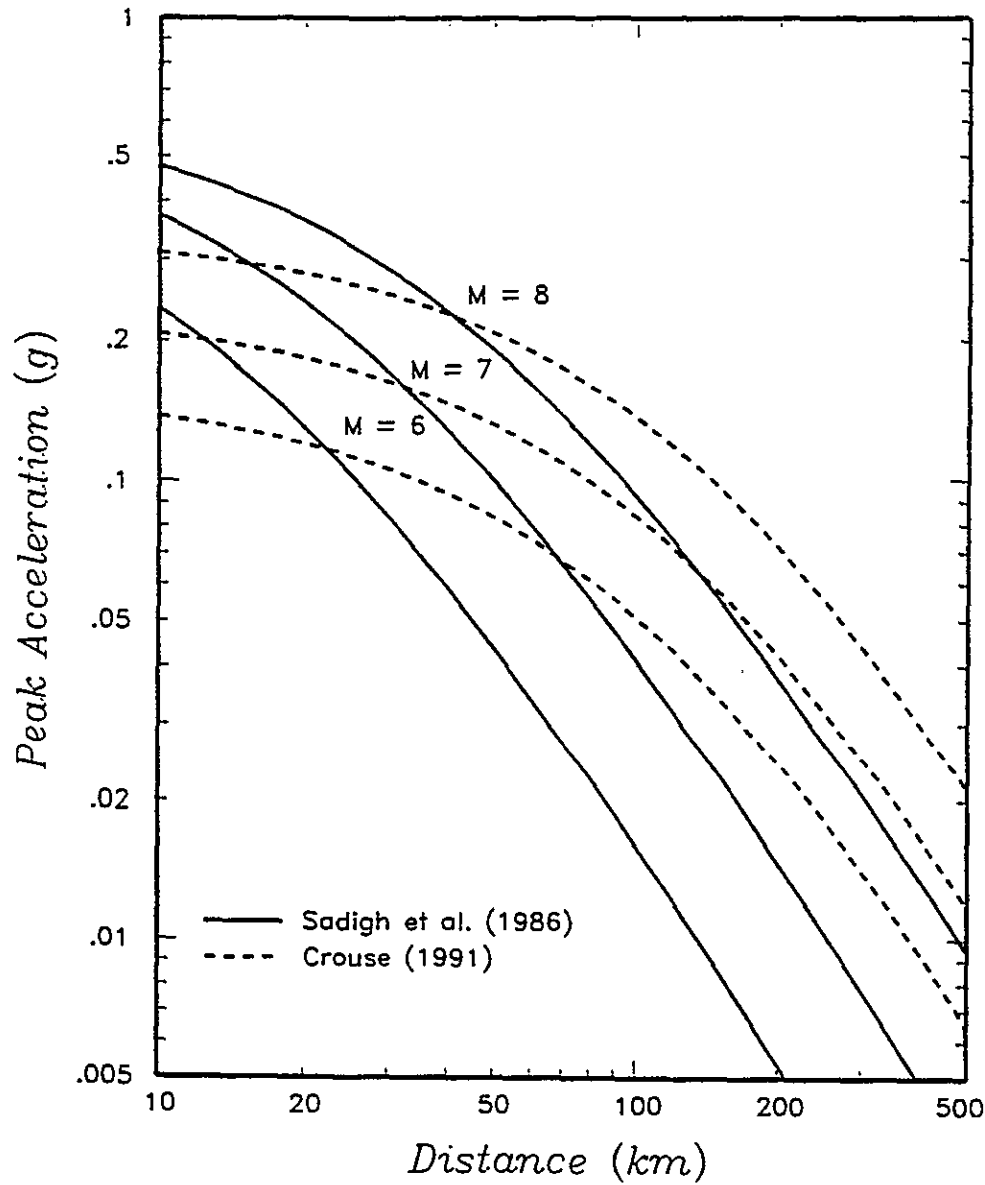amplitude for the attenuation relationships used in this study.

Figure 4-4 Comparison of attenuation relationship for subduction zone earthquakes (Crouse, 1991) with that for crustal earthquakes.

5.0 SEISMIC HAZARD ANALYSIS RESULTS

5.1 ANALYSIS PROCEDURE

Seismic hazard calculations were made for peak horizontal ground acceleration and 5%-damped response spectral accelerations at periods of 0.3 and 2.0 seconds. For hazard computations, the fault-specific sources were modeled as segmented planar surfaces. The areal source zones were modeled as a set of closely spaced parallel fault planes occupying the source regions outlined in Section 3. The probability density function for distance to earthquake rupture for each source was computed assuming earthquake ruptures were uniformly distributed over the fault planes, except for the case in which the spatial distribution in the shallow basalt is assumed to follow that observed in the recorded seismicity (shown on Figures 3-18 and 3-19). The distance density functions were computed consistent with the distance measure used in each of the attenuation relationships. A rectangular rupture area for a given size earthquake is located at a random point on the fault plane. The closest distance to this rectangle was used as the distance measure in the Sadigh and others (1986) model. The same distance was used in the Campbell (1993) model, except that the rupture was not allowed to come shallower than 1 km for earthquakes occurring solely in the CRBG and three km for all others. For the Joyner and Boore (1982) relationship, the rectangular rupture area on the fault was projected vertically to the surface and the closest distance to this surface projection was used.

The rupture size of an event was specified by the relationship ln(area) = 2M - 7.12 developed from the data presented by Wyss (1979). This relationship yields similar results to those given by the updated relationships provided by Wells and Coppersmith (in press). The specified relationship gives the mean rupture area for a specific magnitude rather than the median (mean log) rupture area. Studies by Bender (1984) have shown that the use of mean estimates of rupture size in the computation of hazard yields results nearly equal to those obtained when the statistical uncertainty in the size of individual ruptures is incorporated in the analysis. The hazard was computed with the distribution in peak ground motion about the median attenuation relationships truncated at three standard deviations.

Distributions for the annual frequency of exceeding various levels of peak ground acceleration and spectral acceleration were developed by performing hazard computations using Equation (2-1) with the input parameters defined by each end branch of the logic trees shown in Section 3. The hazard was computed considering the contributions of earthquakes of magnitude M 5 and larger ($m^0=5$). At each ground motion level, the complete set of results forms a discrete distribution for frequency of exceedance, $\nu(z)$. The computed distributions were used to obtain the mean frequency of exceeding various levels of peak ground motion (mean hazard curve) as well as hazard curves representing various percentiles of the distributions. The logic trees represent our best judgement as to the uncertainty in defining the input parameters and thus the computed distributions represent our confidence in the estimated hazard.

5.2 HAZARD RESULTS AND SENSITIVITY

5.2.1 Computed Hazard

Figures 5-1a through 5-1e presents the computed mean peak hazard and the 5th- to 95th-percentile hazard curves for DOE areas A through E for peak acceleration and 5%-damped spectral accelerations at periods of 0.3 and 2.0 seconds. The uncertainty band varies from about one order of magnitude at low ground motion levels to over two orders of magnitude at large ground motion levels. The uncertainty in the computed hazard also increases as one considers longer periods of vibration. The distribution in computed frequency of exceedance becomes skewed at the higher ground motion levels and the mean hazard lies near the 75th-percentile of the hazard distribution.

Based on the mean hazard curves for each site, the following ground motion levels were computed for return periods of 100, 500, 1,000, 2,500, 5,000, 10,000, and 100,000 years:

Site A - 200 West Area

Peak or 5%-damped Spectral Acceleration (g) for Return Periods (yrs) of:

Period	100	500	1,000	2,500	5,000	10,000	100,000
PGA	0.040	0.096	0.138	0.218	0.295	0.387	0.779
0.3 sec	0.091	0.243	0.354	0.546	0.738	0.978	1.803
2.0 sec	0.013	0.056	0.086	0.126	0.184	0.239	-0.538

Site B - 200 East Area
Peak or 5%-damped Spectral Acceleration (g) for Return Periods (yrs) of:

Period	100	500	1,000	2,500	5,000	10,000	100,000
PGA	0.039	0.092	0.132	0.206	0.280	0.37	0.775
0.3 sec	0.089	0.236	0.341	0.521	0.704	0.938	1.776
2.0 sec	0.013	0.055	0.084	0.123	0.181	0.232	0.506

Site C - 300 Area
Peak or 5%-damped Spectral Acceleration (g) for Return Periods (yrs) of:

Period	100	500	1,000	2,500	5,000	10,000	100,000
PGA	0.035	0.081	0.119	0.186	0.251	0.327	0.659
0.3 sec	0.080	0.213	0.307	0.471	0.633	0.830	1.755
2.0 sec	0.012	0.051	0.080	0.117	0.173	0.221	0.479

Site D - 400 Area
Peak or 5%-damped Spectral Acceleration (g) for Return Periods (yrs) of:

Period	100	500	1,000	2,500	5,000	10,000	100,000
PGA	0.037	0.084	0.121	0.186	0.247	0.320	0.639
0.3 sec	0.083	0.219	0.314	0.472	0.627	0.814	1.693
2.0 sec	0.012	0.052	0.081	0.118	0.173	0.221	0.467

Site E - 100 K area
Peak or 5%-damped Spectral Acceleration (g) for Return Periods (yrs) of:

Period	100	500	1,000	2,500	5,000	10,000	100,000
PGA	0.040	0.097	0.139	0.216	0.295	0.398	0.884
0.3 sec	0.090	0.244	0.354	0.543	0.739	0.996	1.890
2.0 sec	0.012	0.056	0.085	0.124	0.182	0.234	0.511

Figures 5-2a through 5-2e show the contribution of the three shallow crustal source types - folds, shallow basalt and basement sources, and the two subduction zone source types - interface and intraslab - to the mean hazard at sites A, B, C, D, and E. The results indicate that at sites A, B, and E, the Yakima Fold sources are the largest contributors to the hazard for high frequency motions (peak acceleration) and intermediate frequency motions (0.3 second spectral acceleration). At sites C and D, which are further from the folds, the basement source becomes the largest contributor to the ground motions. At all sites, the distant Cascadia interface source becomes the dominant contributor to long period (2 second spectral acceleration) ground motion hazard.

Figures 5-3a through 5-3e show the contribution of the three nearest folds to the total hazard from the Yakima Fold sources. The dominant contribution at sites A, B, and E for high levels of ground motion from the Umtanum-Gable Mountain fold. At sites C and D the Rattlesnake-Wallula (RAW) source is the dominate Yakima fold source. At low levels of ground motion a number of the other folds contribute to the hazard because they are more likely to be active and/or have higher activity rates. This is illustrated on Figures 5-3a through 5-3e by the large contribution from the Saddle Mountains source.

Figures 5-4a through 5-4e show the relative contribution of events in different magnitude intervals to the computed mean hazard at the five sites. Each plot in the figure presents a histogram of the percent contributions of events in 0.25 magnitude unit-wide intervals. Histograms are presented for peak acceleration and spectral acceleration at periods of 0.3 and 2.0 seconds for mean annual frequencies of exceedance of 10^3, and 10^{-4} (return periods of 1,000 and 10,000 years). The hazard from high frequency ground motions is dominated by the contributions from events in the range of M 5 to 6. As the period of the ground motion increases the larger magnitude events become increasingly important, dominating the hazard at a period of 2.0 seconds. This shift in magnitude contribution results from the shift in relative ground motion amplitude as a function of period shown in the response spectral acceleration estimates for various magnitude earthquakes (Figure 4-2). For long vibration period motions, there is a much greater difference between the peak amplitude observed for large and small magnitude earthquakes than is observed at short vibration periods. In addition, the very large, distant Cascadia interface events dominate the hazard because of their large long period component.

5.2.2 Sources of Uncertainty and Sensitivity

The distributions in the computed hazard shown in Figures 5-1a through 5-1d represent the cumulative effect of all levels of parameter uncertainty included in the hazard model logic trees (Figures 2-1, 3-10, 3-16, and 3-20). The relative contribution of various components of the model to the overall uncertainty can be readily identified from the logic tree formulation. This is accomplished by selecting the node for the parameter to be examined and

then computing the hazard, giving each branch in succession a weight of unity and all other branches at that node zero weight. For example, the contribution of uncertainty in selecting the appropriate attenuation relationship can be obtained by computing the mean hazard assuming each of the three attenuation relationships is, in turn, the "correct" relationship. with weight of 1.0, and the other two have zero weight. The resulting hazard curves are shown in Figures 5-5a and 5-5b for sites A and C, respectively. Results are not shown for sites B and E or D because they are very similar to sites A and C, respectively. In the plots, the heavy solid curve corresponds to the mean hazard and the light solid curves to the 5th- and 95th-percentiles of the distribution in exceedance frequency shown in Figures 5-1a and 5-1c. The three labeled curves are the resulting mean hazard for each of the attenuation relationships and the differences between them represent the uncertainty in the computed hazard due to uncertainty in selecting the appropriate attenuation relationship.

The results shown in Figure 5-5a and 5-5b indicate that the effect of choice of attenuation relationship is a significant contributor to uncertainty in the hazard only at low probabilities of exceedance and for long-vibration period ground motions. The larger sensitivity of the long-vibration period hazard results to the choice of attenuation relationship results primarily from the large difference in the estimates of the variance in long-vibration period ground motion about the median relationships associated with the different sets of attenuation relationships (Figure 4-3).

Figures 5-6a and 5-6b show the effect of the choice of tectonic model for the Yakima Fold sources (coupled versus uncoupled) on the computed hazard from the fold sources only for sites A and C. The hazard results are similar for both models for high and intermediate frequency ground motions. The hazard at long period ground motions shows greater sensitivity to the choice of models due to the increased dominance of the hazard by larger magnitude events (Figures 5-4a and 5-4c). Examination of the logic trees shown in Section 3 indicates that the assessed distributions of maximum magnitude for the coupled fold model seismic sources (Table 3-1) leads to larger expected maximum magnitudes than those for the uncoupled fold model sources (Table 3-2).

Figures 5-7a and 5-7b show the sensitivity of the hazard resulting from the shallow basalt source to the choice of the appropriate spatial distribution of earthquakes. (Note that the 5th-percentile hazard curve is not shown because there is a 65 percent probability that the largest events that can occur in the shallow basalt layer are less than or equal to the lower bound magnitude considered in the hazard analysis, magnitude 5.0.) As indicated on the figures, there is some sensitivity of the hazard results to the choice of spatial distribution. These differences can be related directly to the various earthquake-to-site distributions developed for the three models of spatial distribution of earthquakes (e.g., Figure 3-19). The "smoothed observed" model results in the highest hazard at site C because of the continued high rate of activity in the Wooded Island area, located near the site.

Figures 5-8a and 5-8b show the sensitivity of the hazard resulting from the basement sources to consideration of the three tectonic models for the basement sources. The failed rift model produces the highest hazard because the predicted seismicity rate is significantly higher than the observed seismicity rate, which is used by the other two basement models (Figure 3-24). The differences between the random and basement block models reflect differences in the boundary of the zones used to collect seismicity for estimation of the seismicity rate in the basement sources.

5.2.3 Effect of Lower Bound Magnitude

The hazard analysis described above was computed using a lower bound magnitude, m^0, of 5.0. As indicated by the magnitude contribution plots on Figures 5-4a through 5-4e, there is a large contribution to the peak acceleration hazard from events near the lower bound, particularly for the short return period hazard levels. Thus, reducing m^0 would increase the computed peak accelerations for the low hazard designation facilities (return periods of 100 and 500 years). It should be noted that the seismic hazard maps on which the Uniform Building Code seismic coefficients (Algermissen and others, 1982) are based were computed using a lower bound magnitude of 4.0. However, Algermissen and others (1982) did not include randomness in the attenuation relationship (equivalent to setting the standard error in peak amplitude to zero). Figure 5-9 compares the peak acceleration hazard computed for

Site A using the Sadigh and others (1986) model with $m^0 = 5.0$ and the standard error values shown on Figure 4-3 compared with the peak acceleration hazard computed with $m^0 = 4.0$ and the standard error in peak acceleration set to zero. As can be seen, use of a minimum magnitude of 5.0 with ground motion randomness results in higher hazard levels. Thus, one can consider that the results presented above are reasonable for use for all hazard level facilities.

5.3 SUMMARY

The seismic hazard estimates presented in this report represents the results of an updated seismic hazard model for the Hanford region. The seismic hazard computed from this model is somewhat higher than that computed from the previous models (e.g., Woodward-Clyde Consultants, 1989). The reasons for these differences are threefold: (1) use of multiple attenuation models, some with higher levels of dispersion; (2) updated estimates of earthquake occurrence; and (3) inclusion of additional sources of potential future earthquakes (the basement source and the Cascadia interface).
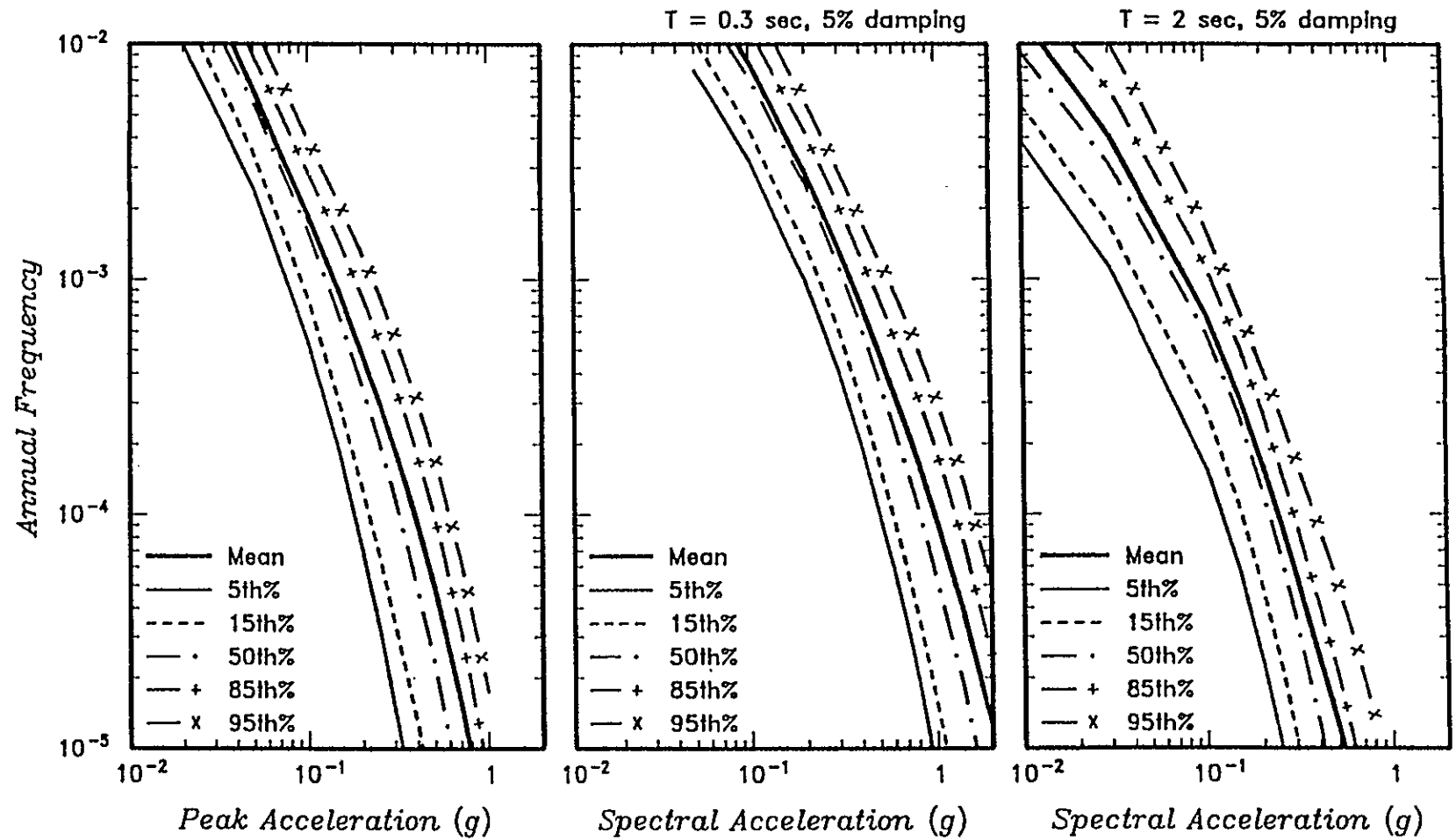
site a with subduction zone 12/7/93

Figure 5-1a   Computed mean and 5th- to 95th-percentile hazard curves for DOE Site A. Shown are results for peak horizontal acceleration and 5%-damped spectral acceleration at 0.3 and 2.0 seconds.
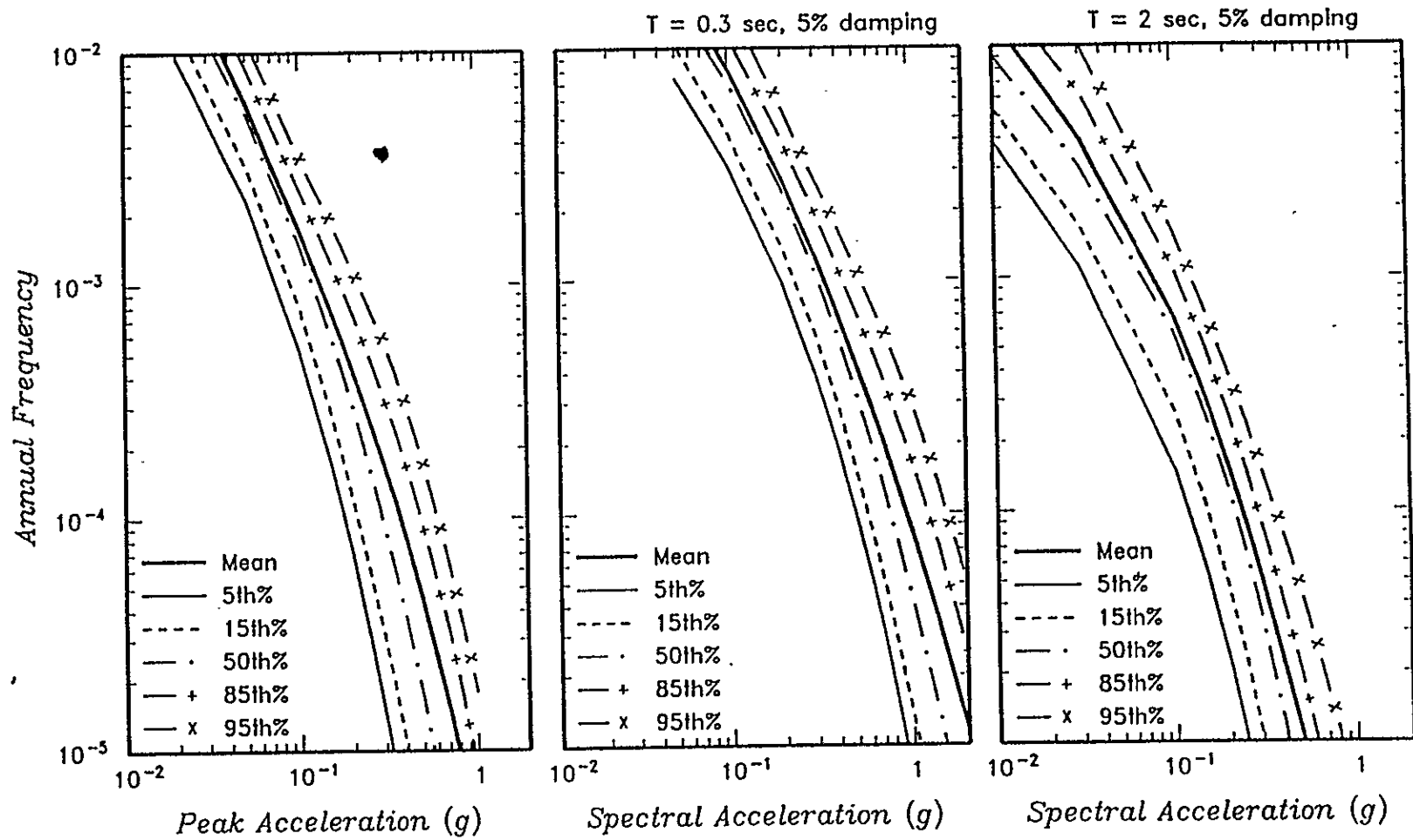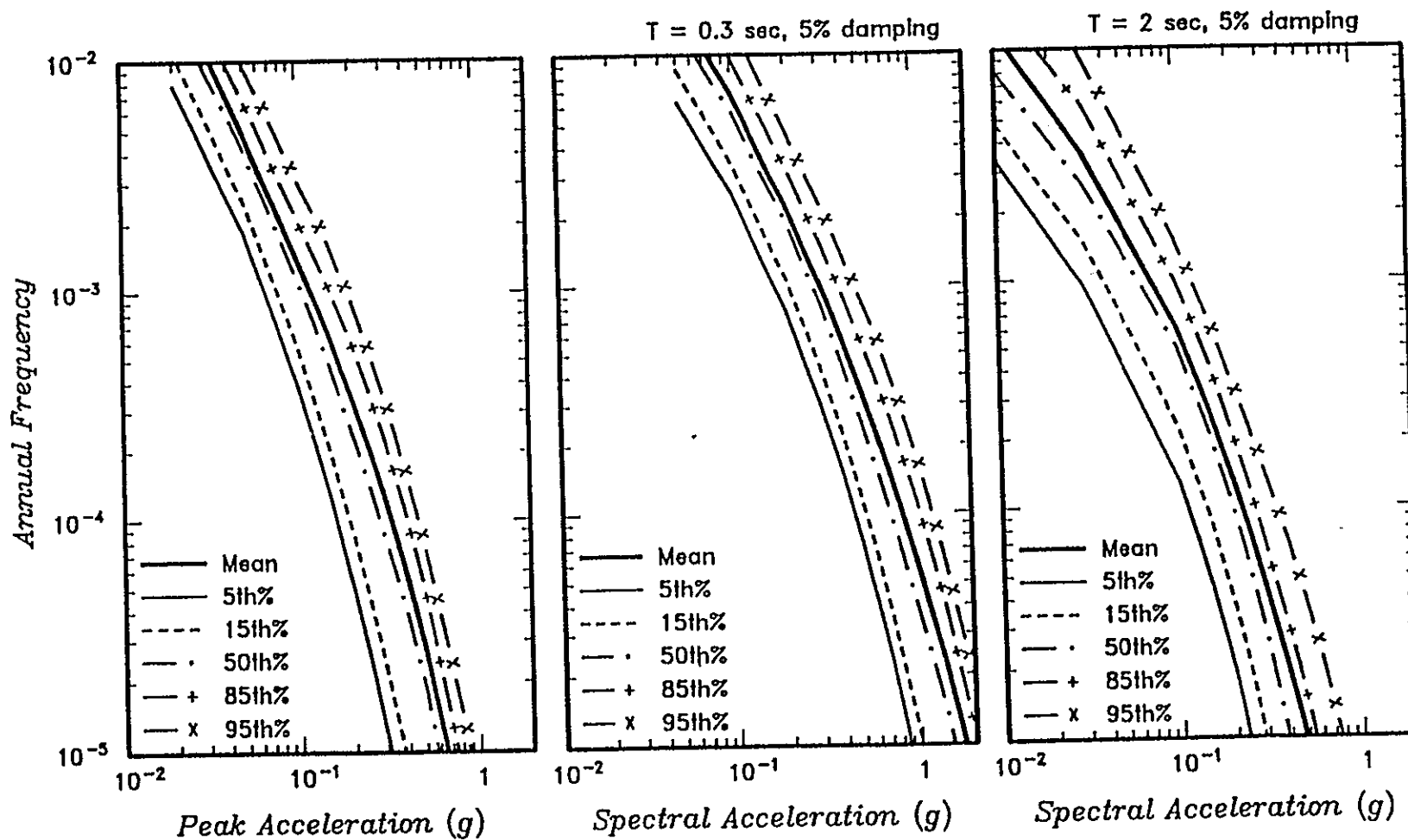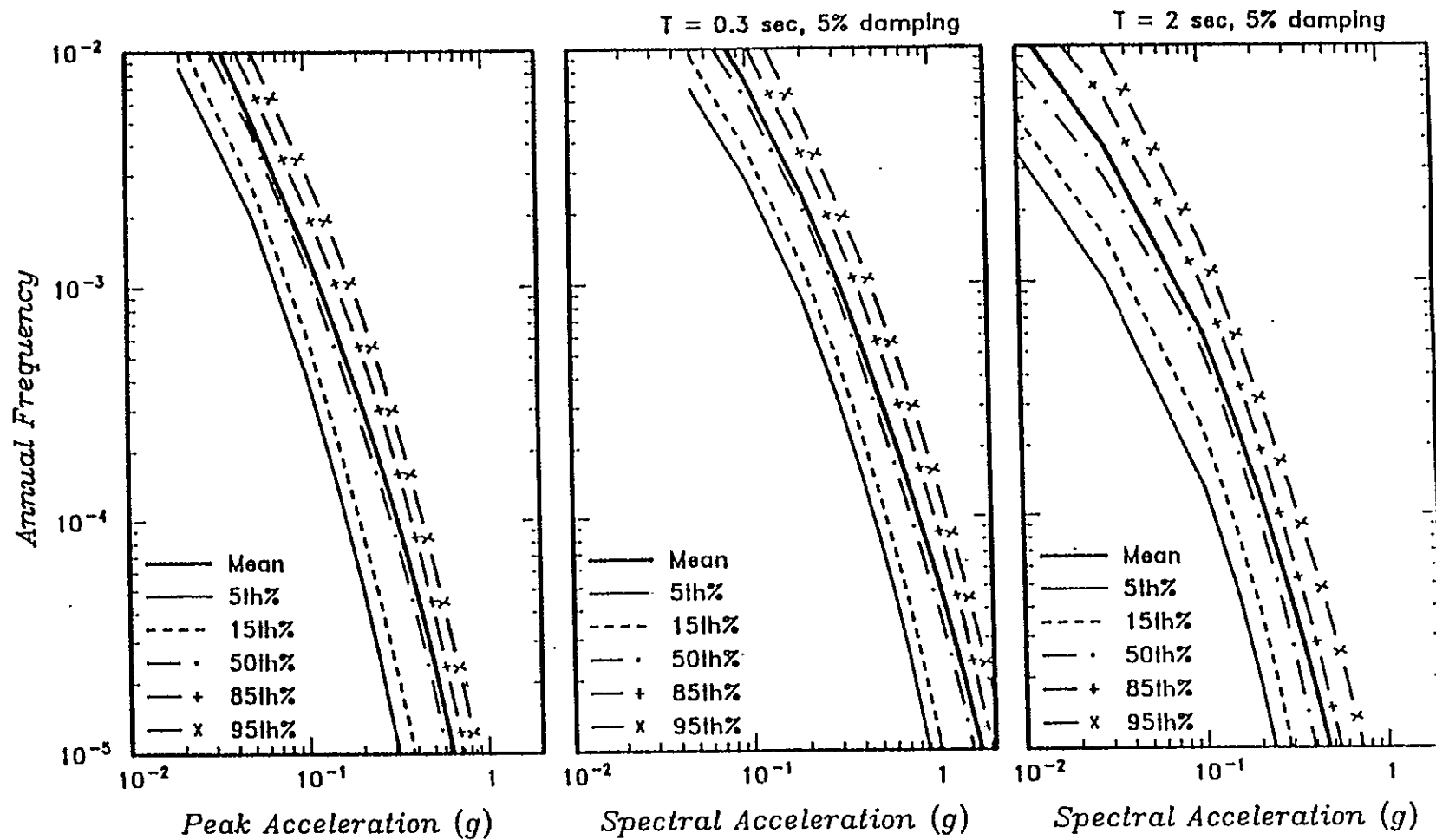
Figure 5-1b   Computed mean and 5th- to 95th-percentile hazard curves for DOE Site B. Shown are results for peak horizontal acceleration and 5%-damped spectral acceleration at 0.3 and 2.0 seconds.
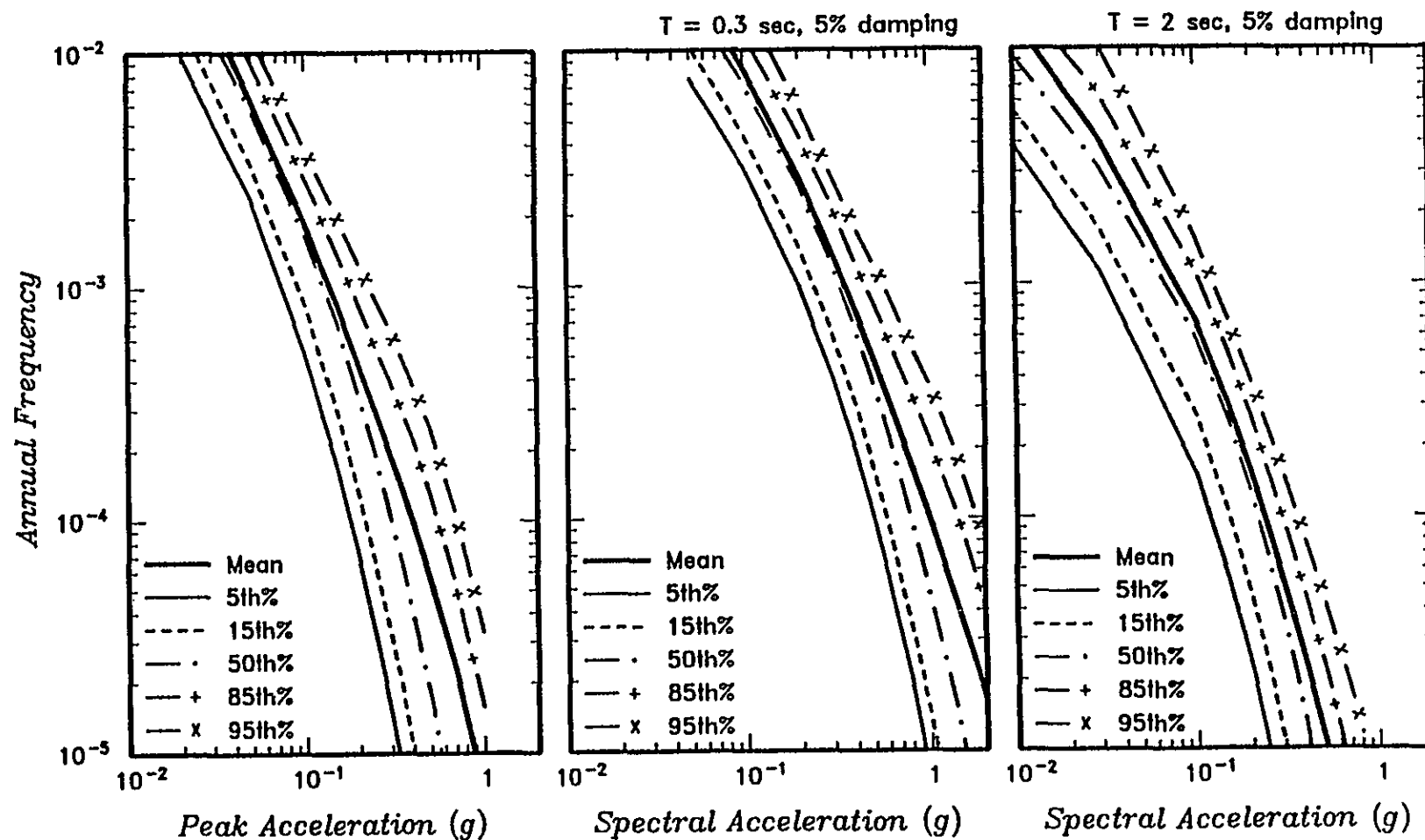
Figure 5-1c   Computed mean and 5th- to 95th-percentile hazard curves for DOE Site C. Shown are results for peak horizontal acceleration and 5%-damped spectral acceleration at 0.3 and 2.0 seconds.
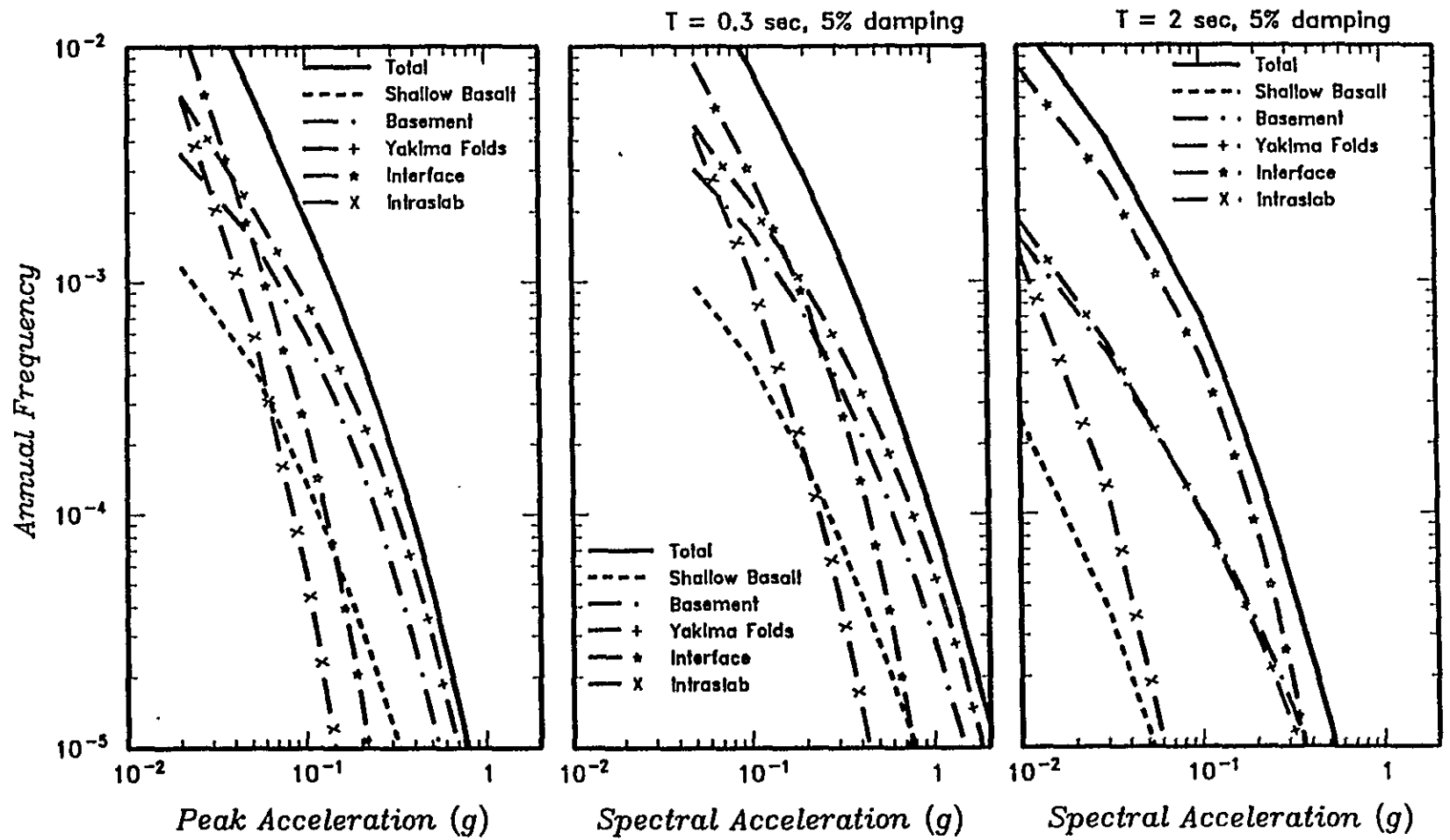
Figure 5-1d Computed mean and 5th- to 95th-percentile hazard curves for DOE Site D. Shown are results for peak horizontal acceleration and 5%-damped spectral acceleration at 0.3 and 2.0 seconds.

Figure 5-1e   Computed mean and 5th- to 95th-percentile hazard curves for DOE Site E. Shown are results for peak horizontal acceleration and 5%-damped spectral acceleration at 0.3 and 2.0 seconds.

T = 0.3 sec, 5% damping

T = 2 sec, 5% damping

Total
Shallow Basalt
Basement
+ Yakima Folds
* Interface
X Intraslab

Total
Shallow Basalt
Basement
+ Yakima Folds
* Interface
X Intraslab

Total
Shallow Basalt
Basement
+ Yakima Folds
* Interface
X Intraslab

Annual Frequency

10^{-2}

10^{-3}

10^{-4}

10^{-5}

10^{-2} 10^{-1} 1

Peak Acceleration (g)

Spectral Acceleration (g)

Spectral Acceleration (g)

Figure 5-2a   Contributions of the five source types to mean hazard at DOE Site A. Shown are results for peak horizontal acceleration and 5%-damped spectral acceleration at 0.3 and 2.0 seconds.
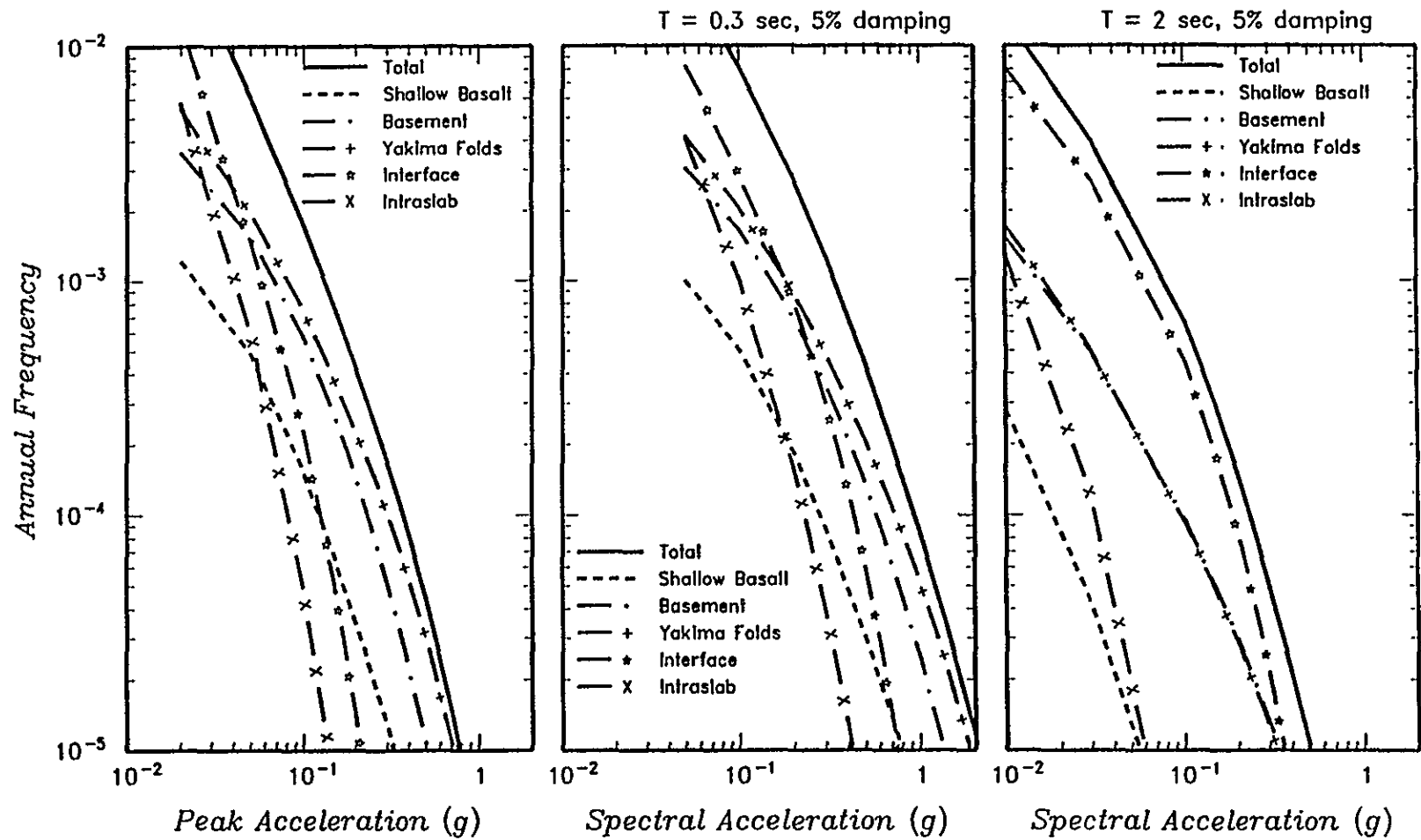
Figure 5-2b   Contributions of the five source types to mean hazard at DOE Site B.   Shown are results for peak horizontal acceleration and 5%-damped spectral acceleration at 0.3 and 2.0 seconds.
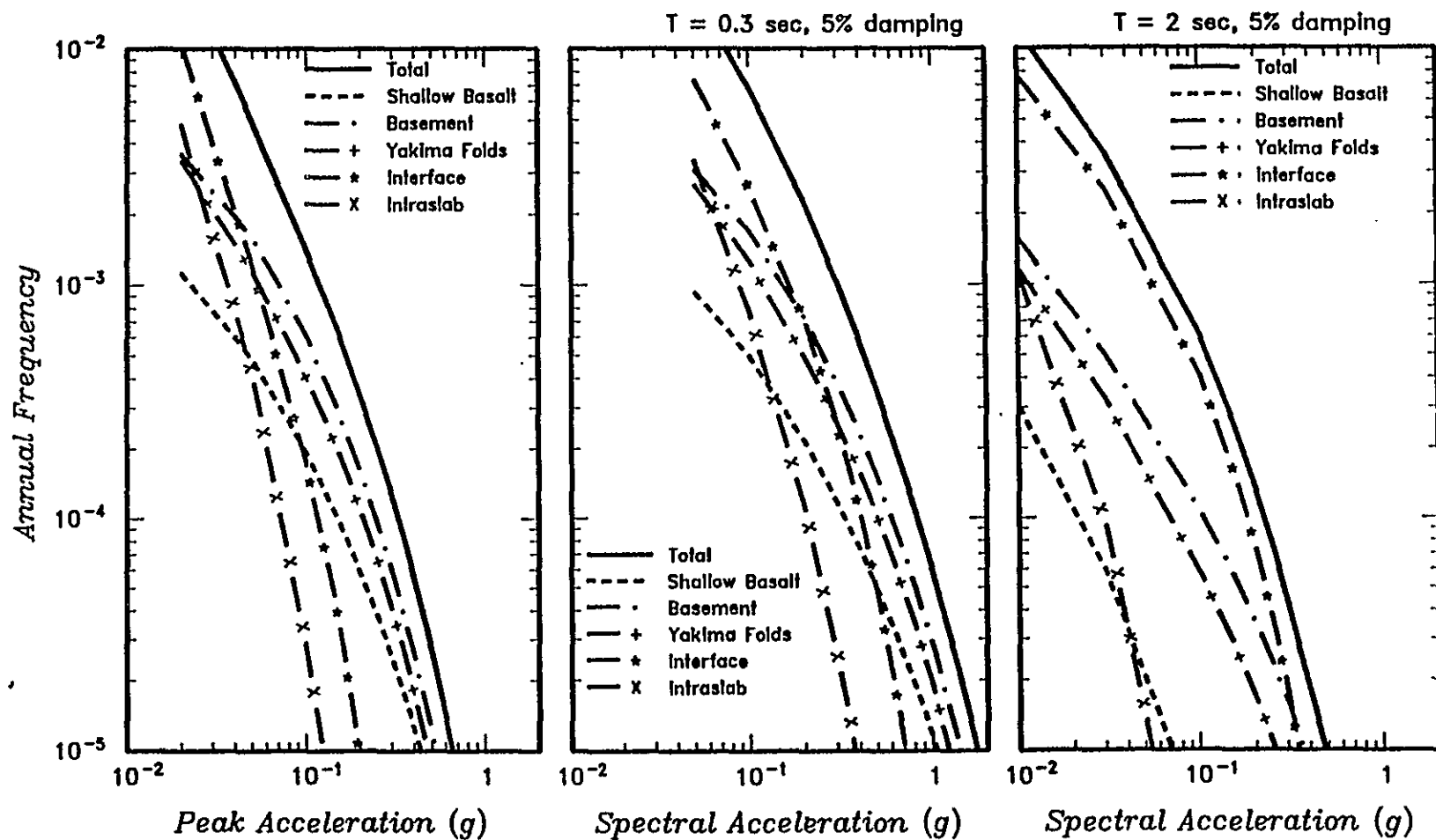
T = 0.3 sec, 5% damping

T = 2 sec, 5% damping

Total
Shallow Basalt
Basement
Yakima Folds
Interface
Intraslab

Annual Frequency

Peak Acceleration (g)

Spectral Acceleration (g)

Spectral Acceleration (g)

Figure 5-2c   Contributions of the five source types to mean hazard at DOE Site C. Shown are results for peak horizontal acceleration and 5%-damped spectral acceleration at 0.3 and 2.0 seconds.
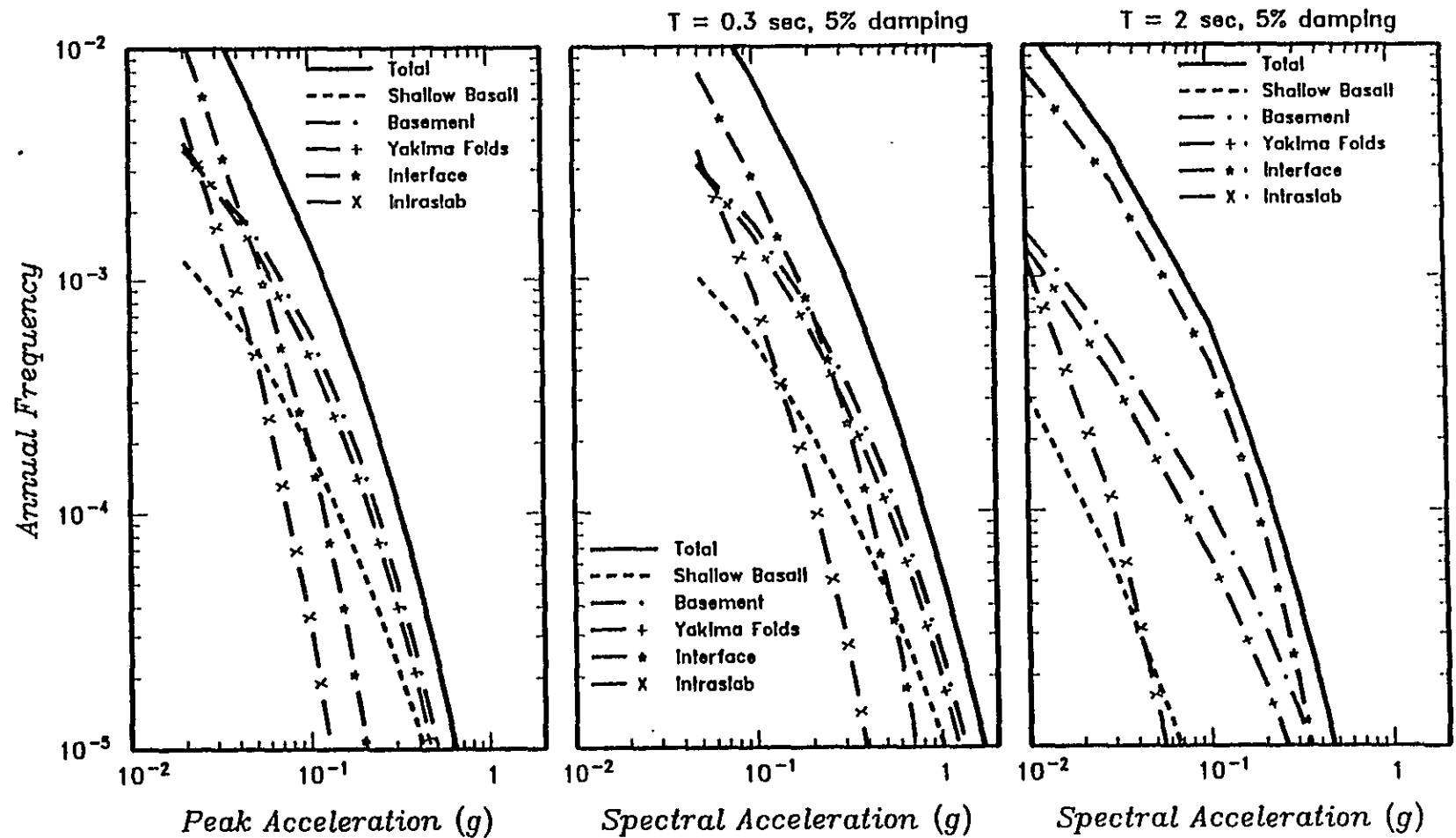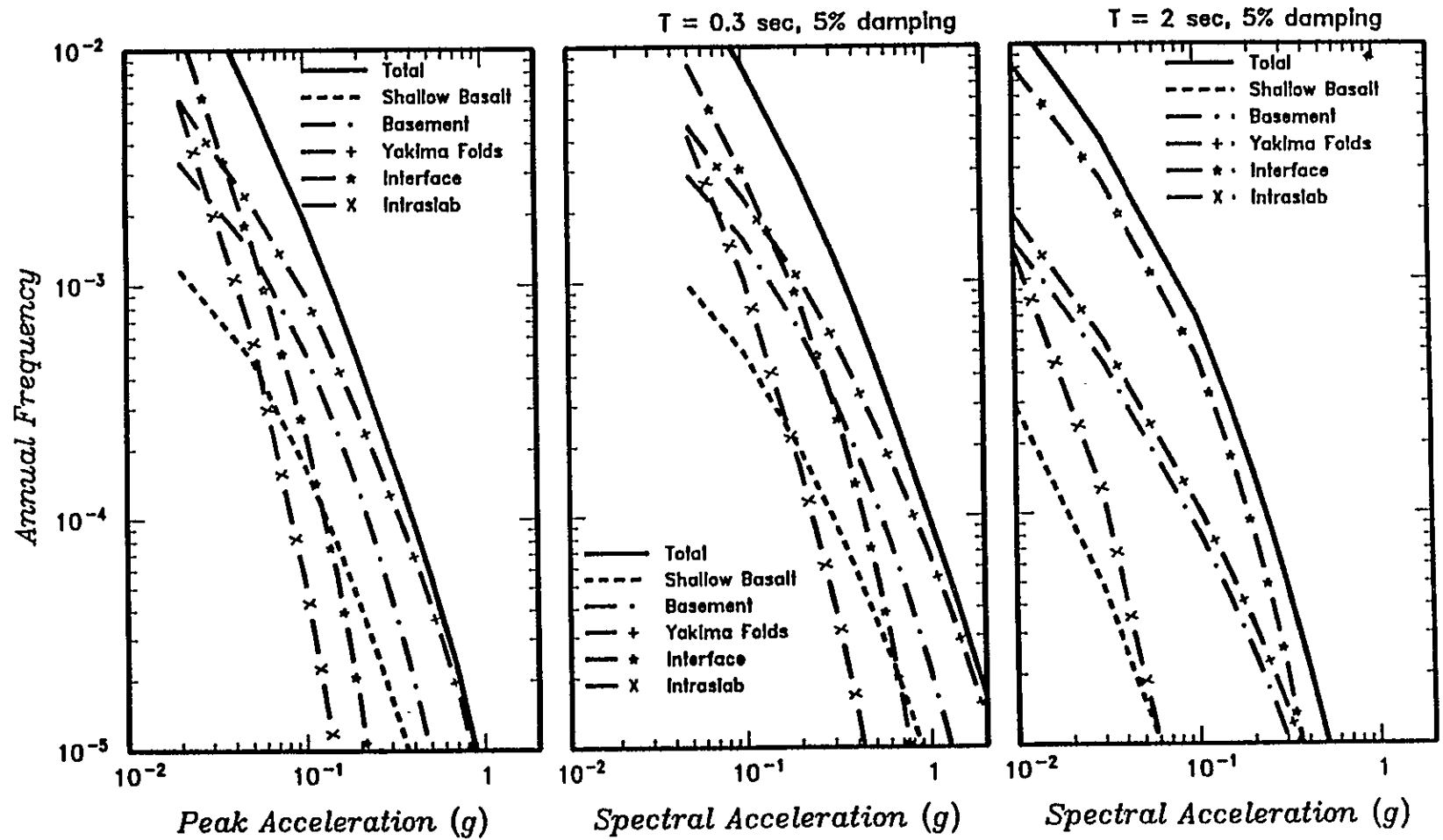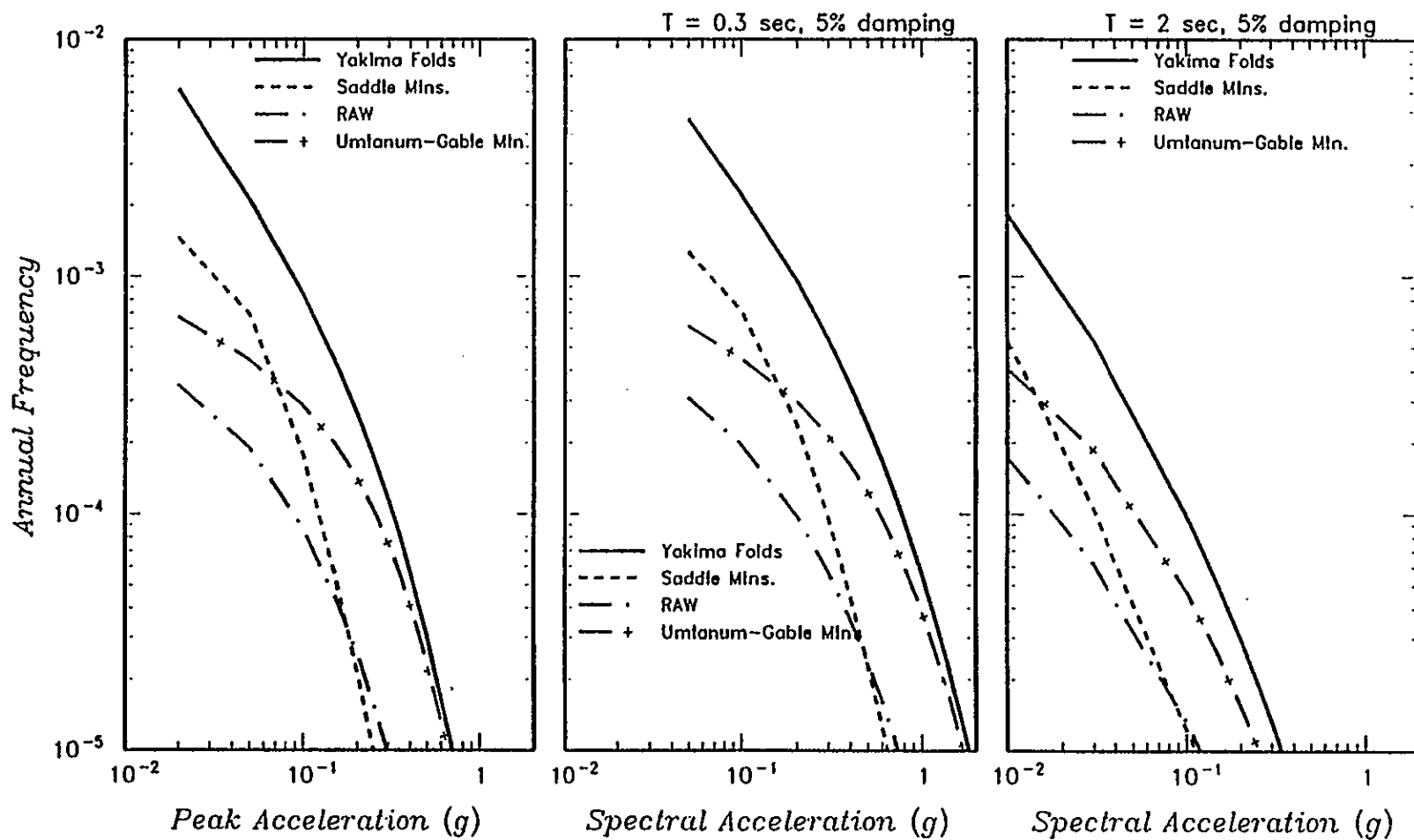
Figure 5-2d Contributions of the three source types to mean hazard at DOE Site D. Shown are results for peak horizontal acceleration and 5%-damped spectral acceleration at 0.3 and 2.0 seconds.

Figure 5-2e   Contributions of the five source types to mean hazard at DOE Site E. Shown are results for peak horizontal acceleration and 5%-damped spectral acceleration at 0.3 and 2.0 seconds.

Figure 5-3a Contributions of the three nearest folds to total hazard from the Yakima Folds of Site A. Shown are results for peak horizontal acceleration and 5%-damped spectral accelerations at 0.3 and 2.0 seconds.
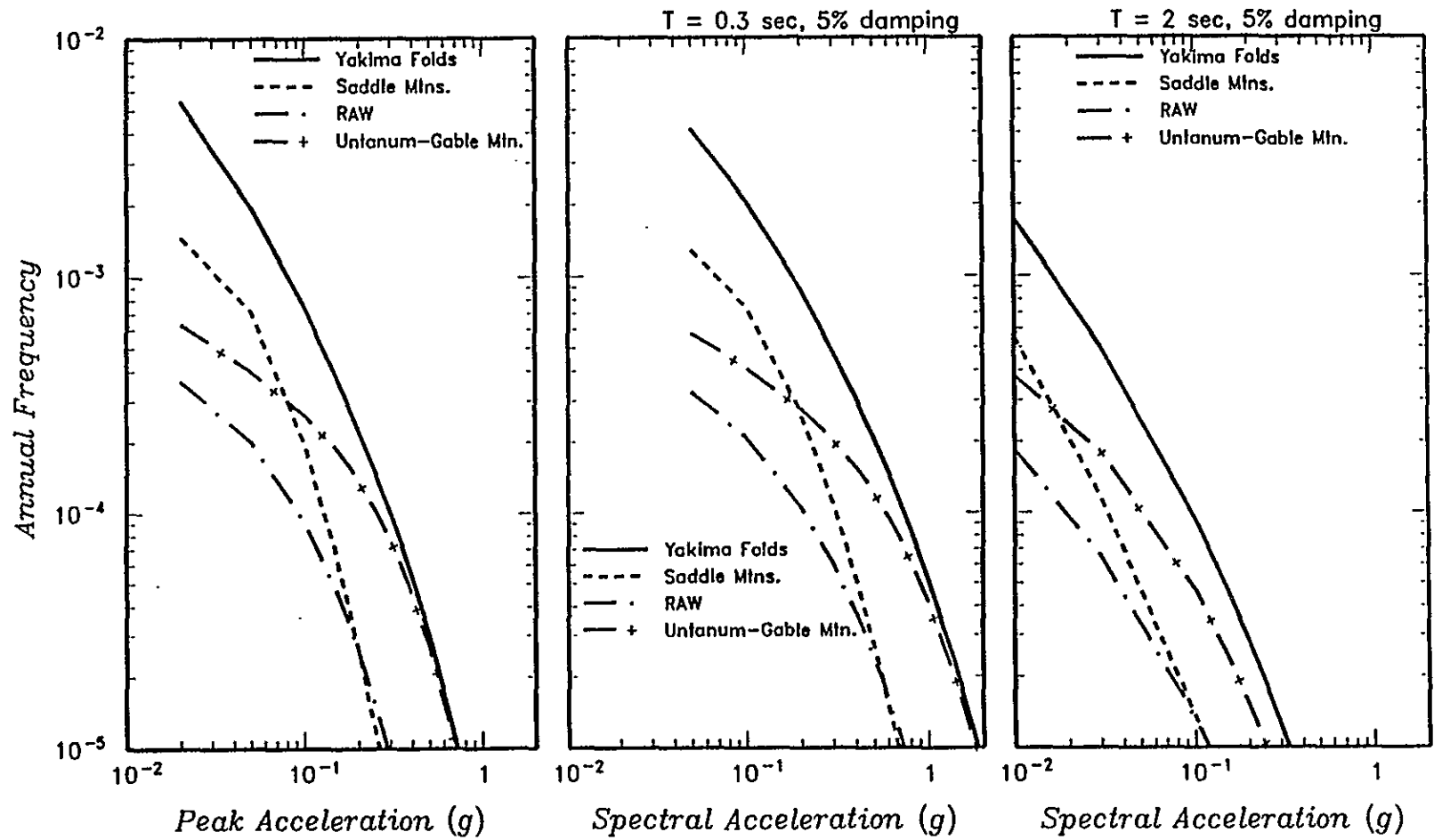
Figure 5-3b Contributions of the three nearest folds to total hazard from the Yakima Folds of Site B. Shown are results for peak horizontal acceleration and 5%-damped spectral accelerations at 0.3 and 2.0 seconds.
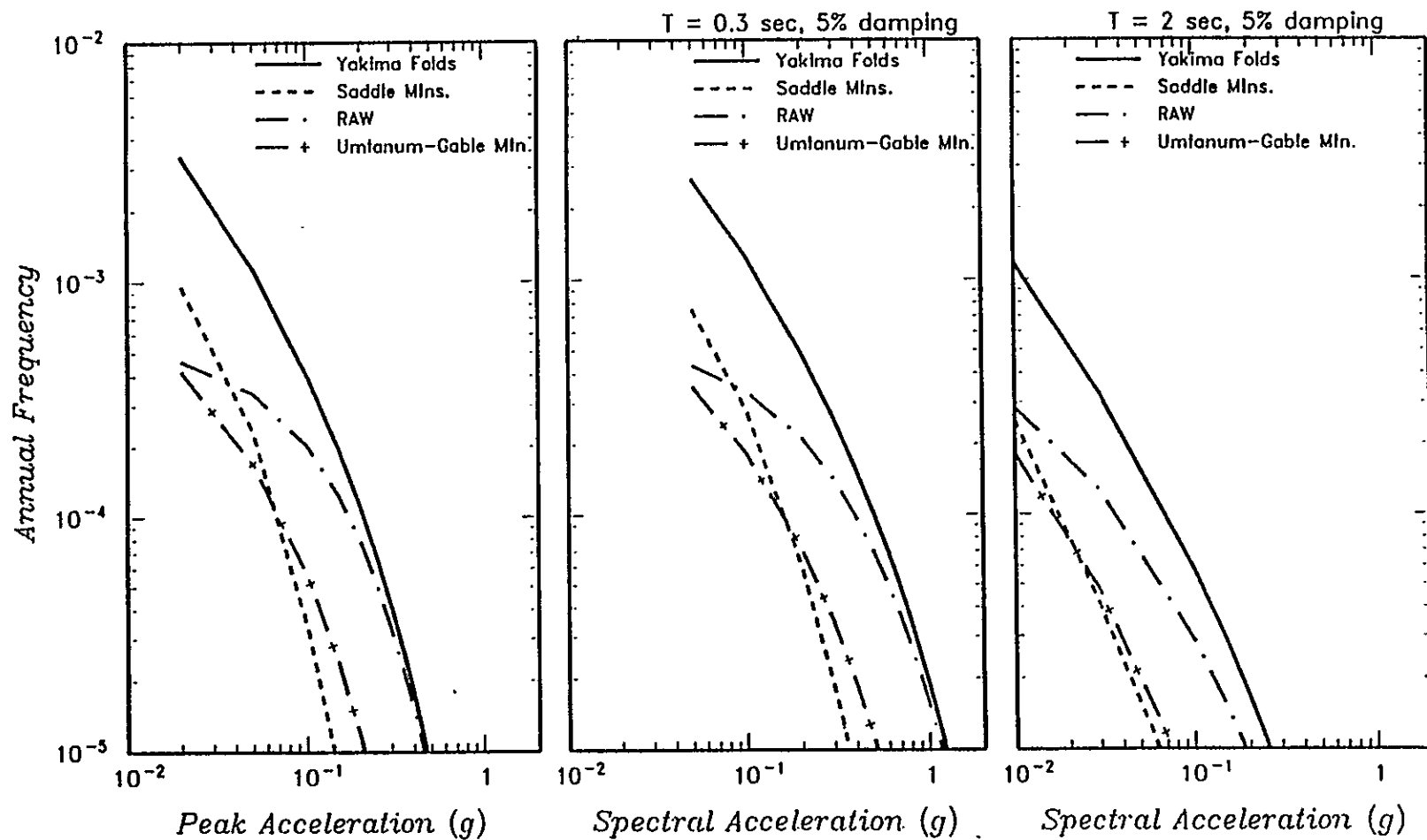
Figure 5-3c Contributions of the three nearest folds to total hazard from the Yakima Folds of Site C. Shown are results for peak horizontal acceleration and 5%-damped spectral accelerations at 0.3 and 2.0 seconds.
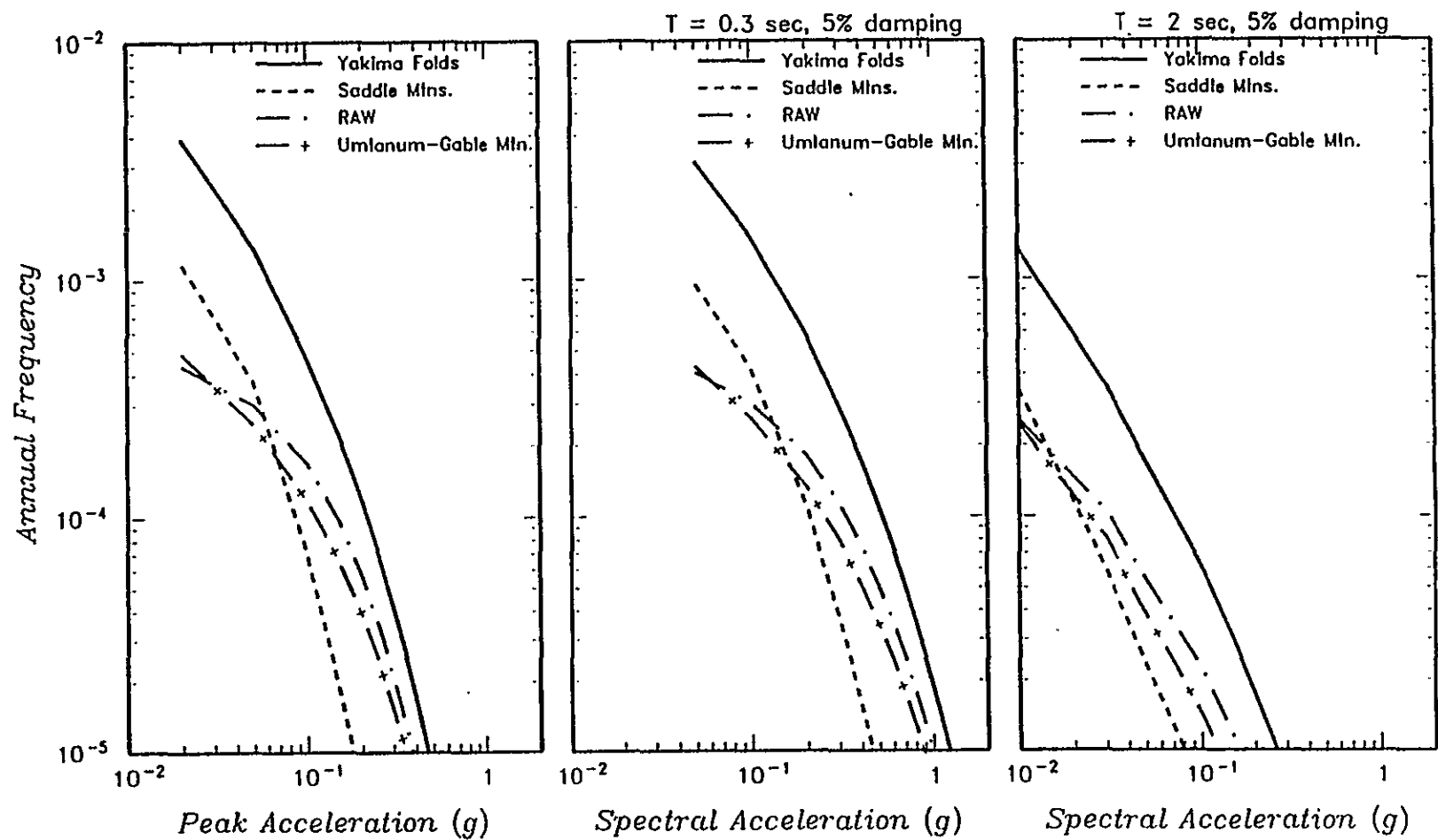
Figure 5-3d Contributions of the three nearest folds to total hazard from the Yakima Folds of Site D. Shown are results for peak horizontal acceleration and 5%-damped spectral accelerations at 0.3 and 2.0 seconds.
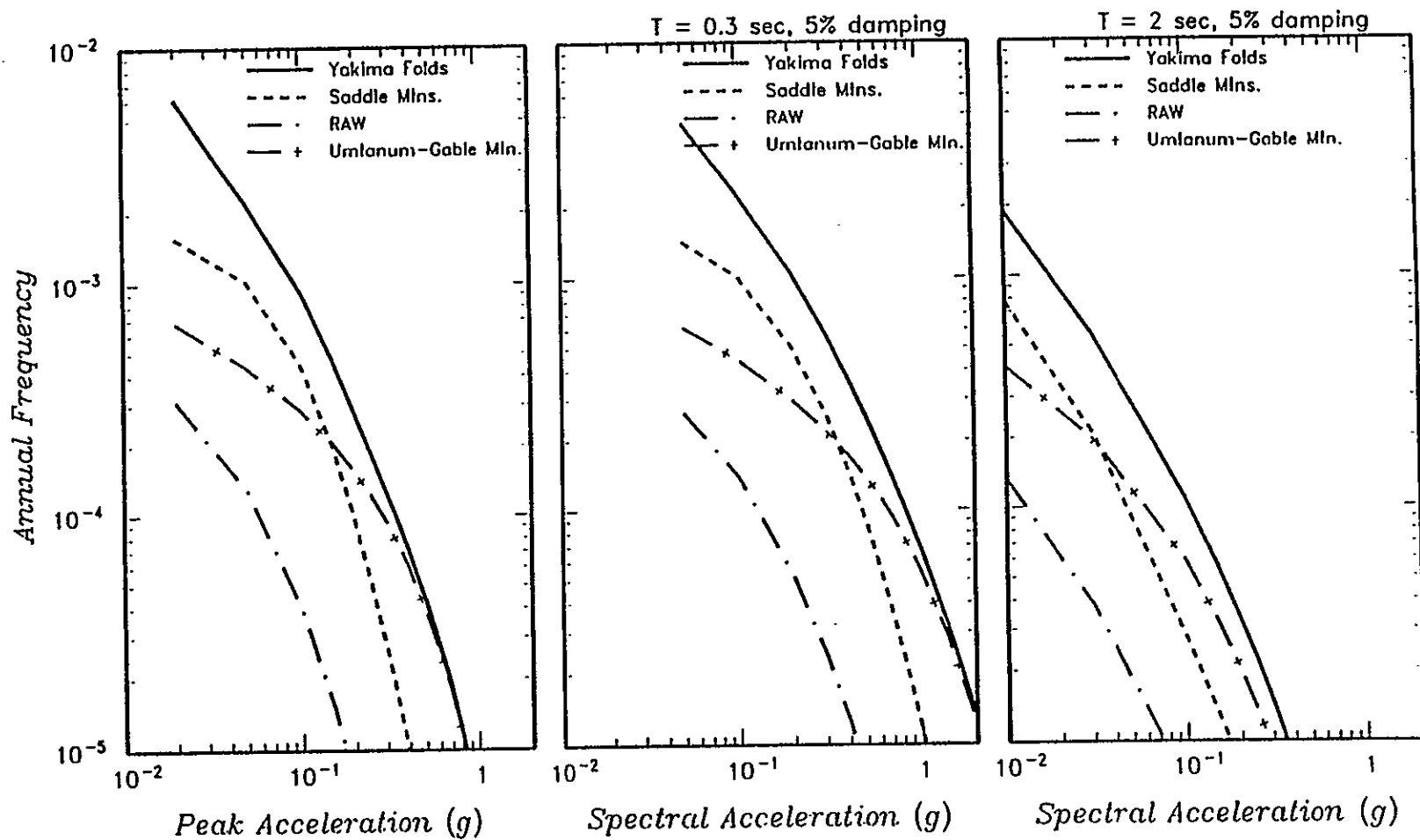
Figure 5-3e Contributions of the three nearest folds to total hazard from the Yakima Folds of Site E. Shown are results for peak horizontal acceleration and 5%-damped spectral accelerations at 0.3 and 2.0 seconds.
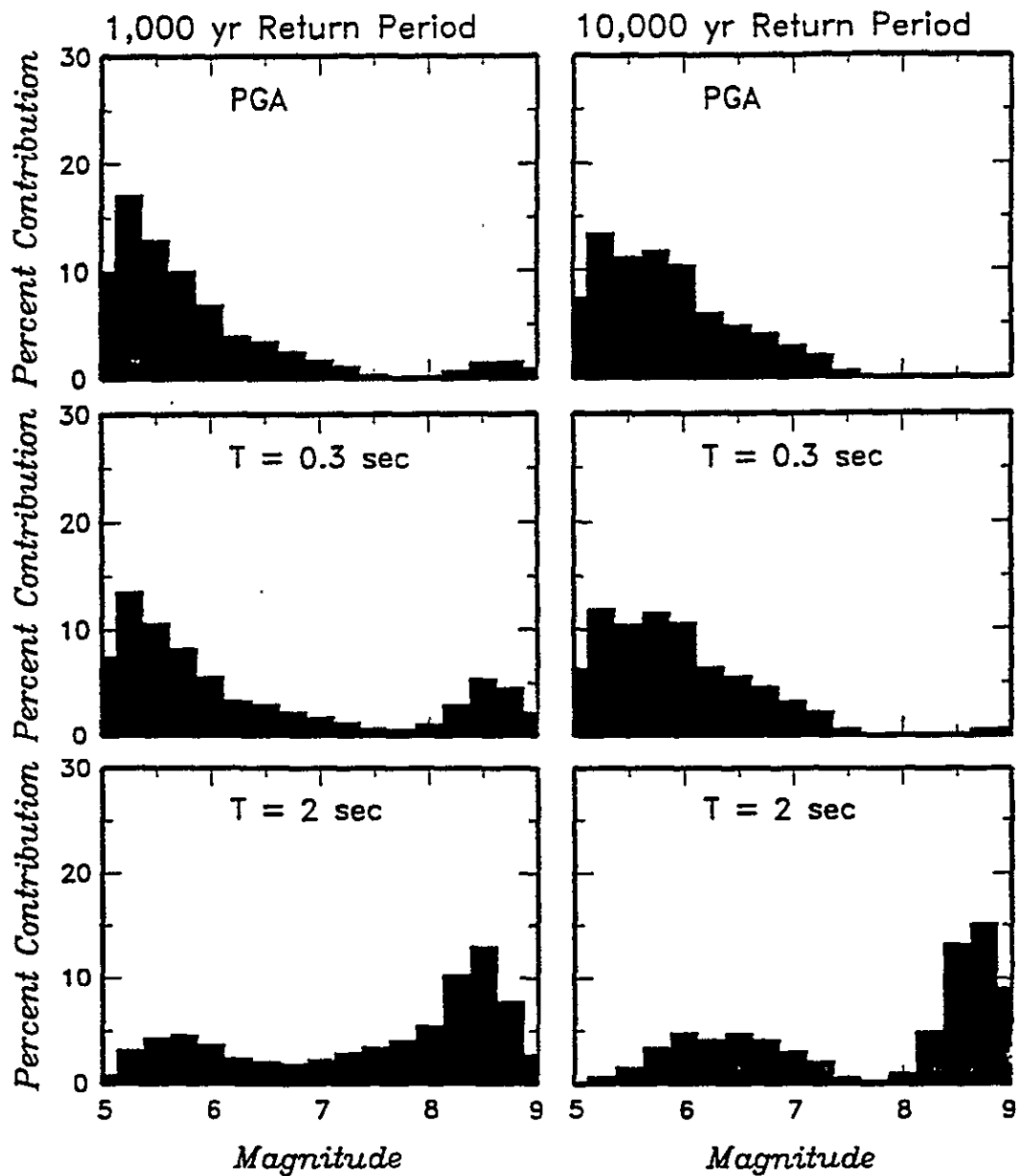
Figure 5-4a Relative contribution of events in various magnitude intervals to mean hazard at DOE Site A. Shown are results for peak horizontal acceleration and 5%-damped spectral acceleration at 0.3 and 2.0 seconds.

Figure 5-4b Relative contribution of events in various magnitude intervals to mean
hazard at DOE Site B. Shown are results for peak horizontal acceleration
and 5%-damped spectral acceleration at 0.3 and 2.0 seconds.

GEOMATRIX

Figure 5-4c   Relative contribution of events in various magnitude intervals to mean hazard at DOE Site C. Shown are results for peak horizontal acceleration and 5%-damped spectral acceleration at 0.3 and 2.0 seconds.
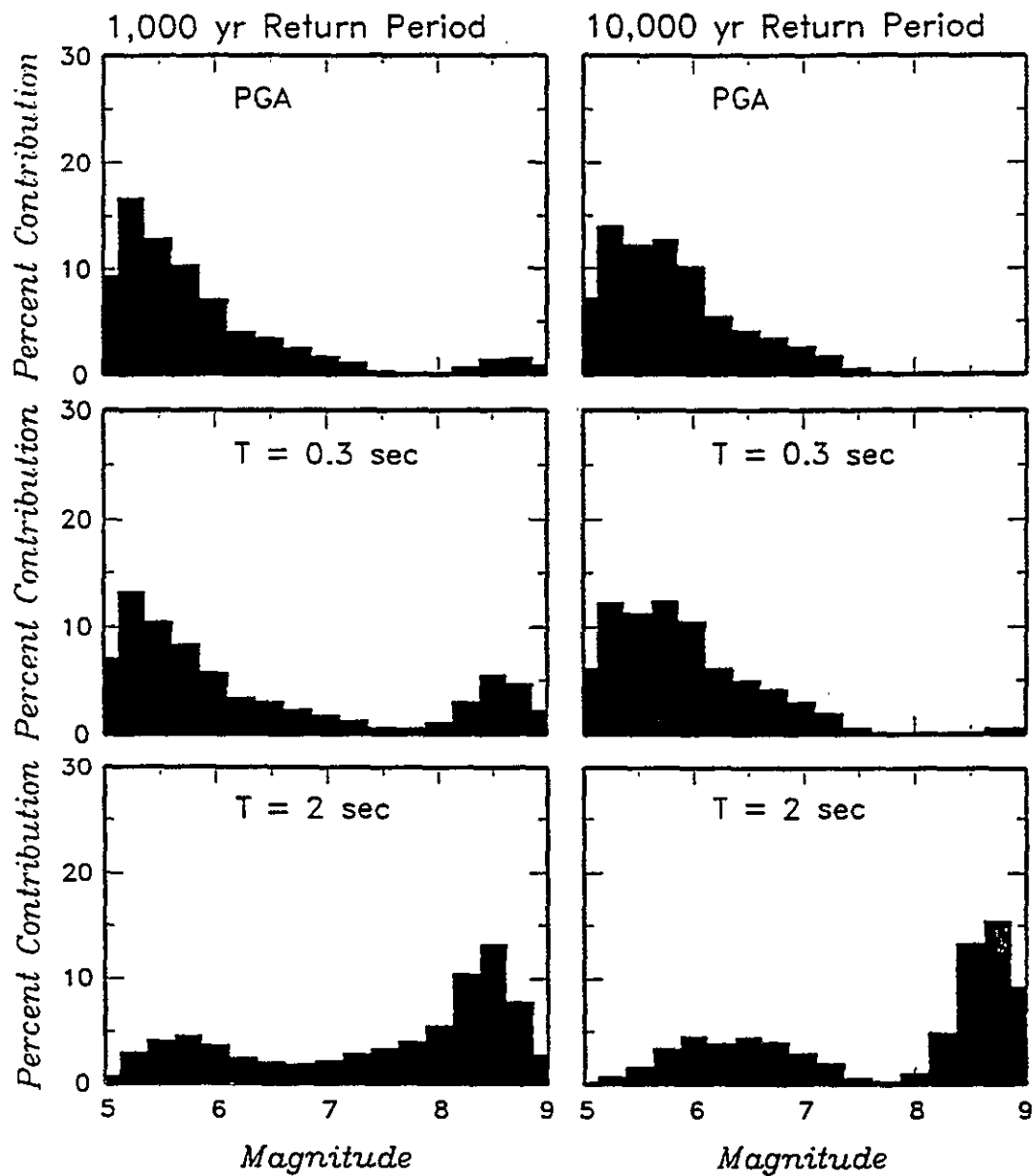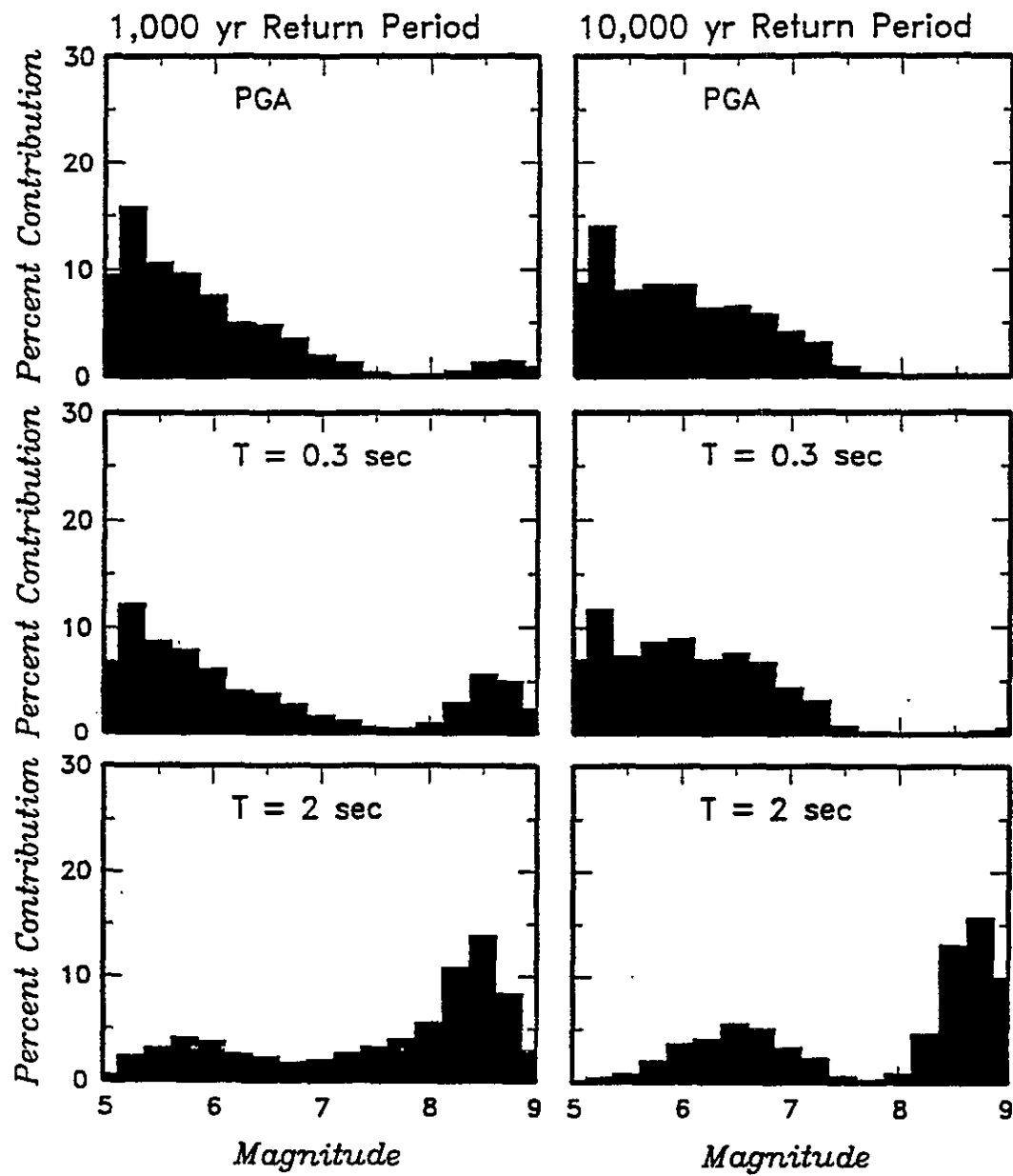
Figure 5-5a   Effect of choice of attenuation relationship on mean hazard from crustal sources at DOE Site A. Shown are results for peak horizontal acceleration and 5%-damped spectral acceleration at 0.3 and 2.0 seconds.
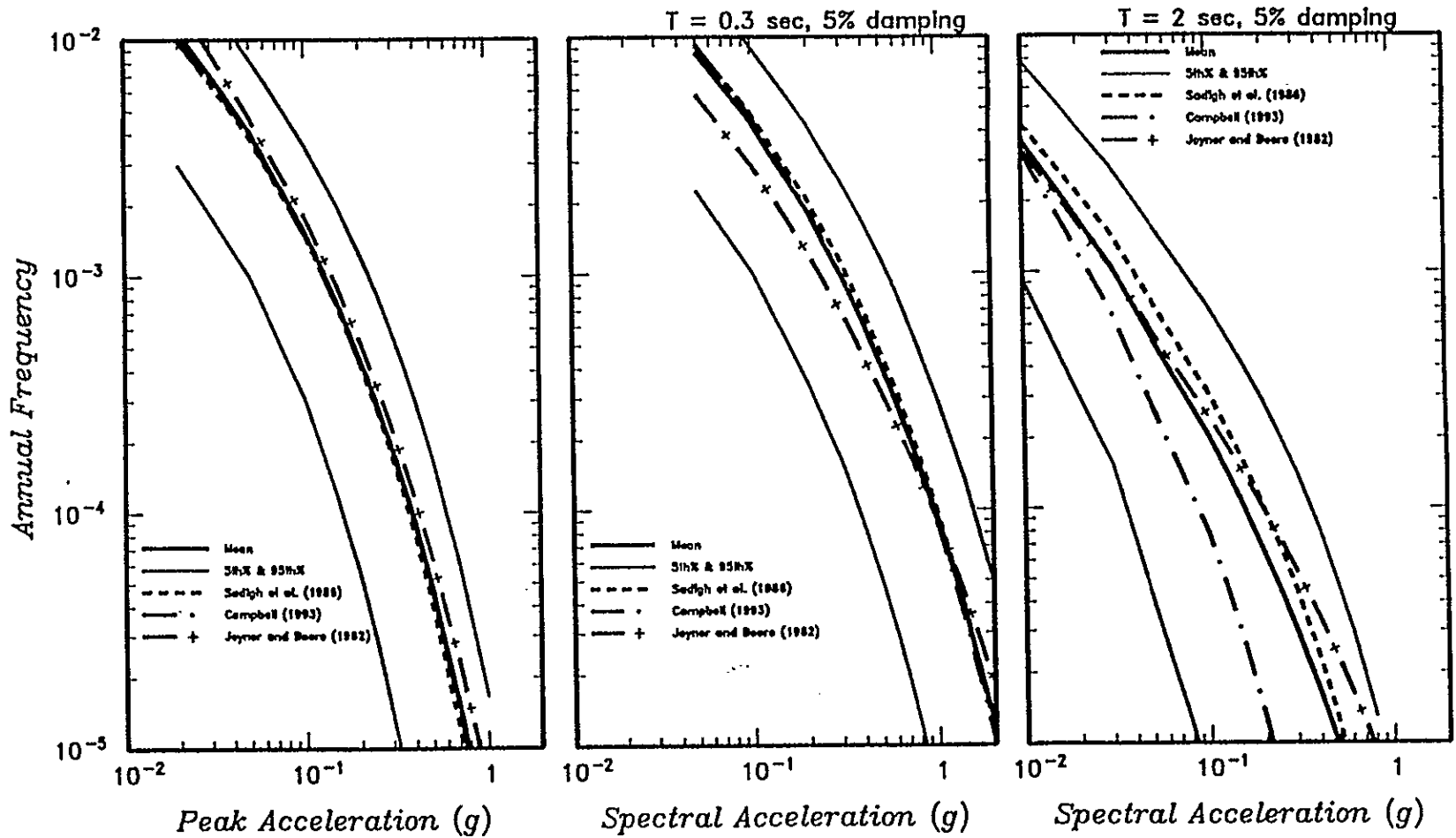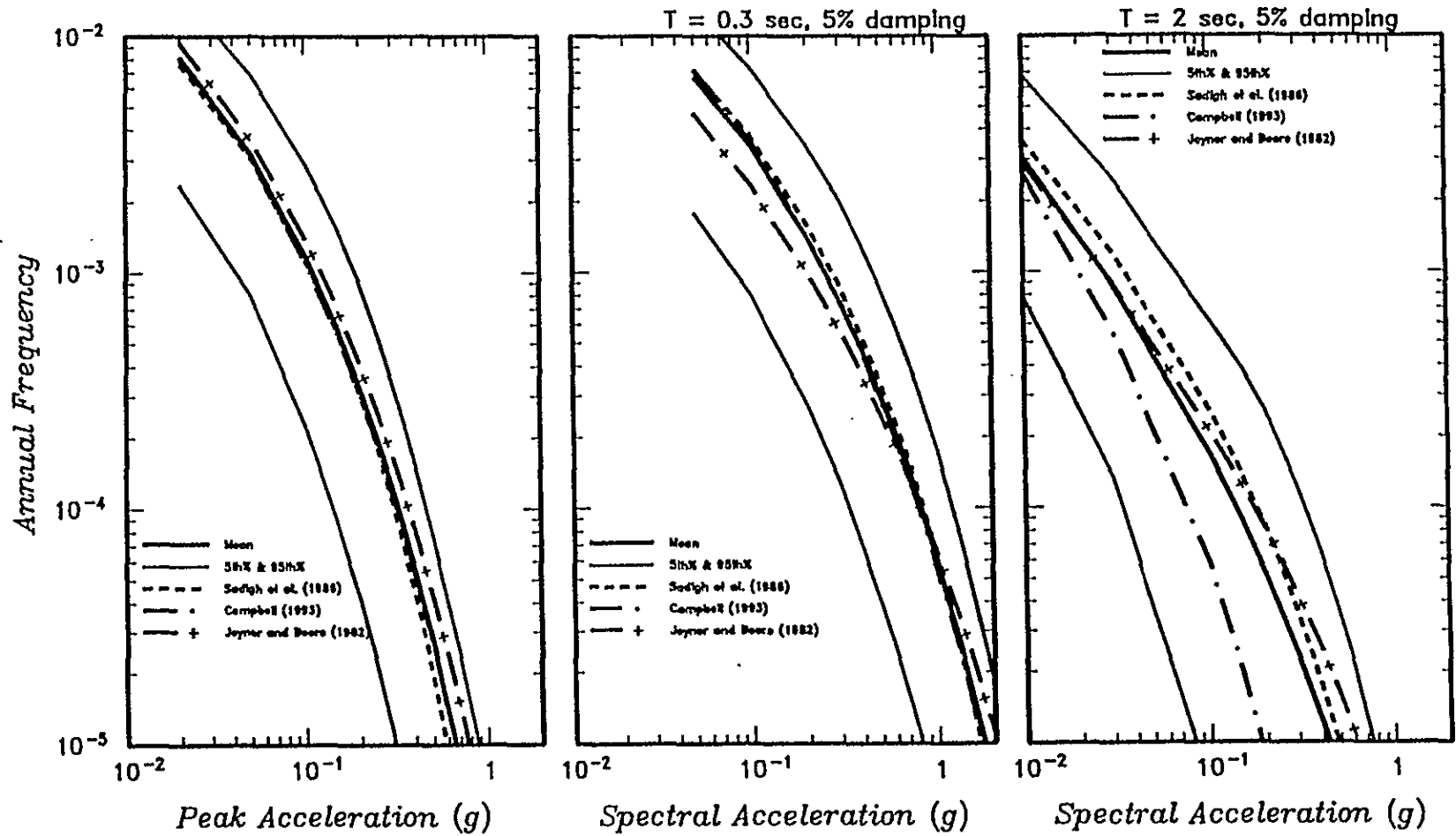
Figure 5-5b   Effect of choice of attenuation relationship on mean hazard from crustal sources at DOE Site C. Shown are results for peak horizontal acceleration and 5%-damped spectral acceleration at 0.3 and 2.0 seconds.

Figure 5-6a   Effect of coupled versus uncoupled fold models on mean hazard from fold sources only at DOE Site A. Shown
are results for peak horizontal acceleration and 5%-damped spectral acceleration at 0.3 and 2.0 seconds.
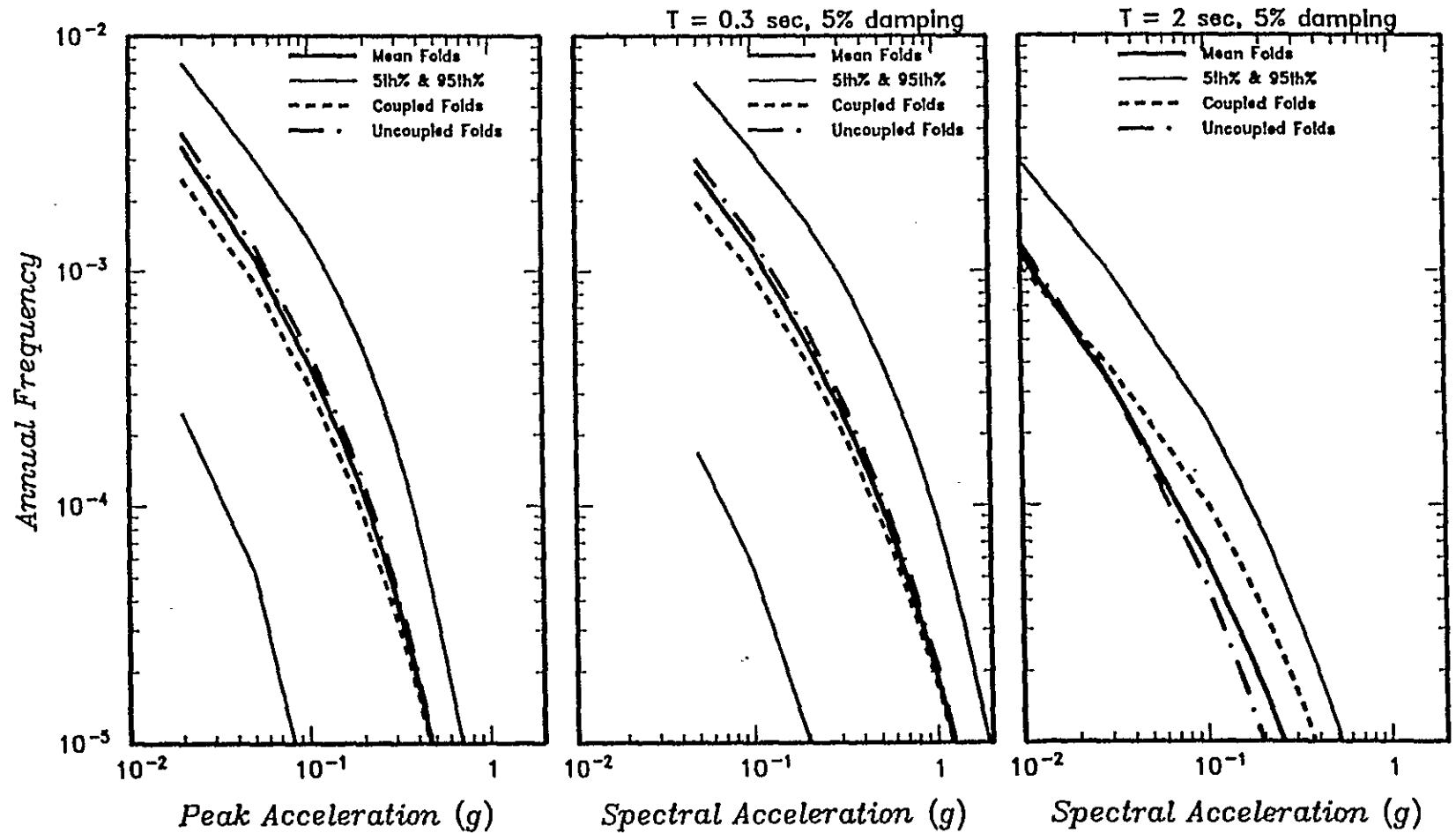
Figure 5-6b   Effect of coupled versus uncoupled fold models on mean hazard from fold sources only at DOE Site C. Shown are results for peak horizontal acceleration and 5%-damped spectral acceleration at 0.3 and 2.0 seconds.

Figure 5-7a   Effect of alternative spatial distributions of earthquakes on mean hazard from the shallow basalt source at DOE Site A. Shown are results for peak horizontal acceleration and 5%-damped spectral acceleration at 0.3 and 2.0 seconds.

Figure 5-7b   Effect of alternative spatial distributions of earthquakes on mean hazard from the shallow basalt source at DOE Site C. Shown are results for peak horizontal acceleration and 5%-damped spectral acceleration at 0.3 and 2.0 seconds.

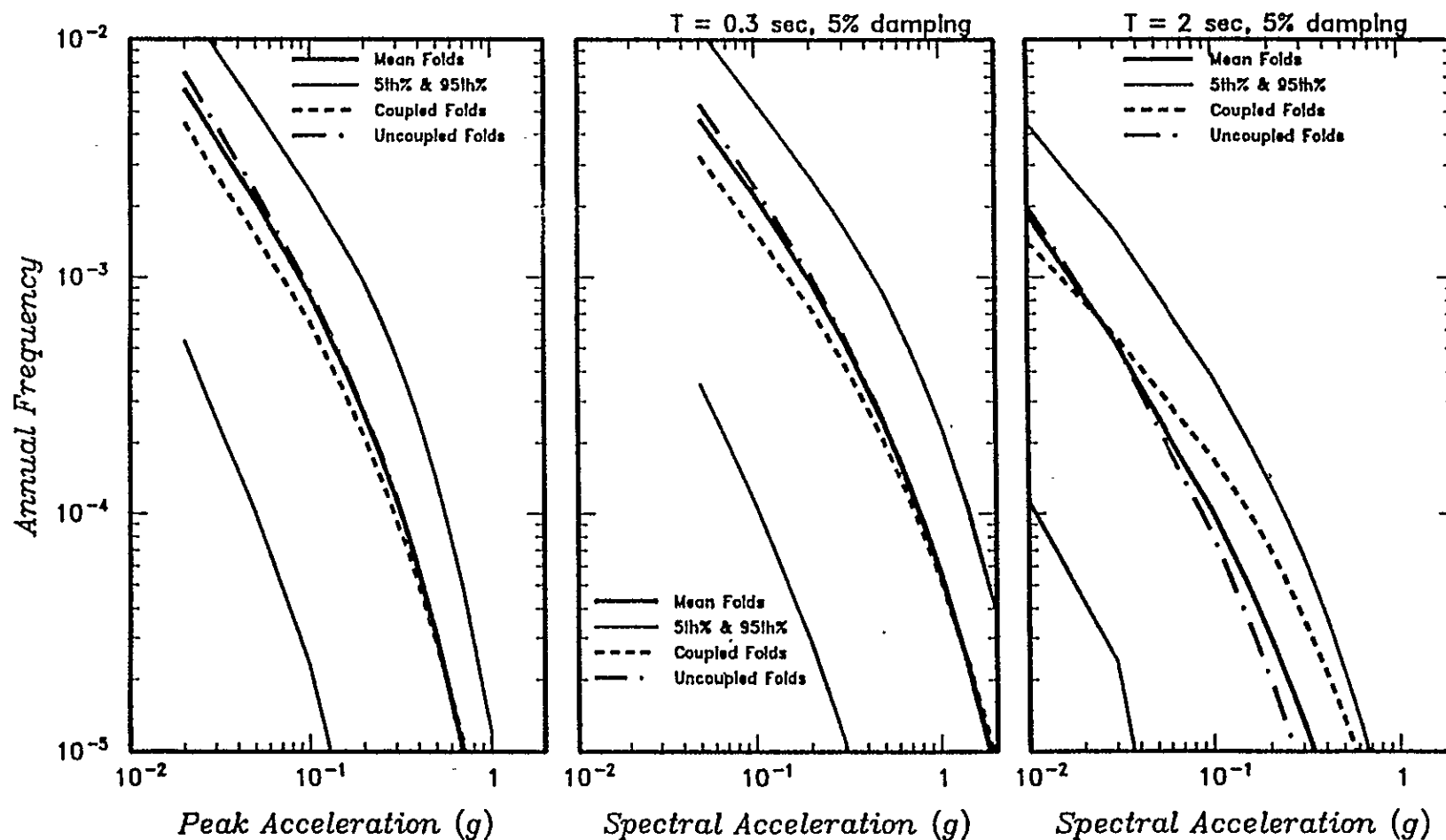Figure 5-8a   Effect of alternative models of earthquake sources on mean hazard from the deep crystalline basement source at DOE Site A. Shown are results for peak horizontal acceleration and 5%-damped spectral acceleration at 0.3 and 2.0 seconds.

Figure 5-8b   Effect of alternative models of earthquake sources on mean hazard from the deep crystalline basement source at DOE Site C. Shown are results for peak horizontal acceleration and 5%-damped spectral acceleration at 0.3 and 2.0 seconds.

GEOMATRIX

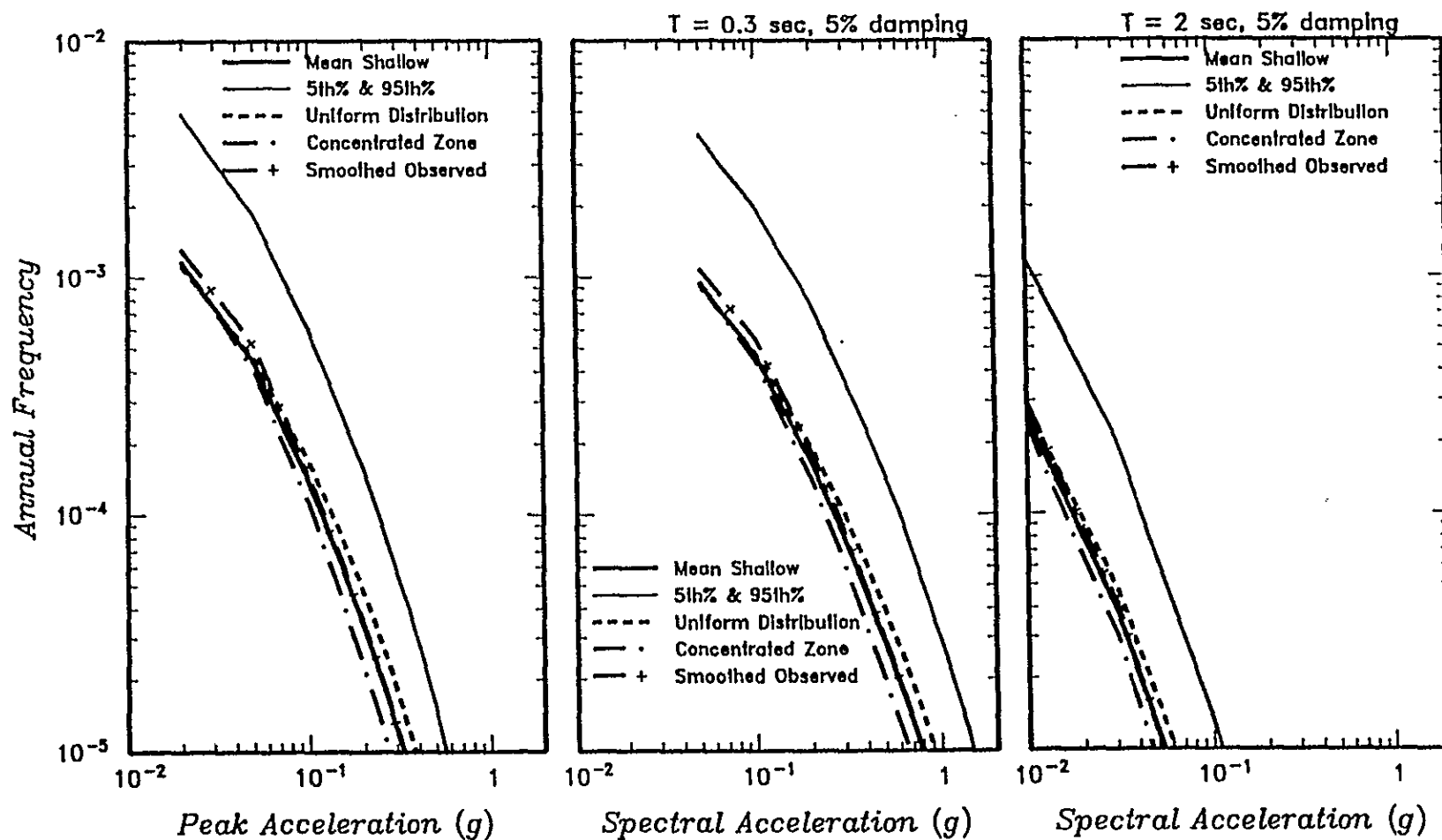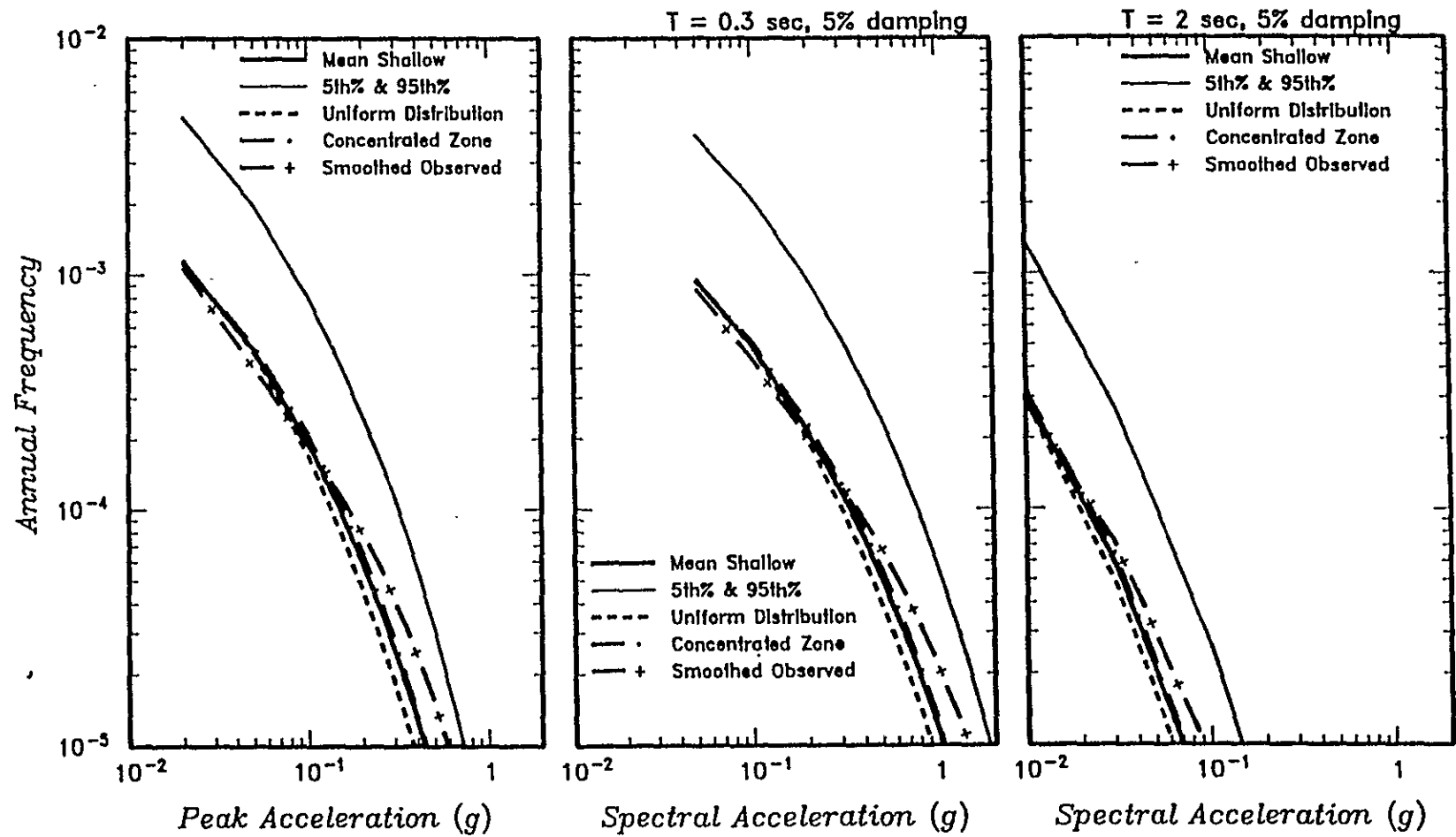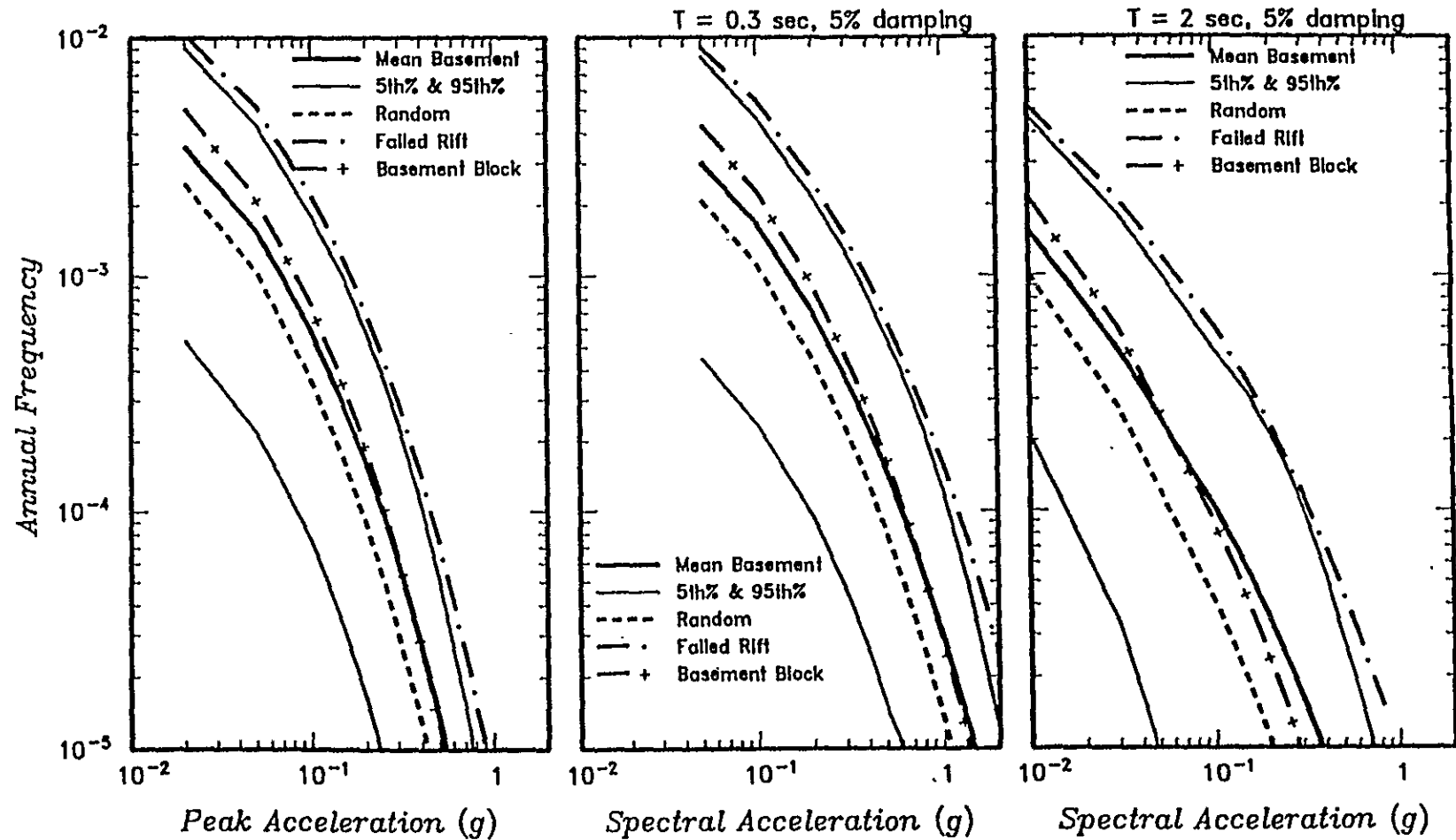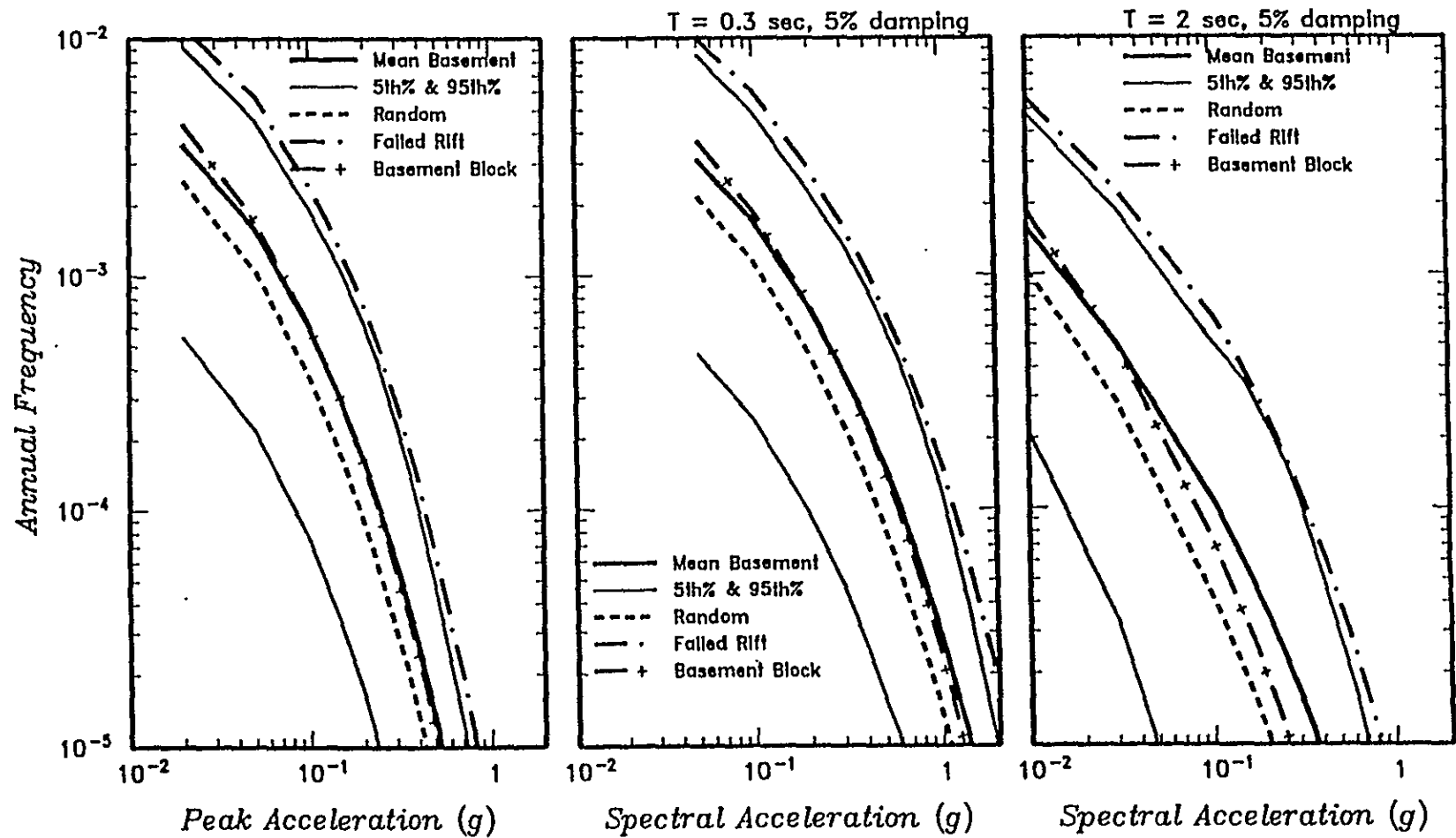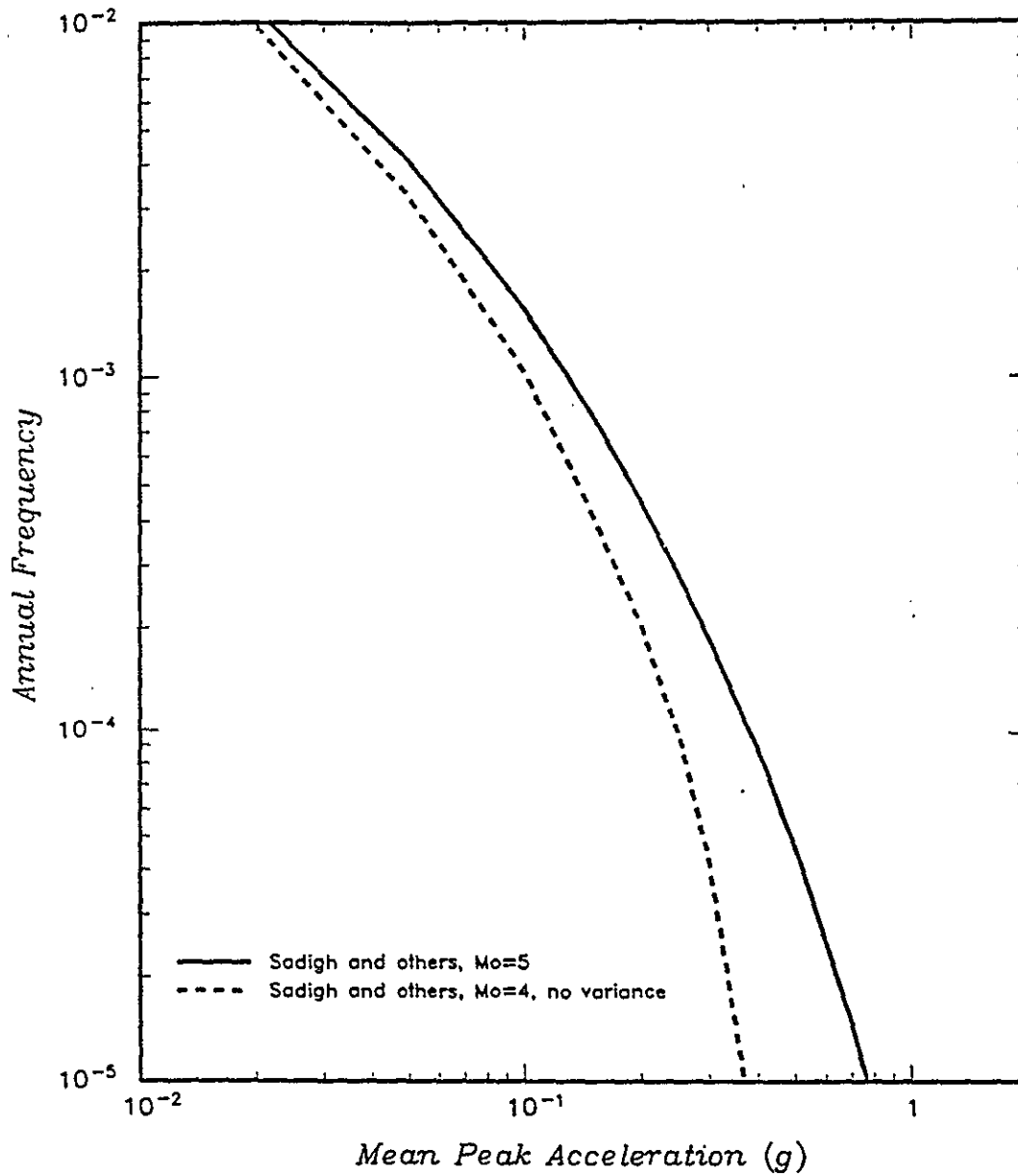Figure 5-9   Peak acceleration hazard at DOE Site A computed using $m^0 = 5.0$ and ground motion randomness compared with the peak acceleration hazard computed using $m^0 = 4.0$ and no ground motion variability.

Catchings, R.D., and W.D. Mooney, 1988, Crustal structure of the Columbia Plateau:
Evaluation for continental rifting: Journal of Geophysical Research, v. 93, p. 459-474.

Cloos, H., 1939, Hebung - Spaltung - Vulkanismus: Geologische Rundschau, v. XXX,
Zwischenheft 4A, Fredinand Enke Verlag, Stuttgart.

Coppersmith, K.J., 1991, Seismic source characterization for engineering seismic hazard
analysis: Proceedings of the Fourth International Seismic Zonation Conference, v. 1,
p. 1-60.

Coppersmith, K.J. and R.R. Youngs, 1986, Capturing uncertainty in probabilistic seismic
hazard assessments within intraplate environments: in Proceedings of the 3rd National
Conference on Earthquake Engineering, Charleston, South Carolina, August 24-28, v. I,
p. 301-312.

Coppersmith, K.J., and R.R. Youngs, 1990, Improved methods for seismic hazard analysis
in the western United States: Proceedings of the Forth U.S. National Conference on
Earthquake Engineering, Palm Springs, Calif. May 20-24, v. I, p. 723-731.

Cornell, C.A., 1968, Engineering seismic risk analysis: Bulletin of the Seismological Society
of America, v. 58, p. 1583-1606.

Cornell, C.A. and E.H. Van Marke, 1969, The major influences on seismic risk: in
Proceedings of the Third World Conference on Earthquake Engineering, Santiago Chile,
v. A-1, p. 69-93.

Cornforth Consultants and Geomatrix, 1992, Seismic hazard evaluation, Bull Run Dam sites
near Sandy Oregon: report prepared for the City of Portland, Oregon Hydraulic Power
Section, Bureau of Public Works, November.

Coward, M.P., 1983, Thrust tectonics, thin skinned or thick skinned, and the continuation of
thrust to deep in the crust: Journal of Structural Geology, v. 5, p. 113-123.

Crouse, C.B., 1991, Ground-motion attenuation equations for earthquakes on the Cascadia
subduction zone: Earthquake Spectra, v. 7, p. 210-236.

Crouse, C.B., and B.E. Turner, 1980, Processing of Japanese accelerograms and comparisons
with U.S. strong-motion data: Proceedings of the 7th World Conference on Earthquake
Engineering, v. 2, p. 419-428.

Davis, G.A., 1977, Tectonic evolution of the Pacific Northwest Precambrian to present,
Preliminary Safety Analysis Report, Amendment 23, Subappendix 2R C, Washington
Public Power Supply System Nuclear Project WNP-2, Richland Washington.

DOE, 1988, Site characterization plan, reference repository location, Hanford Site, Washington: U.S. Department of Energy Report DOE/RW-0164, v. 1 and 2.

Doser, D.I. and R. B. Smith, 1982, Seismic moment rates in the Utah region: Bulletin of the Seismological Society of America, v. 72, p. 525-552.

Foxall, W., W.U. Savage, M.R. Schnapp, and L.C. Seekins, 1981, Analysis of the instrumental seismicity of the Columbia Plateau: Appendix 2.5J to Amendment N. 18 Final Safety Analysis Report WNP-2, for Washington Public Power Supply System, Richland Washington, September.

Gardner, J.K. and L. Knopoff, 1974, Is the sequence of earthquakes in Southern California, with aftershocks removed, Poissonian: Bulletin of the Seismological Society of America, v. 64, p. 1363-1367.

Geomatrix, 1990, Seismotectonic evaluation - Walla Walla section of the Columbia Plateau Geomorphic Province: Report prepared for the US Department of the Interior, Bureau of Reclamation.

Geomatrix, 1993, Seismic ground motion study for Humboldt Bay bridges on Route 255: report prepared for the California Department of Transportation (CALTRANS), Division of Structures, Contract No. 59N772, June.

Glover, D.W., 1985, Crustal structure of the Columbia Basin, Washington, from borehole and refraction data: MS thesis, University of Washington, Seattle, Washington.

Glover, D.W., S.D. Malone, and A. Rohay, 1985, Crustal structure of the Columbia Basin, Washington, form borehole and refraction data (abs.): Earthquake Notes, v, 55, n. 1, p. 22.

Grolier, M.J., and J.W. Bingham, 1971, Geologic map and sections of parts of Grant, Adams, and Franklin Counties, Washington: U.S. Geological Survey Miscellaneous Geologic Investigations Series Map I-589, scale 1:62,500.

Gutenberg B. and C.F. Richter, 1954, Seismicity of the Earth and Associated Phenomena, 2nd ed., Princeton University Press, Princeton, New Jersey, 310 p.

Gutenberg B. and C.F. Richter, 1956, Earthquake magnitude, intensity, energy, and acceleration: Bulletin of the Seismological Society of America, v. 46, p. 105-145.

Hagood, M.A., 1986, Structure and evolution of the Horse Heaven Hills, south-central Washington: Rockwell Hanford Operations Report RHO-BW-SA-344, 176 p.

Hanks, T.C., and H. Kanamori, 1979, A moment magnitude scale: Journal of Geophysical Research, v. 84, p. 2348-2350.

Hyndman, R.D., and Wang, K., 1993, Thermal constraints on the zone of major thrust earthquake failure: the Cascadia subduction zone: Journal of Geophysical Research, v. 98, p. 2039-2060.

Johnson, P.A., 1989a, Cluster analysis of eastern Washington Seismicity: Master of Science Thesis, University of Washington, August, 86 p.

Johnson, P.A., 1989b, Central Washington seismicity: evidence for a reactivated buried continental rift and northwest-trending structural zones: Geophysical Research Letters, v. 16, p. 1325-1328.

Joyner, W.B., and D.M. Boore, 1982, Prediction of earthquake response spectra: US Geological Survey Open File Report 82-977.

Kim, K., S.A. Dischler, J.R. Aggson, and M.P. Hardy, 1986, The state of in-situ stresses determined by hydraulic fracturing at the Hanford Site: RHO-BW-ST-73 P, Rockwell Hanford Operations, Richland Washington.

Kulkarni, R.B., R.R. Youngs, and K.J. Coppersmith, 1984, Assessment of confidence intervals for results of seismic hazard analysis: in Proceedings of the Eight World Conference on Earthquake Engineering, San Francisco, California, v. 1, p. 263-270.

Laubscher, H., 1981, Models of the development of Yakima deformation: Appendix 2.5-O to the Washington Public Power Supply System Nuclear Project No. 2 Final Safety Analysis Report, V. 3, Amendment 18, Washington Public Power Supply System, Richland Washington, September.

Ludwin, R.S., C.S. Weaver, and R.S. Crosson, 1992, Seismicity of Washington and Oregon: in Slemmons, D.B., E.R. Engdahl, M.D. Zoback, M.L. Zoback, and D. Blackwell, eds., Neotectonics of North America, The Geological Society of America, Boulder, Colorado.

Malone, S. ,1979, Annual technical report on micro-earthquake monitoring of the Hanford Region: University of Washington, Seattle, Washington.

Mann, G.M., and C.H. Meyer, 1993, Late Cenozoic structure and correlations to seismicity along the Olympia-Wallowa Lineament: The Geologic Society of America Bulletin, v. 105, p. 853-871.

Merz, H.A., and C.A. Cornell, 1973, Aftershocks in engineering seismic risk analysis: M.I.T. Department of Civil Engineering Research Report R73-25, Cambridge, Massachusetts.

OASES (Offshore Alaska Seismic Exposure Study), 1978, Attenuation: Volume II of a report prepared for Alaska Subarctic Operators Committee by Woodward-Clyde Consultants, March.

Pezzopane, S.K., and R.J. Weldon, III, 1993, Tectonic role of active faulting in central Oregon: Tectonics.

Power, M.S., K.J. Coppersmith, R.R. Youngs, D.P. Schwartz, and F.H. Swan III, 1981, Seismic exposure analysis for the WNP-2 and WNP-1/4 site: Appendix 2.5K to Amendment N. 18 Final Safety Analysis Report WNP-2, for Washington Public Power Supply System, Richland, Washington, September.

Prescott, W.H., and J.C. Savage, 1984, Crustal deformation near Hanford: U.S. Geological Survey Open-File Report 84-797, 28 p.

Price, E.H., and A.J. Watkinson, 1989, Structural geometry and strain distribution within eastern Umtanum fold ridge, south-central Washington: in Reidel, S.P., and P.R. Hooper. eds., Volcanism and Tectonics in the Columbia River Flood-Basalt Province, Geological Society of America, Special Paper 239, p. 265-282.

Purcaru, G., and H. Berkhemer, 1982, Quantitative relations of seismic source parameters and a classification of earthquakes: Tectonophysics, v. 84, p. 57-128.

Reidel, S.P., 1984, The Saddle Mountains: the evolution of an anticline in the Yakima Fold Belt: American Journal of Science, v. 284, p. 942-978.

Reidel, S.P., 1988, Geologic map of the Saddle Mountains, south-central Washington: Washington Division of Geology and Earth Resources Geologic Map GM-38.

Reidel, S.P., and N.P. Campbell, 1989, Structure of the Yakima Fold Belt, central Washington: in Joseph, N.L., and others (eds.) Geologic guidebook for Washington and adjacent areas: Washington Division of Geology and Earth Resources Information Circular 86.

Reidel, S.P., K.R. Fecht, M.C. Hagood, and T.L. Tolan, 1989, The geologic evolution of the central Columbia Plateau: in Reidel, S.P., and P.R. Hooper, eds., Volcanism and Tectonics in the Columbia River Flood-Basalt Province, Geological Society of America, Special Paper 239, p. 247-264.

Reidel, S.P., T.L. Tolan, P.R. Hooper, M.H. Beeson, K.R. Fecht, R.D. Bently, and J.L. Anderson, 1989b, The Grand Ronde Basalt, Columbia River Basalt Group; stratigraphic descriptions and correlations in Washington, Oregon, and Idaho: in Reidel, S.P., and P.R. Hooper, eds., Volcanism and Tectonics in the Columbia River Flood-Basalt Province, Geological Society of America, Special Paper 239, p. 21-53.

Reidel, S.P., N.P. Campbell, K.R. Fecht, and K.A. Lindsey, in press, Late cenozoic structure and stratigraphy of south-central Washington: Washington Division of Geology and Earth Resources Bulletin No. 80, 2nd Symposium on Geology of Washington.

Ringdal, F., E.S. Husebye, H. Bungum, S. Mykkeltveit, and O. Sandvin, 1982, Earthquake hazard offshore Norway: report prepared for the NTNF "Safety Offshore" Committee, NORSAR Contribution 302.

Rohay, A.C., 1989, Earthquake recurrence rate estimates for eastern Washington and the Hanford site: Proceedings of the Second DOE Natural Phenomena Hazards Mitigation Conference, Knoxville, Tennessee, October 3-5, p. 272-281.

Rohay, A.C., and J.D. Davis, 1983, Contemporary deformation in the Pasco Basin area of the central Columbia Plateau: in J.A. Caggiano and D.W. Duncan, eds., Preliminary interpretation of the tectonic stability of the Reference Repository Location, Cold Creek Syncline, Hanford Site: RHO-BWI-ST-19 P, Rockwell Hanford Operations, Richland Washington.

Rohay, A.C., and S.D. Malone, 1983, Crustal structure of the Columbia Plateau Region, Washington: Rockwell Hanford Operations Report RHO-BW-SA-289 P.

Rohay A.C., D.W. Glover, and S.D. Malone, 1985, Time-term analysis of upper crustal structure in the Columbia Basin, Washington: Rockwell Hanford Operations Report RHO-BW-SA-435 P., 4 p.

Sadigh, K., J.A. Egan, and R.R. Youngs, 1986, Specification of ground motion for seismic design of long period structures (abs.): Earthquake Notes, v. 57, n. 1, p. 13. relationships printed in W.B. Joyner and D.M. Boore, 1988, Measurement, characterization, and prediction of strong ground motion: in Earthquake Engineering and Soil Dynamics II - Recent Advances in Ground Motion Evaluation, ASCE Geotechnical Special Publication 20, p. 43-102.

Schwartz, D.P., 1988, Geology and seismic hazards - moving into the 1990's: in Earthquake Engineering and Soil Dynamics II - Recent Advances in Ground Motion Evaluation, ASCE Geotechnical Special Publication 20, p. 1-42.

Shannon and Wilson, Inc., 1977, Geologic reconnaissance of the Cle-Elum-Wallula Lineament and related structures: Report to Washington Public Power Supply System.

Sharp, R.V., 1981, Variable rates of Quaternary strike slip on the San Jacinto fault zone, southern California: Journal of Geophysical Research, v. 86, p. 1754-1762.

Shemeta, J.E., and J.C. Pechmann, 1989, New analysis of three-component digital seismograms for aftershocks of the 1983 Borah Peak, Idaho, earthquake - source parameters and refined hypocenters (abs.): Seismological Research Letters, v.60, n. 1, p. 30.

Singh, S., and R.B. Herrmann, 1983, Regionalization of crustal coda Q in the continental United States: Journal of Geophysical Research, v. 88, p. 527-538.

Slemmons, D.B., 1982, Determination of design earthquake magnitudes for microzonation: Proceedings of the Third International Microzonation Conference, v. 1, p. 119-130.

Suppe, J., 1988, Short Course on cross-section balancing in petroleum structural geology: Pacific Section AAPG, Santa Barbara, California, 20-21 April, 220 p.

Swan, F.H., 1988, Temporal clustering of paleoseismic events on the Oued Fodda fault, Algeria: Geology, v. 16, p. 1092-1095.

Swanson, D.A., J.L. Anderson, R.D. Bentley, V.E. Camp, J.N. Gardner, and T.L. Wright, 1979, Reconnaissance geologic map of the Columbia River Basalt Group in Washington and adjacent Idaho: U.S. Geological Survey Open-File Report 79-1363, scale 1:250,000.

Swanson, D.A., and seven others, 1980, Reconnaissance geologic map of the Columbia River Basalt Group, Pullman and Walla Walla Quadrangles, southwest Washington and adjacent Idaho: U.S. Geological Survey Miscellaneous Investigations Map I-1139, scale 1:250,000.

Tabor, R.W., V.A. Frizzell Jr., J.A. Vance, and C.W. Naeser, 1984, Ages and stratigraphy of lower and middle Tertiary sedimentary and volcanic rocks of the central Cascades, Washington - Application to the tectonic history of the Straight Creek fault: Geological Society of America Bulletin, v. 95, p. 26-44.

University of Washington, 1985, Annual technical report, 1985, on earthquake monitoring of eastern Washington: Geophysics Program, University of Washington, Seattle, report prepared for the U.S. Department of Energy under contract no. EY-76-S-06-2225.

University of Washington, 1986, Annual technical report, 1986, on earthquake monitoring of eastern Washington: Geophysics Program, University of Washington, Seattle, report prepared for the U.S. Department of Energy under contract no. EY-76-S-06-2225.

Uhrhammer, R.A., 1986, Characteristics of northern and central California seismicity (abs.): Earthquake Notes, v. 57, n. 1, p. 21.

Veneziano, D. and J. Van Dyck, 1985, Analysis of earthquake catalogs for incompleteness and recurrence rates: Seismic Hazard Methodology for Nuclear Facilities in the Eastern United States, EPRI Research Project N. P101-29, EPRI/SOG Draft 85-1, v. 2, Appendix A-6, April 30.

Wallace, R.E., 1987, Grouping and migration of surface faulting and variations in slip rates on faults in the Great Basin province: Bulletin of the Seismological Society of America, v. 77, p. 868-876.

Washington Public Power Supply System, 1981, Final Safety Analysis Report for Unit WNP-2, Admendment No. 18, September.

Washington Public Power Supply System, 1985, Site-specific response spectra for the WNP-2 power plant: Final Safety Analysis Report for Unit WNP-2, Appendix 2.5Q, Admendment No. 36, December.

Watters, T.R., 1989, Periodically spaced anticlines of the Columbia Plateau: in Reidel, S.P., and P.R. Hooper, eds., Volcanism and Tectonics in the Columbia River Flood-Basalt Province, Geological Society of America, Special Paper 239, p. 283-292.

Weichert, D.H., 1980, Estimation of the earthquake recurrence parameters for unequal observation periods for different magnitudes: Bulletin of the Seismological Society of America, v. 70, p. 1337-1346.

Wells, D., and K.J. Coppersmith, 1991, Analysis of fault dip and sense of slip for historical earthquakes (abs.): Seismological Research Letters, v. 62, p. 38

Wells, D., and K.J. Coppersmith, in press, Updated empirical relationships among magnitude, rupture length, rupture area, and surface displacement: Bulletin of the Seismological Society of America.

West, M.W., and M.E. Shaffer, 1989, Late Quaternary surface deformation in the Smyrna Bench and Saddle Gap segments, Saddle Mountains anticline, Yakima fold belt, central Columbia Basin, Washington (abs): Geological Society of America Abstracts with Program, v. 21, no. 5, p. 157-158.

Weston Geophysical Corporation, 1981, Geologic models in the Columbia Plateau constrained by gravity data: report prepared for Washington Public Power Supply System, Contract H.O. 44010, June, 9 p.

Woodward-Clyde Consultants, 1989, Seismic Hazard Assessment for Hanford DOE Site: report prepared for Westinghouse Hanford Company, Richland Washington, WHC-MR-0023.

Wyss, M., 1979, Estimating maximum expectable magnitude of earthquakes from fault dimensions: Geology, v. 7, p. 336-340.

Yelin, T.S., and H.J. Patton, 1991, Seismotectonics of the Portland, Oregon, region: Bulletin of the Seismological Society of America, v. 81, p. 109-130.

Youngs, R.R. and K.J. Coppersmith, 1985a, Development of a fault-specific recurrence model: Earthquake Notes (abs.), v. 56, n. 1, p. 16.

Youngs, R.R. and K.J. Coppersmith, 1985b, Implications of fault slip rates and earthquake recurrence models to probabilistic seismic hazard estimates: Bulletin of the Seismological Society of America, v. 75, p. 939-964.

Youngs, R.R., K.J. Coppersmith, M.S. Power and F.H. Swan III, 1985, Seismic hazard assessment of the Hanford region, eastern Washington State: in Proceedings of the DOE Natural Phenomena Hazards Mitigation Conference, Las Vegas, Nevada, October 7-11, p. 169-176.

Youngs, R.R., F.H. Swan, M.S. Power, D.P. Schwartz, and R.K. Green, 1987, Probabilistic analysis of earthquake ground shaking hazard along the Wasatch Front, Utah: Assessment of Regional Earthquake Hazards and Risk Along the Wasatch Front, Utah, U.S. Geological Survey Open File Report 87-585, v. II, p. M-1-110.

Youngs, R.R., F.H. Swan, and M.S. Power, 1988, Use of detailed geologic data in regional probabilistic seismic hazard analysis - an example from the Wasatch Front, Utah: in Earthquake Engineering and Soil Dynamics II -Recent Advances in Ground Motion Evaluation, ASCE Geotechnical Special Publication 20, p. 156-172.

Youngs, R.R., F. Makdisi, K. Sadigh, and N.A. Abrahamson, 1990, The case for magnitude dependent dispersion in peak ground acceleration (abs.): Seismological Research Letters, v. 61, n. 1, p. 30, submitted to the Bulletin of the Seismological Society of America in 1993.

Youngs, R.R., K.J. Coppersmith, C.L. Taylor, M.S. Power, L.A. Di Silvestro, M.L. Angell, N.T. Hall, J.R. Wesling, and L. Mualchin, 1992, A Comprehensive Seismic Hazard Model for the San Francisco Bay Region, Proceedings of the Second Conference on Seismic Hazard in the east San Francisco Bay Region, California, California Department of Conservation, Division of Mines and Geology Special Publication 113, p. 431-441.

Youngs, R.R., N.A. Abrahamson, F. Makdisi, and K. Sadigh, in review, Magnitude dependent dispersion in peak ground acceleration: Bulletin of the Seismological Society of America.